An electrospun protein-and chromophore-loaded patch: Application to laser-assisted vascular anastomosis

Inauguraldissertation

zur Erlangung des akademischen Grades
Doktor der Medizinwissenschaften
der Universitätsmedizin Rostock

vorgelegt von

Annemarie Schönfeld

aus Zwickau

2017

Leiter der Arbeit:
PD Dr. Kirsten Peters, Arbeitsbereich Zellbiologie der Universitätsmedizin Rostock
Prof. Dr. Martin Frenz, Institut für Angewandte Physik der Universität Bern

Aus dem Arbeitsbereich Zellbiologie
Leiter: Prof. Dr. Barbara Nebe

An electrospun protein-and chromophore-loaded patch: Application to laser-assisted vascular anastomosis

Inauguraldissertation

zur Erlangung des akademischen Grades
Doktor der Medizinwissenschaften
der Universitätsmedizin Rostock

vorgelegt von

Annemarie Schönfeld

geboren am 27.03.1986 in Zwickau

2017

Leiter der Arbeit:
PD Dr. Kirsten Peters, Arbeitsbereich Zellbiologie der Universitätsmedizin Rostock
Prof. Dr. Martin Frenz, Institut für Angewandte Physik der Universität Bern

Aus dem Arbeitsbereich Zellbiologie
Rostock,   Leiter: Prof. Dr. Barbara Nebe

Contents

Abstract

Laser-assisted vascular anastomosis (LAVA) is a technique to fuse blood vessels by using laser energy with possible applications in almost all medical fields. This technique is based on the energy absorption by a chromophore with subsequent heating of the underlying tissue. Generally, this heat results in alteration of the molecular structure of the tissue which can then form bonds with neighboring molecules. The application of a proteinaceous solder increases the strength of the tissue fusion by forming additional bonds with the tissue and acts as a biological glue.

Even though LAVA has been studied for more than 50 years, it has not yet reached the stage of clinical applicability. Main challenges include either too strong thermal damage or too low bonding strengths, the tedious handling of the solder material during surgery, and the flow-off of the solder from the tissue, leading to staining and heating of peripheral tissue.

The objective of this thesis was to improve LAVA by introducing a new soldering material, by elaborating the soldering setup, and by investigating alternative temperature profiles. A two-layer solder patch was produced by electrospinning, entrapping the chromophore indocyanine green and the protein bovine serum albumin into polymer fibers. An intraluminal soldering setup with a balloon catheter and a diffusor laser-fiber was used to characterize the behavior of the patch during soldering. *In vitro* studies using rabbit aortas confirmed the feasibility of the electrospun patch for sutureless LAVA. Applying the patch improved the handling during surgery significantly and vanished the staining of the tissue, while ensuring strong bonding strengths. The flow-off of indocyanine green was reduced due to its protection from aqueous environment in polycaprolactone fibers. Preclinical experiments, involving pigs, demonstrated a sufficient immediate bonding strength. However, occlusion of the anastomosis was observed after a few days. Therefore, the temperature curve during soldering, using continuous and pulsed laser irradiation, was analyzed in order to reduce thermal damage. By testing the patches *in vitro*, it was demonstrated that endothelial and stem cells do not adhere to the laser-irradiated patch. This thesis discusses the current challenges in the development of a new biomaterial and soldering technique for sutureless LAVA and can guide future research.

I. Introduction

The application of laser techniques for surgery provides an exciting and innovative research field, especially for minimally invasive surgery. The fusion of two blood vessels is a vital step in most surgical procedures. Conventional techniques to fuse blood vessels are sutures [1, 2] and mechanical closure devices such as clips and staples [3, 4]. These techniques are well accepted, inexpensive, reliable and applicable for many purposes. A huge drawback is the damage to the tissue during the passage of the needle or staples, which can result in tissue inflammation, scar formation, and stenosis. Foreign body reactions may occur due to the introduction of a foreign material, namely the thread or clips. Moreover, sutures are not immediately watertight due to the small holes that are created. Additionally, suture ligation is a time consuming and skill intensive process especially in microsurgery [5, 6]. Other closure techniques such as glues made of fibrin [7–9], albumin [10, 11], or cyanoacrylate [12, 13] are easy to apply. However, they require stay sutures to achieve a reasonable bonding strength, and can lead to allergic reactions and anaphylaxis [5, 9].

Laser-assisted vascular anastomosis

Laser-assisted vascular anastomosis (LAVA) was first reported by Yahr *et al.* in 1964, where they fused arteries using a neodymium laser [14]. In 1979, Jain and Gorisch demonstrated the application of a Nd:YAG laser for the anastomosis of rat arteries [15]. A few years later, early attempts achieved stable tissue bonds with a CO_2 laser [16, 17]. The CO_2 wavelength in the mid-infrared range is strongly absorbed by water, which leads to a strong absorption of the laser energy in the outermost layers of the tissue. Hence, only a small area of the tissue is heated and the underlying layers are not affected. As a consequence, anastomoses with a CO_2 laser suffered from aneurisms, and low bonding strengths [18, 19]. Recent research with the CO_2 laser focuses on the bonding of superficial surgical incisions, such as the cornea [20], or involves multi-wavelength systems [21]. The argon laser was used to produce more even tissue heating, leading to stronger bonds. The absorption of typical argon laser wavelengths, 488.0 and 514.5 nm, is mainly mediated by hemoglobin, occurring in blood. Hence, variations in the hemoglobin content lead to irreproducible results. Successful vascular anastomosis in dogs with an argon laser was demonstrated by Chikamatsu [22] and Vlasak [23]. Chuck *et al.* used an argon laser in combination with the dye fluorescein isothiocyanate for selective energy absorption for the anastomosis of rabbit aorta [24], being the advent of dye-enhanced laser soldering. Nowadays, most research towards LAVA focuses on the application of a diode laser in combination with the chromophore dye indocyanine green (ICG) [25–29] or methylene blue [30]. By adding a dye, the tissue is selectively heated, which could avoid heating of surrounding tissue. Both dyes are used with laser in the near-infrared range, which minimizes thermal damage to the tissue, since the tissue absorbs least in the so called "diagnostic window".

LAVA can potentially overcome the limitations of mechanical closures. Yet, LAVA is still only used experimentally. The clinical application of LAVA is mainly hampered by irreproducible

temperature regimes, resulting in either strong thermal damage or in low bonding strengths. Other challenges include difficult handling of the soldering material, and the flow-off of the solder during surgery, causing the staining and unwanted heating of peripheral tissue. Blood vessels require good control of the soldering procedure due to their thin and delicate tissue layer, resulting in high risk of thermal damage across the whole vessel wall and therefore risk of thrombosis and the occlusion of the blood vessel.

Interactions of laser light with tissue are scattering, absorption, and reflection and refraction, with absorption being the most important in dye-enhanced LAVA. The absorption of laser light by the dye results in heating of the dye, followed by heat diffusion and heating of underlying tissue. Since the heating depends on the absorption coefficient of the dye, controlling the amount of ICG during the soldering process is a prerequisite for ensuring reproducible temperatures and bonding strengths. The first goal of this thesis is to bind ICG to a solder carrier material, ensuring a constant spatial and temporal concentration of ICG during soldering.

The application of a solder, consisting of a protein substance, contributed to optimizing LAVA. Heating results in the denaturation of proteins from both, the solder and the tissue, leading to subsequent cross-linking [19, 31]. The first reported solders were blood [32], followed by fibrin [33, 34], and albumin [31, 35, 36]. One problem of addition of liquid solder during surgery is its hardly controllable amount, leading to irreproducible results. Over the last years, the reliability of LAVA has been significantly improved by applying membranes or strips [27, 28, 35]. These membranes/strips increase the overall area that is involved in the bonding and therefore the strength of the weld. The second objective of this thesis was thus to incorporate albumin into the solder carrier material.

Electrospinning

Electrospinning of nanofibers was first mentioned in a US patent by Formhals in 1934, where cellulose acetate was used for preparing artificial threads [37]. Since then, publications on electrospinning appeared only occasionally until the 1990s. Today, electrospinning-related research raises great interest and is used in the fields of filters [38], wound healing [39–41], tissue engineering [42–44], and drug delivery [45–48], to name some examples. Electrospun fibers are prepared by applying a high voltage between a polymeric solution and a metallic collector. The polymeric solution, allowing macromolecular entanglement, is pumped through a metallic needle, using a syringe pump, that ensures a constant flow. When the electric charges overcome the surface tension of the solution, a fluid jet is released from the needle tip. The ejected liquid jet is then drawn towards the collector and the fibers are deposited as non-wovens onto the collector. The fiber formation is comprised of different physical phenomena, which are the droplet formation at the needle tip, the development of a jet, the bending deformations, and the deposition of the jet. The details of the physical process can be found in numerous articles [49–52].

Electrospinning can produce mechanically strong and elastic membranes [53, 54], and is a versatile, relatively simple, and cheap technique. The variation of the solution and process parameters allows tailoring of the fiber diameter and pore size, the modulation of the fiber surface, and the uniformity of the fibers [55]. Furthermore, functional compounds, such as proteins [56–61], growth factors [62, 63], drugs [48, 64], and chromophores [65–68], can be entrapped into the fibers in relatively large quantities.

Setup of this thesis

The focus of this thesis is the development of an electrospun solder patch and the exploration of the applicability of the patch for LAVA using medium-sized arteries (diameter 3.5 to 4.5 mm).

In this thesis, all chapters can be read independently. In chapter II, I present the development of a solder patch by binding ICG in polycaprolactone (PCL) fibers using blend electrospinning. This patch was soaked in liquid bovine serum albumin (BSA), and subsequently applied to end-to-end LAVA, without the use of stay sutures. Chapter III evaluates auxiliary polymers for electrospinning of the globular protein BSA, with a high BSA-concentration. The BSA-loaded layer is directly electrospun onto the PCL/ICG-layer, producing a two-layer patch. The next section, chapter IV, applies the two-layer electrospun patch to preclinical LAVA, involving a muscle flap model in pigs. Chapter V investigates the adhesion of cells onto the solder patch and its toxicology. The last section, chapter VI, focuses on the reduction of thermal damage by applying different end-point temperatures during LAVA, as well as pulsed laser irradiation.

Bibliography

[1] P. L. Harris. Arterial suture and anastomosis. In Crawford W. Jamieson and James S. T. Yao, editors, *Vascular Surgery*, pages 51–58. Springer US, Boston, MA, 1994.

[2] Yelena Akelina. Microsurgical Technique for 1mm Vessel End to End Anastomosis. *Journal of Medical Insight*, 2014(4), 2014.

[3] Ari Leppäniemi, David Wherry, Emmanouil Pikoulis, Howard Hufnagel, Christine Waasdorp, Nancy Fishback, and Norman Rich. Arterial and venous repair with vascular clips: Comparison with suture closure. *Journal of Vascular Surgery*, 26(1):24–28, jul 1997.

[4] Subrato Deb, Barry Martin, Leon Sun, David Burris, David Wherry, Emmanuel Pikoulis, and Peter Rhee. Comparison of Titanium Vascular Closure Staples With Suture Repair of the Thoracic Aorta in Swine. *Chest*, 118(6):1762–1768, dec 2000.

[5] C. J. Zeebregts, R. H. Heijmen, J. J. van den Dungen, and R. van Schilfgaarde. Non-suture methods of vascular anastomosis. *British Journal of Surgery*, 90(3):261–271, mar 2003.

[6] Disa Lidman and Rollin K Daniel. The Normal Healing Process of Microvascular Anastomoses. *Scandinavian Journal of Plastic and Reconstructive Surgery*, 15(2):103–110, jan 1981.

[7] Dean H. Whitman, Ronald L. Berry, and David M. Green. Platelet gel: An autologous alternative to fibrin glue with applications in oral and maxillofacial surgery. *Journal of Oral and Maxillofacial Surgery*, 55(11):1294–1299, nov 1997.

[8] Silvestro Canonico. The use of human fibrin glue in the surgical operations. *Acta biomedica: Atenei Parmensis*, 74 Suppl 2:21–5, 2003.

[9] George F. Pratt, Warren M. Rozen, Angie Westwood, Angela Hancock, Daniel Chubb, Mark W. Ashton, and Iain S. Whitaker. Technology-assisted and sutureless microvascular anastomoses: Evidence for current techniques. *Microsurgery*, 32(1):68–76, jan 2012.

[10] Joshua Weiner, Shannon Widman, Zygmunt Golek, Maryann Tranquilli, and John A. Elefteriades. Role of Bovine Serum Albumin-Glutaraldehyde Glue in the Formation of Anastomatic Pseudoaneurysms. *Journal of Cardiac Surgery*, 26(1):76–81, jan 2011.

[11] Edward L Jones, Clay Cothren Burlew, and Ernest E Moore. BioGlue hemostasis of penetrating cardiac wounds in proximity to the left anterior descending coronary artery. *The Journal of Trauma and Acute Care Surgery*, 72(3):796–798, mar 2012.

[12] J. Izaaryene, M. Saeed Kilani, P.-H. Rolland, J.-Y. Gaubert, A. Jacquier, J.-M. Bartoli, and V. Vidal. Preclinical study on an animal model of a new non-adhesive cyanoacrylate (Purefill®) for arterial embolization. *Diagnostic and Interventional Imaging*, 97(11):1109–1116, nov 2016.

[13] R. Loffroy. Glubran2®, Histoacryl® or Trufill®: Which cyanoacrylate glue for endovascular use? *Diagnostic and Interventional Imaging*, 97(1):119, jan 2016.

[14] W. Z. Yahr, K. J. Strully, and E. S. Hurwiit. Non-occlusive small arterial anastomosis with a neodymium laser. *Surgical forum*, 15:224–6, 1964.

[15] K K Jain and W Gorisch. Repair of small blood vessels with the neodymium-YAG laser: a preliminary report. *Surgery*, 85(6):684–8, jun 1979.

[16] M. R. Quigley, J. E. Bailes, H. C. Kwaan, L. J. Cerullo, and J. T. Brown. Aneurysm formation after low power carbon dioxide laser-assisted vascular anastomosis. *Neurosurgery*, 18(3):292–9, mar 1986.

[17] Amado Ruiz-Razura, Ma Lan, Carlos Hita, Zahid Khan, Ned Hwang, and Benjamin Cohen. Bursting Strength in Co 2 Laser-Assisted Microvascular Anastomoses. *Journal of Reconstructive Microsurgery*, 4(04):291–296, jul 1988.

[18] I.C.D.Y.M. Wolf -de Jonge, J.F. Beek, and R. Balm. 25 Years of Laser Assisted Vascular Anastomosis (LAVA): What Have We Learned? *European Journal of Vascular and Endovascular Surgery*, 27(5):466–476, may 2004.

[19] Lawrence S. Bass and Michael R. Treat. Laser tissue welding: A comprehensive review of current and future. *Lasers in Surgery and Medicine*, 17(4):315–349, 1995.

[20] Ilan Gabay, Irina Barequet, David Varssano, Mordechai Rosner, and Abraham Katzir. Bonding surgical incisions using a temperature-controlled laser system based on a single infrared fiber. *Journal of Biomedical Optics*, 18(11):111416, sep 2013.

[21] A. Abergel, I. Gabay, D. M. Fliss, A. Katzir, and Z. Gil. A Multi-wavelength Fiber-Optic Temperature-Controlled Laser Soldering System for Upper Aerodigestive Tract Reconstruction: An Animal Model. *Otolaryngology - Head and Neck Surgery*, 144(6):872–876, jun 2011.

[22] Eiji Chikamatsu, Tsunehisa Sakurai, Naomichi Nishikimi, Takashi Yano, and Yuji Nimura. Comparison of laser vascular welding, interrupted sutures, and continuous sutures in growing vascular anastomoses. *Lasers in Surgery and Medicine*, 16(1):34–40, 1995.

[23] Jerry W. Vlasak, George E. Kopchok, Roy M. Fujitani, and Rodney A. White. Argon laser vascular fusion: Venous and arterial bursting pressures. *Lasers in Surgery and Medicine*, 9(5):478–481, 1989.

[24] Roy S. Chuck, Mehmet C. Oz, Thomas M. Delohery, Jeffrey P. Johnson, Lawrence S. Bass, Roman Nowygrod, and Michael R. Treat. Dye-enhanced laser tissue welding. *Lasers in Surgery and Medicine*, 9(5):471–477, 1989.

[25] Paolo Matteini, Fulvio Ratto, F Rossi, and Roberto Pini. Laser-activated nano-biomaterials for tissue repair and controlled drug release. *Quantum Electronics*, 44(7):675–682, jul 2014.

[26] Amadé Bregy, Serge Bogni, Vianney J.P. Bernau, Istvan Vajtai, Felix Vollbach, Alke Petri-Fink, Mihai Constantinescu, Heinrich Hofmann, Martin Frenz, and Michael Reinert. Solder doped polycaprolactone scaffold enables reproducible laser tissue soldering. *Lasers in Surgery and Medicine*, 40(10):716–725, dec 2008.

[27] Daniel S. Schöni, Serge Bogni, Amadé Bregy, Amina Wirth, Andreas Raabe, Istvan Vajtai, Uwe Pieles, Michael Reinert, and Martin Frenz. Nanoshell assisted laser soldering of vascular tissue. *Lasers in Surgery and Medicine*, 43(10):975–983, dec 2011.

[28] Giuseppe Esposito, Francesca Rossi, Paolo Matteini, Alba Scerrati, Alfredo Puca, Alessio Albanese, Giacomo Rossi, Fulvio Ratto, Giulio Maira, and Roberto Pini. In vivo laser assisted microvascular repair and end-to-end anastomosis by means of indocyanine green-infused chitosan patches: A pilot study. *Lasers in Surgery and Medicine*, 45(5):318–325, jul 2013.

[29] M.E. Khosroshahi, M.S. Nourbakhsh, S Saremi, A Hooshyar, Sh Rabbani, F Tabatabai, and M Sotudeh Anvari. Application of Albumin Protein and Indocyanine Green Chromophore for Tissue Soldering by Using an IR Diode Laser: Ex Vivo and In Vivo Studies. *Photomedicine and Laser Surgery*, 28(6):723–733, dec 2010.

[30] Dara R. Pabittei, Michal Heger, Sjoerd van Tuijl, Marc Simonet, Wadim de Boon, Allard C. van der Wal, Ron Balm, and Bas A. de Mol. Ex vivo proof-of-concept of end-to-end scaffold-enhanced laser-assisted vascular anastomosis of porcine arteries. *Journal of Vascular Surgery*, 62(1):200–209, jul 2015.

[31] Karen M McNally, Brian S Sorg, Ashley J Welch, Judith M Dawes, and Earl R Owen. Photothermal effects of laser tissue soldering. *Physics in Medicine and Biology*, 44(4):983–1002, apr 1999.

[32] R. R. Krueger and E. E. Almquist. Argon laser coagulation of blood for the anastomosis of small vessels. *Lasers in Surgery and Medicine*, 5(1):55–60, 1985.

[33] S K Forman, M C Oz, J F Lontz, M R Treat, T a Forman, and H a Kiernan. Laser-assisted fibrin clot soldering of human menisci. *Clinical orthopaedics and related research*, 310(310):37–41, jan 1995.

[34] Philip E Grubbs, Su Wang, Corrado Marini, Samir Basu, Daniel M Rose, and Joseph N Cunningham. Enhancement of CO2 laser microvascular anastomoses by fibrin glue. *Journal of Surgical Research*, 45(1):112–119, jul 1988.

[35] Dara R. Pabittei, Michal Heger, Johan F. Beek, Sjoerd Van Tuijl, Marc Simonet, Allard C. Van Der Wal, Bas A. De Mol, and Ron Balm. Optimization of suture-free laser-assisted vessel repair by solder-doped electrospun poly(ϵ-caprolactone) scaffold. *Annals of Biomedical Engineering*, 39(1):223–234, may 2011.

[36] Beat Ott, Mihai A. Constantinescu, Dominique Erni, Andrej Banic, Thomas Schaffner, and Martin Frenz. Intraluminal laser light source and external solder: In vivo evaluation of a new technique for microvascular anastomosis. *Lasers in Surgery and Medicine*, 35(4):312–316, oct 2004.

[37] Anton Formhals. Process and apparatus for preparing artificial threats, 1934.

[38] S. Ramakrishna, R. Jose, P. S. Archana, A. S. Nair, R. Balamurugan, J. Venugopal, and W. E. Teo. Science and engineering of electrospun nanofibers for advances in clean energy, water filtration, and regenerative medicine. *Journal of Materials Science*, 45(23):6283–6312, dec 2010.

[39] Payam Zahedi, Iraj Rezaeian, Seyed-Omid Ranaei-Siadat, Seyed-Hassan Jafari, and Pitt Supaphol. A review on wound dressings with an emphasis on electrospun nanofibrous polymeric bandages. *Polymers for Advanced Technologies*, 21(2):n/a–n/a, 2009.

[40] Pim-on Rujitanaroj, Nuttaporn Pimpha, and Pitt Supaphol. Wound-dressing materials with antibacterial activity from electrospun gelatin fiber mats containing silver nanoparticles. *Polymer*, 49(21):4723–4732, oct 2008.

[41] Martina Abrigo, Sally L. McArthur, and Peter Kingshott. Electrospun Nanofibers as Dressings for Chronic Wound Care: Advances, Challenges, and Future Prospects. *Macromolecular Bioscience*, 14(6):772–792, jun 2014.

[42] Nae Gyune Rim, Choongsoo S Shin, and Heungsoo Shin. Current approaches to electrospun nanofibers for tissue engineering. *Biomedical Materials*, 8(1):014102, feb 2013.

[43] J. Lannutti, D. Reneker, T. Ma, D. Tomasko, and D. Farson. Electrospinning for tissue engineering scaffolds. *Materials Science and Engineering: C*, 27(3):504–509, apr 2007.

[44] Ali Tamayol, Mohsen Akbari, Nasim Annabi, Arghya Paul, Ali Khademhosseini, and David Juncker. Fiber-based tissue engineering: Progress, challenges, and opportunities. *Biotechnology Advances*, 31(5):669–687, sep 2013.

[45] Gareth R Williams, Nicholas P Chatterton, Tahir Nazir, Deng-Guang Yu, Li-Min Zhu, and Christopher J Branford-White. Electrospun nanofibers in drug delivery: recent developments and perspectives. *Therapeutic Delivery*, 3(4):515–533, apr 2012.

[46] Seeram Ramakrishna, Maedeh Zamani, and Molamma P Prabhakaran. Advances in drug delivery via electrospun and electrosprayed nanomaterials. *International Journal of Nanomedicine*, 8(1):2997, aug 2013.

[47] Young Ju Son, Woo Jin Kim, and Hyuk Sang Yoo. Therapeutic applications of electrospun nanofibers for drug delivery systems. *Archives of Pharmacal Research*, 37(1):69–78, jan 2014.

[48] Travis J. Sill and Horst A. von Recum. Electrospinning: Applications in drug delivery and tissue engineering. *Biomaterials*, 29(13):1989–2006, may 2008.

[49] A. L. Yarin, S. Koombhongse, and D. H. Reneker. Taylor cone and jetting from liquid droplets in electrospinning of nanofibers. *Journal of Applied Physics*, 90(9):4836, nov 2001.

[50] Y.M. Shin, M.M. Hohman, M.P. Brenner, and G.C. Rutledge. Experimental characterization of electrospinning: the electrically forced jet and instabilities. *Polymer*, 42(25):09955–09967, dec 2001.

[51] Darrell H. Reneker, Alexander L. Yarin, Hao Fong, and Sureeporn Koombhongse. Bending instability of electrically charged liquid jets of polymer solutions in electrospinning. *Journal of Applied Physics*, 87(9):4531, 2000.

[52] Moses M Hohman, Michael Shin, Gregory Rutledge, and Michael P Brenner. Electrospinning and electrically forced jets. I. Stability theory. *Physics of Fluids*, 13(8):2201, 2001.

[53] Stephen R. Baker, Soham Banerjee, Keith Bonin, and Martin Guthold. Determining the mechanical properties of electrospun poly-ϵ-caprolactone (PCL) nanofibers using AFM and a novel fiber anchoring technique. *Materials Science and Engineering: C*, 59:203–212, feb 2016.

[54] A. Doustgani, E. Vasheghani-Farahani, M. Soleimani, and S. Hashemi-Najafabadi. Optimizing the mechanical properties of electrospun polycaprolactone and nanohydroxyapatite composite nanofibers. *Composites Part B: Engineering*, 43(4):1830–1836, jun 2012.

[55] Joachim H. Wendorff, Seema Agarwal, and Andreas. Greiner. *Electrospinning*. Wiley-VCH Verlag GmbH & Co. KGaA, Weinheim, Germany, 1. edition, apr 2012.

[56] Fatemeh Roozbahani, Naznin Sultana, Davood Almasi, and Farnaz Naghizadeh. Effects of Chitosan Concentration on the Protein Release Behaviour of Electrospun Poly(ϵ-caprolactone)/Chitosan Nanofibers. *Journal of Nanomaterials*, 2015:1–11, apr 2015.

[57] Ericka N J Ford, Nisaraporn Suthiwangcharoen, Paola A. D'Angelo, and Ramanathan Nagarajan. Role of Single-Walled Carbon Nanotubes on Ester Hydrolysis and Topography of Electrospun Bovine Serum Albumin/Poly(vinyl alcohol) Membranes. *ACS Applied Materials & Interfaces*, 6(14):11741–11748, jul 2014.

[58] Sebastian Puhl, Linhao Li, Lorenz Meinel, and Oliver Germershaus. Controlled Protein Delivery from Electrospun Non-Wovens: Novel Combination of Protein Crystals and a Biodegradable Release Matrix. *Molecular Pharmaceutics*, 11(7):2372–2380, jul 2014.

[59] Christina Tang, A. Evren Ozcam, Brendon Stout, and Saad A. Khan. Effect of pH on Protein Distribution in Electrospun PVA/BSA Composite Nanofibers. *Biomacromolecules*, 13(5):1269–1278, may 2012.

[60] Chandra M. Valmikinathan, Steven Defroda, and Xiaojun Yu. Polycaprolactone and Bovine Serum Albumin Based Nanofibers for Controlled Release of Nerve Growth Factor. *Biomacromolecules*, 10(5):1084–1089, may 2009.

[61] Tomasz Kowalczyk, Aleksandra Nowicka, Danek Elbaum, and Tomasz A. Kowalewski. Electrospinning of Bovine Serum Albumin. Optimization and the Use for Production of Biosensors. *Biomacromolecules*, 9(7):2087–2090, jul 2008.

[62] Wei Ji, Yan Sun, Fang Yang, Jeroen J J P Van Den Beucken, Mingwen Fan, Zhi Chen, and John A. Jansen. Bioactive electrospun scaffolds delivering growth factors and genes for tissue engineering applications. *Pharmaceutical Research*, 28(6):1259–1272, may 2011.

[63] Sambit Sahoo, Lay Teng Ang, James Cho-Hong Goh, and Siew-Lok Toh. Growth factor delivery through electrospun nanofibers in scaffolds for tissue engineering applications. *Journal of Biomedical Materials Research Part A*, 93(4):1539–1550, 2009.

[64] Anne J. Meinel, Oliver Germershaus, Tessa Luhmann, Hans P. Merkle, and Lorenz Meinel. Electrospun matrices for localized drug delivery: Current technologies and selected biomedical applications. *European Journal of Pharmaceutics and Biopharmaceutics*, 81(1):1–13, may 2012.

[65] Luigi Romano, Andrea Camposeo, Rita Manco, Maria Moffa, and Dario Pisignano. Core-Shell Electrospun Fibers Encapsulating Chromophores or Luminescent Proteins for Microscopically Controlled Molecular Release. *Molecular Pharmaceutics*, 13(3):729–736, mar 2016.

[66] Nikodem Tomczak, Shuying Gu, Mingyong Han, Niek F. van Hulst, and G. Julius Vancso. Single light emitters in electrospun polymer nanofibers: Effect of local confinement on radiative decay. *European Polymer Journal*, 42(10):2205–2210, oct 2006.

[67] Nikodem Tomczak, Niek F. van Hulst, and G Julius Vancso. Beaded Electrospun Fibers for Photonic Applications. *Macromolecules*, 38(18):7863–7866, sep 2005.

[68] Stefano Pagliara, Andrea Camposeo, Alessandro Polini, Roberto Cingolani, and Dario Pisignano. Electrospun light-emitting nanofibers as excitation source in microfluidic devices. *Lab on a Chip*, 9(19):2851, 2009.

II. Binding of indocyanine green in polycaprolactone fibers using blend electrospinning for laser-assisted vascular anastomosis

Abstract

Background and Objective: The clinical application of laser-assisted vascular anastomosis is impeded by unreliable and low bonding strengths and tedious handling during microvascular surgery. The challenge to be met arises from the flow-off of the chromophore during soldering that changes the absorption coefficient and stains peripheral tissue, leading to an uncontrollable thermal damage zone. In this study, we investigated the feasibility to produce an indocyanine green (ICG)-loaded patch by electrospinning and tested its applicability to laser soldering.

Materials and Methods: A blend of polycaprolactone and ICG was electrospun to produce a pliable patch. Prior to soldering, the patch was soaked in 40 % (w/w) bovine serum albumin solution. The solder patch was wrapped *in vitro* around blood vessel stumps of rabbit aortas. An intraluminal balloon catheter enabled an easy alignment and held the setup in place. The soldering energy was delivered via a diffusor fiber from the vessel lumen using a diode laser at 810 nm. During the procedure the surface temperature was monitored with an infrared camera. Afterwards, samples were embedded in methylmethacrylate and in epon to study thermal damage. The quality of the fusion was assessed by measuring the tensile strength. After *in vitro* tests with rabbit aortas, 8 large white pigs were subjected to an acute *in vivo* experiment, and the artery of the latissimus dorsi flap was anastomosed to the distal femoral artery.

Results: The indocyanine green-loaded patch, produced by electrospinning, has a thickness of $279\pm62\,\mu m$, a fiber diameter of $1.20\pm0.19\,\mu m$, and an attenuation coefficient of $1119\pm183\,cm^{-1}$ at a wavelength of 790 nm. The patch was pliable and easy to handle during surgery. No leakage of the chromophore was observed. Thermal damage was restricted to the Tunica adventitia and Tunica media and the area of the vessel wall that was covered with the patch. Six pigs were successfully treated, without any bleeding and with a continuous blood flow. The *in vivo* flap model yielded a similar tensile strength compared to *in vitro* laser-assisted vascular anastomoses ($138\pm52\,mN/mm^2$ versus $117\pm30\,mN/mm^2$).

Conclusion: Our study demonstrated the applicability of the ICG-loaded patch for laser-assisted vascular anastomosis. By using electrospinning, ICG could be bound to polymer fibers, avoiding its flow-off and the staining of the peripheral tissue. This patch demonstrated several advantages over liquid solder as it was easier to apply, ensured a high and reliable bonding strength while maintaining a constant concentration of ICG concentration during the surgery.

II.1 Introduction

End-to-end anastomosis is a crucial procedure in microvascular surgery. Conventional anastomosis by suture ligation is a time consuming and skill intensive process. Laser tissue soldering is a promising alternative, where proteins of tissue and solder are denatured by thermal effect and thus coagulate into seals that are strong enough to withstand the blood pressure [2–6]. Laser-assisted vascular anastomosis (LAVA) holds the perspective to reduce suture and needle trauma and might decrease foreign body reactions and bleeding [7]. To become widely accepted LAVA must prove to be reliable, safe, and applicable to a variety of vessel diameters. The usage of a laser-based technique provides a remarkable advantage especially in the field of minimally invasive surgery with applications such as free flap transfer and replantation [8], attachment of arterial and venous grafts [9], and extracranial-intracranial bypass surgery [10].

LAVA has already been reported in 1964 by Yahr et. al. [11]. However, a clinical usage has not yet been introduced. An important aspect is the lack of control on the temperature reached during soldering. Previous studies have shown that the strength of the tissue connection strongly correlates with the temperature profile [2, 12–14]. Dye-enhanced LAVA is based on thermal heating involving localized absorption of laser light using chromophores. A promising chromophore for LAVA is indocyanine green (ICG), that is commonly employed as a liquid solution [3, 6, 15]. Dilution and flow-off of ICG lead to an uncontrollable heating behavior. An additional challenge that is provoked by the flow-off of ICG is staining of circumferential tissue, causing its unintended heating. Few approaches have been tested to face the problem of unfixed absorber: ICG-infused chitosan patches [6], biodegradable polymer films [16], ICG-loaded nanoshells that are integrated in the soldering scaffold made of solvent cast polycaprolactone (PCL) [12, 15, 17], and the usage of absorbing gold nano-chromophores [18]. However, most of these techniques still result in a flow-off of the solder or require the use of fixation sutures. Furthermore, ICG has a poor optical stability in water. Therefore, suitable storage conditions in either dry state or non-aqueous solvents such as methanol, dimethylformamide, or propanediol are required [19].

It was shown that electrospun PCL added on top of a liquid solder [20] or soaked in a semi-liquid solder [5], composed of bovine serum albumin (BSA), methyl cellulose, and methylene blue enhances the soldering strength. The application of electrospun non-wovens is an emerging strategy for addressing several medical problems [21, 22] related to drug delivery [23–26], tissue engineering [27–29] and wound dressing [30–32]. The advantages are easy processing, cost effectiveness and various properties of these meshes. Electrospun fibers that have been prepared from PCL are mechanically resistant, elastic and have a large surface area with defined pores [33–35]. Electrospinning provides the possibility to entrap composites into fibers [36, 37], and can be scaled up to an industrial process [38–40].

In this study we examined the feasibility of electrospinning a blend of PCL and ICG and thus combining the chromophore directly with the polymer fibers. The fiber morphology and size distribution was investigated to inspect the formation of fibers and to control the stability and reproducibility of the electrospinning process. Thereafter, the applicability of the electrospun ICG-loaded patches was tested *in vitro* using rabbit aortas. Accordingly, an intraluminal laser light source in combination with the externally applied patch enabled a homogeneous irradiation of the whole circumference of a defined area of the vessel [3]. A balloon catheter carrying the laser fiber was inserted into the vessel lumen and placed at the side were the soldering had to be performed. The ICG-loaded patch was then soaked in liquid BSA solution and applied onto the vessel stumps. Finally, the vessels were irradiated using an 810 nm diode laser that was coupled into a diffusor fiber producing a homogeneous 360° irradiation. The temperature profile was measured with an infrared camera to control the procedure and thermal damage was

assessed by using light microscopy. The quality of the soldered vessels was determined based on tensile strength measurements and compared to conventionally sutured vessels. After testing this technique *in vitro*, we demonstrated the clinical feasibility of this technique in an acute pig trial with the objective to investigate the handling of the soldering setup and the patch.

II.2   Materials and Methods

II.2.1   Materials

Polycaprolactone (PCL, average M_n = 80000) and lyophilized bovine serum albumin (BSA, lyophilized) were obtained from Sigma Aldrich (Saint Louis, MO). Methanol and chloroform were used in analytical grade from Merck KGaA (Darmstadt, Germany). Indocyanine green (ICG, IR-125) was obtained from Acros Organics (Geel, Belgium). All materials were used as received.

II.2.2   Electrospinning of the soldering patch

Solution preparation

First, PCL was dissolved in chloroform and ICG in methanol. Both solutions were stirred separately overnight to yield a homogenous solution. Then, they were combined to obtain a blend of 9 % (w/w) PCL solution in chloroform/methanol (75/25 (v/v)) with an ICG:PCL ratio of 1:10 (w/w). After addition of ICG, the solution was spun and processed in the dark as the ICG tends to degrade with exposure to light [41].

Electrospinning setup and parameters

For electrospinning of the PCL/ICG blend, a custom-made setup with a single needle was used (shown in figure II.1). The PCL/ICG solution was loaded into a 5 mL syringe with a truncated needle (0.812 mm I.D., BD Microlance 3, Becton Dickinson S.A., Fraga, Spain) that was connected with electrodes to a power supply (gamma series, brandenburg, Applied Kilovolts Ltd., UK). The electrospinning process parameters were varied in order to achieve stable electrospinning. A flow rate of 30 µL/min, a gap distance of 15 cm between the needle tip and the grounded collector plate, and an applied positive potential of 15 kV lead to a stable Taylor cone. The deposited scaffold was visually homogeneous and without spots. The fibers were collected on a rotating aluminum plate at 1 rpm with a diameter of 10 cm to ensure a homogeneous distribution of the fibers. The setup was placed in a chamber, in which temperature and humidity were well controlled to be 22±1 °C and 30±5 % RH. The resulting patch was stored in the dark in a desiccator until further processing to ensure complete removal of the solvent [42].
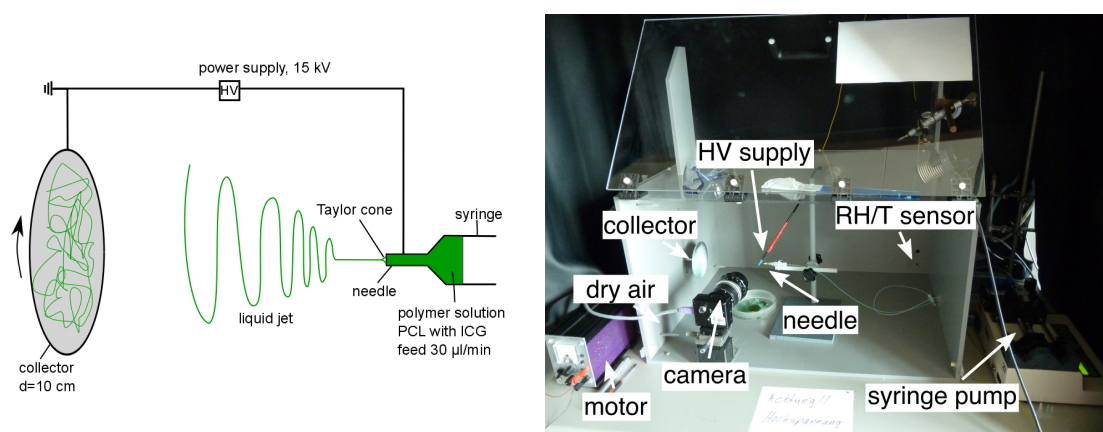
Figure II.1: Electrospinning setup. **Left:** High voltage was applied to a polymer solution to induce the formation of a liquid jet. The jet underwent stretching and whipping processes resulting in a long and thin fiber. During the flight, the solvent evaporated and the diameter was significantly reduced from hundreds of micrometers to a few micrometers. Eventually the jet was deposited on a grounded collector as a random, non-woven mat of fibers. **Right:** Setup used in our lab. The setup was placed in a chamber, curtains were used to keep the setup in the dark. Dry air was supplied via two nozzles and the RH/T sensor measured the humidity and the temperature in the chamber. The motor was rotating the collector.
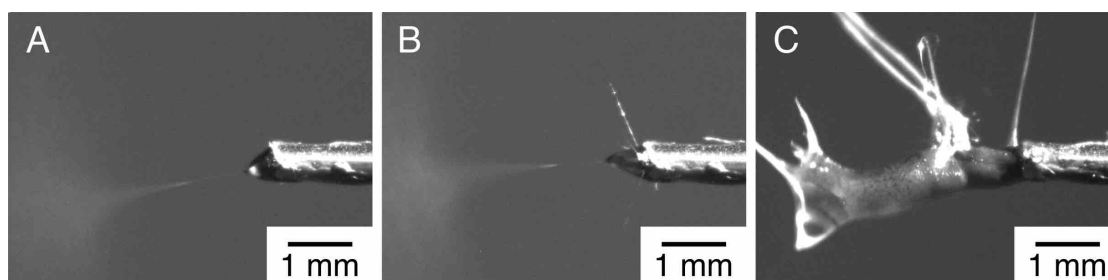
Figure II.2: Droplet shape at the needle tip. **A:** Immediately after the onset of electrospinning. **B:** Branching of the droplet after 5 min of electrospinning using a solution of 1:10 ICG:PCL. **C:** Branching of the droplet continues and long glob is forming. Picture was taking after 15 min of electrospinning. Pictures were obtained with a Dragonfly Express Camera (Point Grey Research Inc., Vancouver, BC, Canada) and a Minolta lens (f=58 mm, 1:1.2).

One difficulty was the reproducibility of the electrospinning process. Using a high concentration of ICG of 10 % (w/w) in the patch, a long glob is forming from the needle tip, and hardens. This drop was removed manually every 15 min. When using ICG concentrations lower than 5 % (w/w), this effect was not observed. A photograph of the droplet shapes at the needle tip is shown in figure II.2. The polymer glob is a regularly occurring phenomenon during electrospinning [57, 58]. Furthermore, it was important to keep the relative humidity in the electrospinning chamber at 30±5 %, as otherwise the solution was dripping regularly. This effect was not observed at low ICG concentrations. Laboratory electrospinning setups differ significantly from industrial-scale systems [38], where the climate-control and the long drop will not be of concern.

Analysis of the patch

To examine the fiber morphology and diameter, samples were sputter coated with a 10 nm layer of gold and analyzed using a scanning electron microscope (SEM, Zeiss DSM982, Carl Zeiss AG, Oberkochen, Germany) with an electron beam of 5.0 kV. For the determination of the thickness of the patches, a patch was inserted between two microscope slides, followed by measuring the displacement with a height gauge (Trimos V600+, Trimos SA, Renens, Switzerland).

For the determination of the attenuation coefficient of the ICG-loaded patch, thin layers with varying electrospinning duration of 1 to 10 min (step-size of 1 min; 3 samples per duration) were electrospun on a microscopy slide and the thickness of the layers was measured. The absorbance was measured at a wavelength of 790 nm, the wavelength of maximum absorption, involving a standard spectrometer (Lambda 750, Perkin Elmer, Waltham, MA, US). The absorbance times the natural logarithm ln(10), divided by the thickness of the layers, equals the attenuation coefficient that was calculated to be $1119\pm183\,\mathrm{cm}^{-1}$. Since these experiments do not provide a differentiation between the scattering nor the absorption coefficient, the patches were irradiated with a Gaussian beam at a wavelength of 785 nm and an image of the transmitted beam was taken with a CMOS detector [43]. As there was hardly any background caused by scattering, it can be assumed that scattering events are negligible, and therefore the attenuation coefficient equals the absorption coefficient.

To estimate the aqueous- and photo-stability of ICG in the patch, the patches were cut to a width of 10±1 mm and a length of 20±1 mm, weighted and immersed in 1 ml of physiological solution (Dulbecco's phosphate-buffered saline (DPBS), Gibco, Thermo Fisher Scientific, Waltham, MA, US), see figure II.3. During immersion, the samples were stored at room temperature, applying gentle agitation, with and without exposure to daylight. The samples were stored for t=0, 1, 8, and 24 h. At timepoint t=0 h, the patch was only dipped in DPBS for 10 s. We additionally added an untreated group, where the patch was not immersed in DPBS and directly processed further. After immersion, the patches were removed from the extract. The removed patches were dissolved in 1 ml chloroform/methanol (75/25 v/v) and further diluted 1000-fold using the same solvent. Thereafter, we measured the absorbance of the extracts and the dissolved patches using a spectrometer at 790 nm (Lambda 750, Perkin Elmer, Waltham, MA, US). For each time-point the samples were prepared 10-fold. The results of the optical measurements were compared to a reference series with known ICG concentrations.

II.2.3   Soldering

Treatment of the patch

Prior to soldering, pieces with a length of 1 cm and a width of 2 cm were cut from the electrospun mesh and immersed in BSA solution. The liquid protein solution was prepared by dissolving 40 % (w/w) BSA in MilliQ water at 37 °C under gentle stirring. The electrospun ICG-loaded patch was soaked in this solution for 10 s and excess was removed by reversing the patch twice on a Teflon plate. Highly concentrated and liquid 40 % (w/w) BSA solution is sticky. Hence, the patches were air-dried in the dark for 15 min, resulting in a slightly humid patch. Due to drying, the patches were less sticky but still pliable. The patches were then vacuum sealed in small plastic bags, stored at 4 °C without light exposure and used within three days.

***In vitro* anastomoses: setup and parameters**

The applicability of the patches to LAVA was first tested in an *in vitro* model, using an end-to-end anastomosis with medium-sized rabbit aortas and an intraluminal soldering setup, that was
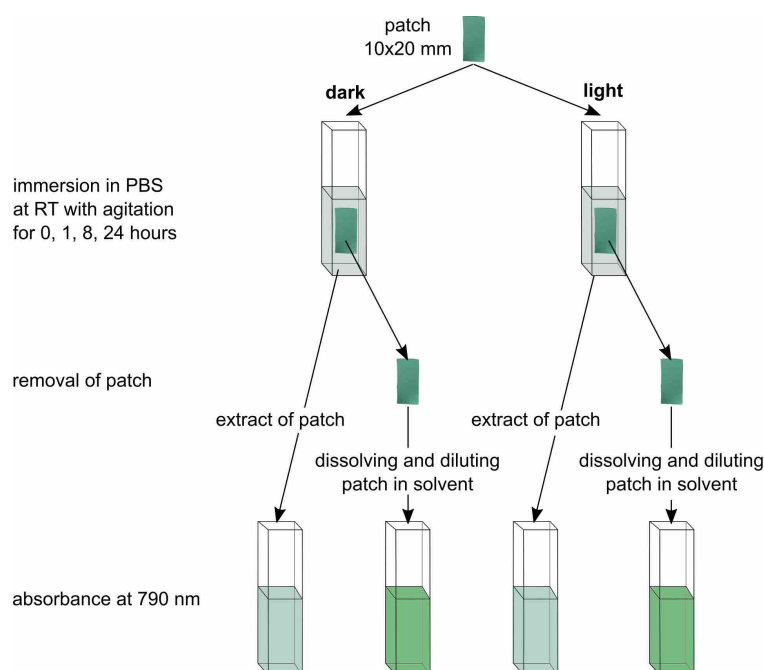
Figure II.3: Scheme of testing the aqueous and photo-stability of ICG in the patch. Patches were cut, immersed in DPBS, and removed from the immersion liquid. The patch was dissolved and diluted in chloroform/methanol (75/25 v/v). The absorbance of the extract of the patch and the dissolved patch was measured.

previously pre-clinically tested [3].

Rabbit aortas were harvested at a local slaughterhouse. Then, the aortas were frozen directly and stored at -80 °C. Prior to use, they were slowly warmed up to room temperature. The perivascular adipose tissue was carefully removed and the aortas were shortened to a length of 3 cm. Subsequently, the aortas were cut transversely and aligned to each other over a balloon catheter (Armada 35 PTA catheter, 3.0 mm balloon diameter, Abbott Laboratories, Illinois, US). The catheter was inflated with a saline solution prior to inserting the laser fiber (Laser und Medizintechnologie Berlin, Berlin, Germany), which was placed exactly at the site where the anastomosis had to be performed. A HeNe-target laser, additionally coupled into the same fiber, helped to align the fiber with respect to the vessel stumps. The laser fiber had a 400 μm quartz core with a diffusor at its distal end, homogeneously illuminating the vessel over a length of 15 mm (figure II.9A). A diode laser (Lina 30d, Intros, Heilbad Heiligenstadt, Germany) emitting radiation in the near infrared at 810 nm was coupled into the fiber. Following, the patch with a size of 2x1 cm was applied around the vessel. To ensure that the whole circumference of the vessel was fully covered, and taking the shrinkage of the patch into account, we left a seam overlap of approximately 2 mm. If the patch extending the vessel too far, the patch was cut accordingly. The patch was then irradiated with the laser operating at an average output power of 4 W in the continuous wave (cw) regime. The vessels used had a diameter of 3.9 ± 0.3 mm (n=30) and the irradiated surface was estimated to be equal to 1.8 cm^2, resulting in an irradiance of 2.2 W/cm^2.

The temperature at the surface of the patches was recorded and controlled during the laser irradiation with a thermal camera (A655, FLIR Systems, Inc., Wilsonville, Oregon, US). The camera was calibrated for a temperature range from -40 to 150 °C allowing an accuracy of ± 2 °C.

To reduce desiccation of the vessel wall and to stay in a clinically acceptable time we irradiated for 30 s after reaching 75 °C at the surface of the patch. The temperature was stabilized between 75 and 85 °C by manually switching the laser on and off. After soldering, the temperature data were analyzed and processed using Matlab (version R2012b, MathWorks, Inc., Natick, Massachusetts, US). The average temperature of a 6 mm² surface was calculated for each camera frame and plotted versus the irradiation time. The surface was determined by a 2 times 3 mm rectangle centered over the hottest spot of the solder surface.

***In vivo* anastomoses: setup and parameters**

The experiments were performed in the experimental surgery unit of the Insel-Hospital Bern on 3 month old pigs weighing approximately 40 kg each. The protocol used for the animal experiments were in accordance with the guidelines of the *National Institutes of Health for the care and use of experimental animals*. The same team of surgeons performed all experiments. General anesthesia was induced with 20 mg/kg body weight ketamine (Vetoquiol AG, Ittigen, Switzerland) and 2 mg/kg xylazine (Vetoquiol AG, Ittigen, Switzerland) given intramuscular. Ten minutes later, 0.5 mg/kg midazolam and 0.05 mg/kg atropine were administered by an intravenous catheter placed in the ear vein. Anesthesia was maintained with 1–1.5 % (v/v) isoflurane and 25 % oxygen in air.

A total of eight animals underwent laser assisted anastomoses in an acute trial. The M. latissimus dorsi was harvested and the A. thoracodorsalis was isolated. After that the distal A. femoralis and the A. saphenous were isolated and clipped with microsurgical vascular clips. The A. femoralis was clamped proximal with a HD-D microsurgical clamp. The A. saphena was then sectioned at about 5 cm from its bifurcation from the A. femoralis and the distal A. femoralis was sectioned at about 2 cm from the bifurcation. Next, via the collateral branch, the balloon catheter was inserted into the A. saphena and advanced to the transected extremity of the distal A. femoralis. The stump of the flap's artery was carefully adjusted over the balloon catheter and kept in contact with the distal A. femoralis with another HD-D clamp. To keep the soldering site away from surrounding tissue, a surgical gauze was placed underneath when necessary. The balloon was inflated with saline solution and the laser fiber was inserted into the working channel of the balloon catheter until it laid exactly at the site were the anastomosis had to be performed. The ICG-loaded patch was wrapped around the coapted vessels (figure II.4). The vessel diameter was 3.3±0.6 mm (n=8), and therefore slightly smaller than the rabbit aortas that we used *in vitro*. To ensure a similar irradiance as for *in vitro* experiments, the laser output power was thus reduced to 3 W instead of 4 W. After soldering, the clamps, the balloon, and the fiber were gently removed and the patency was determined by visual observation of the blood flow at the venous end of the flap and by observation of the pulsatile signal distal to LAVA. At the end of the observation period of 1 min, the A. femoralis was clipped distal to LAVA. The vascular segment was then excised and prepared for tensile strength measurement. The pigs were alive during the whole operation and observation period and then euthanized by intravenous application of 2 mmol/kg potassium chloride.

II.2.4 Conventional suture anastomosis

The bonding strength of the LAVAs was compared to *in vitro* conventional suture anastomosis. Therefore, five rabbit aortas were prepared by removing the adventitia over a length of 2 cm. An Acland micro vascular clamp (Synovis micro companies alliance Inc., Birmingham, US) was used to oppose the vessels to allow for a tension-free anastomosis. The vessels were then flushed with saline water. 8 interrupted sutures were applied using 9-0 Nylon (Ethicon, Somerville,
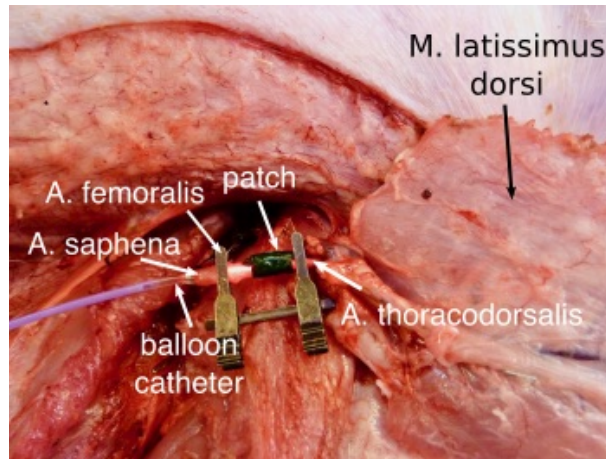
Figure II.4: Intraoperative image of the vessel during soldering. The balloon catheter with the laser fiber is inserted via the A. saphena. The patch is wrapped around the vessel, connecting the A. femoralis and the A. thoracodorsalis. The microsurgical clamp holds the setup in place, adapting the two artery stumps for laser soldering.

New Jersey, US) to perform the anastomosis under the magnification of an operating microscope (Zeiss Surgical microscope, Carl Zeiss AG, Oberkochen, Germany).

II.2.5   Measurement of tensile strength

The tensile strength of *in vitro* and *in vivo* soldered and sutured vessels was evaluated using a test stand with a fixed force gauge (BFG50, Mecmesin Limited, West Sussex, UK) (figure II.5). Vessels were fixed 2 mm from the end of the patch with two surgical clamps attached to a moving table. The table was pulled with an electrically driven motor at a constant velocity of 30 mm/min. The tensile strength was calculated by dividing the maximum load at the rupture time point by the cross-sectional area of the blood vessel. Therefore, the external diameter of the vessel was measured with a caliper before soldering, and the surface area of the cross-section, including the vessel wall and the lumen, was calculated. For comparison with our previous studies, we reported both, the tensile strength as well as the maximum load. The measurement was done within 1 min after soldering to avoid any desiccation of the sample. The *in vivo* vessels had, however, to be transported and were thus stored on gauze imbued in PBS until the tensile strength measurement. The time from excising the vessel until measurement was within 1.5 hours.

II.2.6   Histological assessment

Laser-induced thermal damage was assessed using light microscopy. For histological assessment we used freshly obtained rabbit aortas, in contrast to the tensile strength measurements, where we used frozen rabbit aorta. Immediately after *in vitro* soldering, the tissue samples were fixed in 4 % formaldehyde (G256, Dr. Grogg Chemie AG, Stettlen, Switzerland). The biopsies were processed for the production of undecalcified ground sections. The specimens were rinsed under running tap water, dehydrated in ascending ethanol concentrations, and embedded in methylmethacrylate (MMA). The embedded tissue blocks were cut into approximately 600 µm-thick sections using a slow-speed diamond saw with copious water cooling (Varicut VC-50, Leco, Munich, Germany).
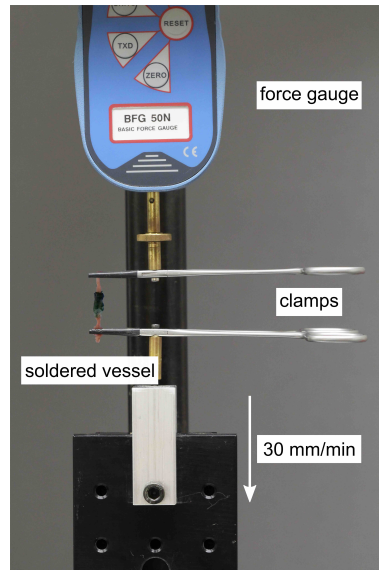
Figure II.5: Tensile strength measurement setup.

After mounting the sections onto acrylic glass slabs, they were ground and polished to a final thickness of about $200\,\mu m$ (Knuth-Rotor-3; Struers, Rødovre/Copenhagen, Denmark) and surface stained with toluidine blue and basic fuchsin [44]. Light microscopic recording was performed using a motorized Zeiss Axio Imager M2 microscope (Carl Zeiss AG, Oberkochen, Germany) with scan table and a high-resolution AxioCam digital camera (Carl Zeiss AG, Oberkochen, Germany).

For detailed study of the structures we used embedding in epon resin, where the tissue samples were fixed for $24\,h$ at $4\,°C$ by immersion in $1\,\%$ glutaraldehyde, $1\,\%$ formaldehyde buffered with $0.08\,M$ sodium cacodylate (pH 7.4). Then the samples were extensively washed in $0.1\,M$ sodium cacodylate buffer containing $5\,\%$ sucrose, pH 7.3, and postfixed with potassium-ferrocyanide-reduced osmium tetroxide. Osmicated samples were processed for embedding in Taab 812 epoxy resin (Merck, Dietikon, Switzerland). Sections measuring $1\,\mu m$ in thickness were cut with glass and diamond knives on a Reichert Ultracut E microtome (Leica Microsystems, Glattbrugg, Switzerland), stained with toluidine blue and basic fuchsin, and observed in a Zeiss Axio Imager M2 microscope (Carl Zeiss AG, Oberkochen, Germany) with scan table and a high-resolution AxioCam digital camera (Carl Zeiss AG, Oberkochen, Germany).

II.2.7   Statistical data evaluation

Values are reported as mean ± standard deviation. The non-parametric Wilcoxon rank test was used to compare the experimental groups and was performed with R 3.3.1 (R Foundation for Statistical Computing, Vienna, Austria). A p-value < 0.05 was considered significant in this study.

II.3   Results

In this study, we characterized electrospun ICG-loaded patches and tested the applicability of these patches to LAVA *in vitro* and under pre-clinical conditions.

As can be seen in figure II.6A, the electrospun ICG-loaded patch with a concentration of 10 % (w/w) ICG consisted of randomly oriented fibers with an average diameter of 1.20±0.19 µm (6 patches with 90 fiber measurements each, maximum diameter 2138 nm, minimum 143 nm). We observed a similar fiber distribution when using lower ICG concentrations or no ICG (data not shown). Concentrations above 5 % (w/w) ICG lead to dripping of the solution from the needle tip and to more droplets landing on the collector.

The thickness of the patch was adjusted by the duration of electrospinning. The spherical collector with a diameter of 10 cm was fully covered with fibers after electrospinning for at least 60 min. After electrospinning for 60, 75, 90 and 120 min the patch thickness was 212±12, 279±62, 351±52 and 473±61 µm, respectively (n=5 patches, for 75 min: n=10), being an almost linear dependence on the duration. Whereas the patches with an electrospinning duration of 60 min were thin and thus difficult to handle, the patches spun for 90 min and longer were too thick and therefore difficult to wrap around blood vessels. Thus, the further investigations were continued with the patch spun for 75 min. The applied amount of BSA is a governing factor for LAVA [2, 45], therefore the native and the soaked patches were weighed to determine the effective BSA amount to be 38.1±7.9 mg.
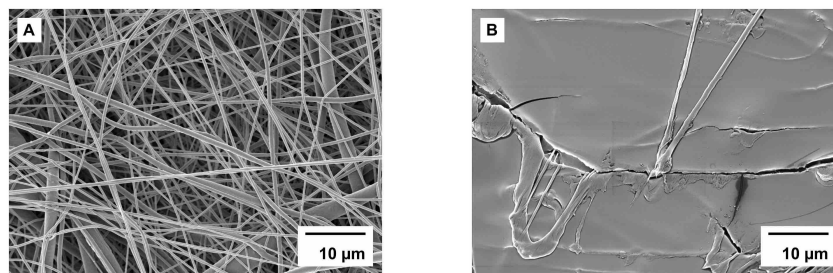
Figure II.6: Scanning electron micrographs. **A:** The fiber morphology of the ICG-loaded patch after electrospinning and before soaking in BSA solution. **B:** Surface of the patch after *in vitro* LAVA using rabbit aorta. The fibers melt to a smooth surface.

II.3.1   Aqueous and photo-stability of ICG in the patch

The ICG-loaded patch was intended to reduce the flow-off of ICG during laser-tissue soldering, ensuring stable optical properties and to avoid staining of the surrounding tissue. To evaluate the leaking behavior of the patch we analyzed the release of ICG in physiological solution for 24 hours. We measured the amount of ICG remaining in the patch after immersion and the amount of ICG in the extract (figure II.7). The calculated amount of ICG of a 10 mg-patch after electrospinning was 910 µg. The amount of ICG in the patches decreased to 798±117 µg after immersion, without significant changes over the immersion duration or exposure to daylight. To further investigate the leakage and photo-degradation of ICG, the absorbance of the extracts was measured. The ICG content ranged from 5±4 µg for samples immersed for 10 s to 57±14 µg for the samples stored in the dark for 8 and 24 hours. Interestingly, the extracts that were stored at daylight did not show changes of absorption over time, with the amount of absorbing ICG being

25±6 µg. We noticed no changes in the visual appearance and the soldering behavior of patches that were stored for several months in the dark, compared to freshly prepared ones.
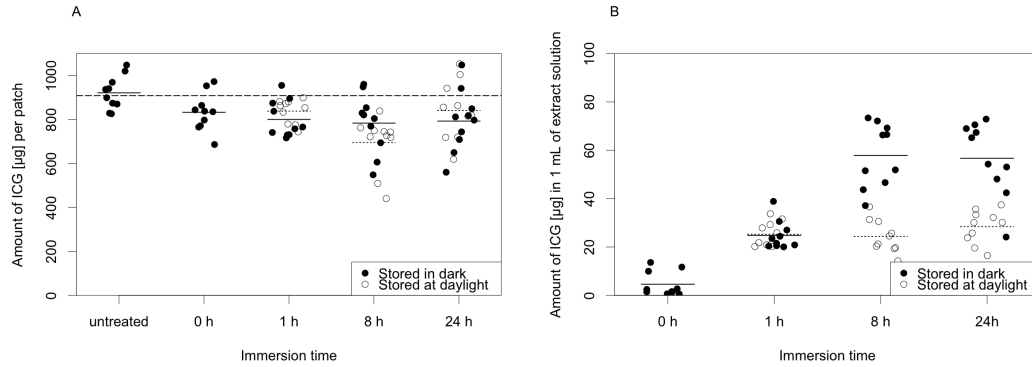
Figure II.7: Testing of ICG-leakage from the ICG-loaded patches. The solid short lines represent the means of the samples stored in the dark, while the dashed short lines show the means of the samples kept at daylight. **A:** Amount of absorbing ICG per 10 mg patch after immersion in PBS. The long-dashed line shows the theoretical amount of ICG per patch, being 910 µg, which is calculated from the ratio of PCL and ICG in the electrospinning blend. **B:** Amount of absorbing ICG found in the extract, normalized per 10 mg patch. These results show that ICG bleached after storage at daylight in aqueous solution.

II.3.2 *In vitro* anastomosis

The average surface temperature curve for 30 independent experiments is shown in figure II.8B. This curve shows that the temperature at the surface of the patch was always between minimum 70 °C and maximum 85 °C. Due to the fast heat diffusion across the patch and taking into account the efficient cooling of the water filled balloon catheter we can assume that the vessel wall did not reach a temperature far above 75 °C. Such a temperature was reported to ensure good tissue fusion [12]. During soldering, the color of the patch did not change and no staining at the edges of the outer border of the patch was observed (compare figure II.9B and II.9C). This observation is confirmed using the thermal camera, where there is a strong temperature gradient at the vessel edges, indicating that there is only few ICG leaking towards the edges, see figure II.8A. Nevertheless, this figure demonstrates lateral heat diffusion after 15 s of laser irradiation that results in some heating of surrounding tissue. The ICG-loaded patch started to melt at temperatures >60 °C, leading to a smooth surface of the patch (see figure II.6B). The patch was shrinking during irradiation. Therefore, it was important that the patch covered the incision lengthwise by 10 mm prior to irradiation, which ensured that the lateral shrinkage during soldering did not cause leakage, even if the patch was not perfectly centered.
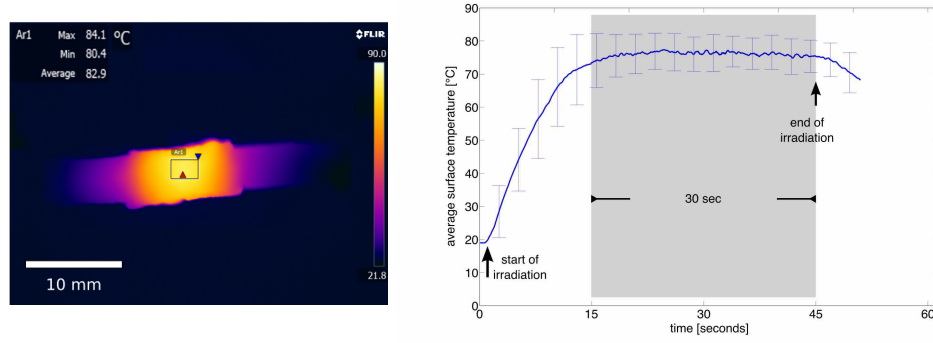
Figure II.8: **A:** Typical temperature distribution after 15 s of laser irradiation. The ICG-loaded patch is irradiated by using an intraluminal laser light source and hence heated homogeneously. A rectangle with an area of 6 mm^2 is centered over the hottest spot of the solder surface to determine the average surface temperature. **B:** Solder-surface temperature of *in vitro* experiments. The graph shows the mean temperature of 30 experiments during laser irradiation. After first measuring 75 °C at the patch surface, we irradiated for further 30 s at a temperature range of 75 to 85 °C. The error bars show the standard deviation.
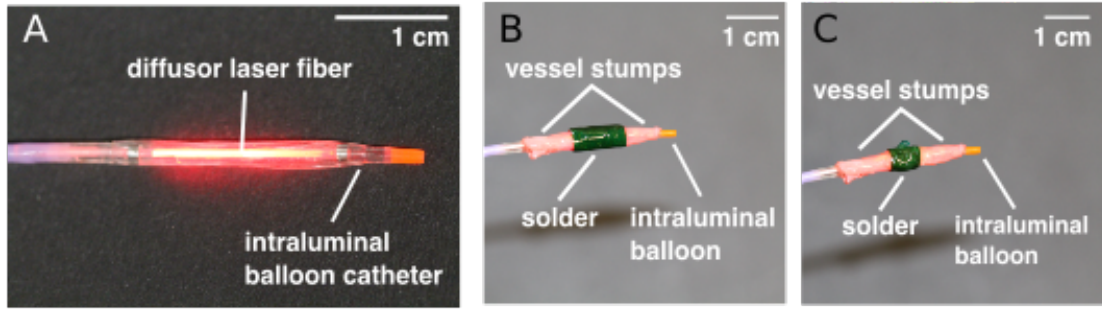
Figure II.9: **A:** Intraluminal balloon catheter with inserted diffusor fiber. A HeNe target laser was coupled into the laser fiber. **B:** *In vitro* experiment showing the aligned vessel stumps with the balloon catheter and the patch that was wrapped around the vessel before irradiation. **C:** *In vitro* experiment after irradiation. The patch was melting around the vessel, giving additional stability, and was shrinking in lateral direction.

The total irradiation time for the vessels was 46±8 s. The maximal load before vessel rupture was 1451±337 mN, and the tensile strength was 117±30 mN/mm^2 (n=30) for the laser-soldered-anastomosis. During tensile strength testing, the rupture took consistently place at the interface between the patch and the vessel wall. This tensile strength was significantly lower (p=0.0094) compared to sutured rabbit aortas where we obtained 171±29 mN/mm^2 (maximum load was 2042±112 mN, n=5).

Figure II.10 shows the histological assessment of the rabbit aorta after LAVA *in vitro*. Comparing the native arterial wall and the laser-treated wall, it is evident that thermal damage occurred in the Tunica adventitia and the Tunica media. The Tunica interna with its endothelium remained intact, which is important to prevent pathological vascular changes [46]. No vacuoles were present in the arterial wall. The thermal damage of the Tunica media, indicated

by the shrinkage of this layer, was restricted to the area that was covered by the patch. The Tunica adventitia was interfused with liquid BSA and seemed to be damaged. This damage can be further seen in some distance from the area beyond the patch, which is probably due to heat diffusion, as mentioned above. The soldered patch was interfused with small to mid-sized bubbles.
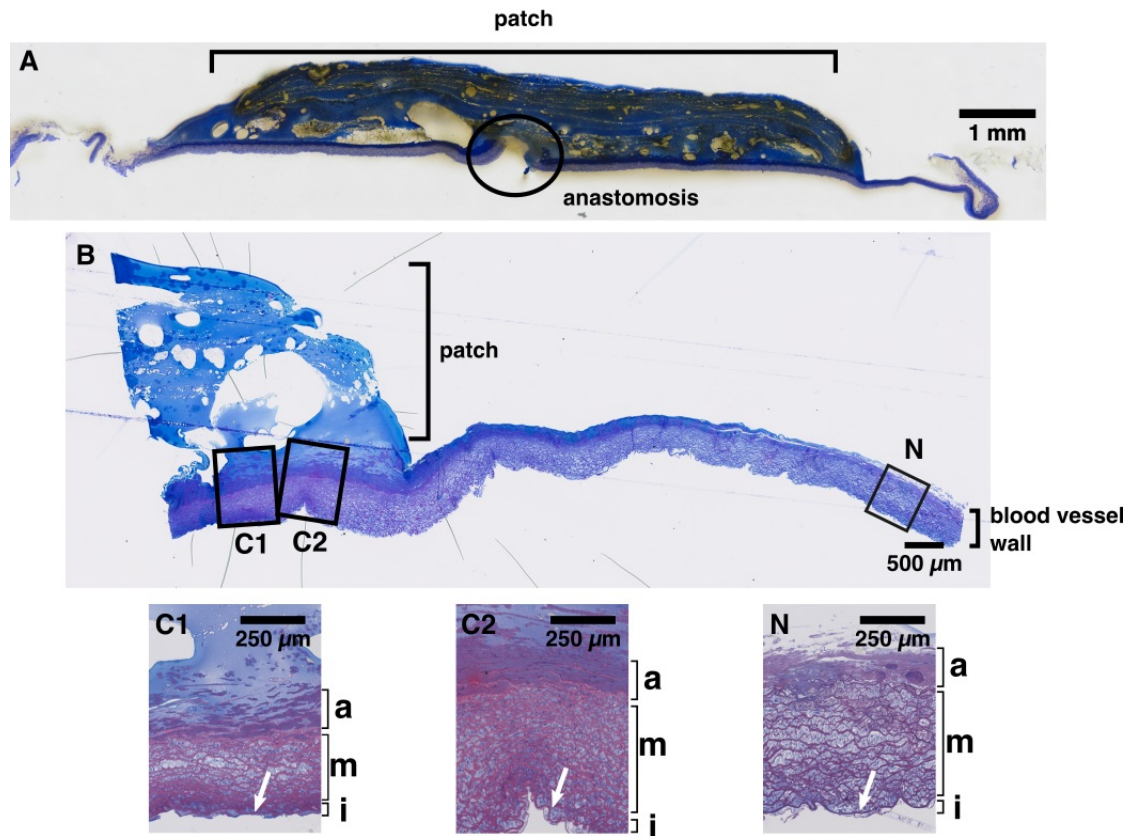
Figure II.10: Histological Analysis. Light micrographs of arterial walls immediately after *in vitro* LAVA . **A**: Longitudinal whole-mount section after MMA embedding shows the patch closely adhering to the blood vessel and the position were the anastomosis was performed. **B**: Overview after embedding in epon resin demonstrating the arterial wall after LAVA and showing the position of the detail views. **N**: The native arterial wall (N) is shown with the Tunica interna (i) and the Tunica media (m), that is formed by smooth muscle cells and loosely arranged collagen fibers. The Tunica adventitia (a) blends with the connective tissue that surrounds the artery. **C1, C2**: After LAVA thermal damage is noticed. The collagen fibers of the Tunica media appear compact and accurately arranged, and in **C1** the Tunica media is clearly compressed. The Tunica interna with its endothelium (arrow) remained intact.

II.3.3   *In vivo* anastomosis

We performed *in vivo* LAVA using eight pigs. The slightly sticky patch simplifies the positioning of the patch, the coaptation of the vessels stumps and holds the stumps together. Furthermore, the patch was stable and did not tear apart. Therefore, the ICG-loaded patch had advantages
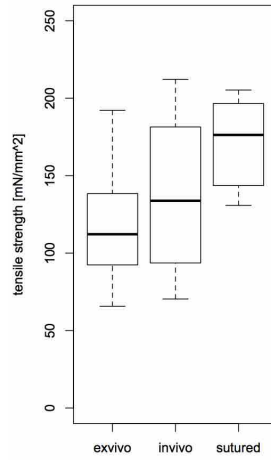
Figure II.11: Tensile strength measurements after soldering using rabbit aorta (*in vitro*) and pig arteries (*in vivo*) compared to conventionally sutured rabbit aorta (*in vitro*). The boxes indicate the median and the interquartile range, the vertical lines depict the ranges (upper/lower quartile ± 1.5*interquartile range).

compared to liquid solder regarding clinical handling. We observed no dripping of the solder and the surrounding tissue was not stained by the green chromophore. Bonding was obtained after an average time of total laser irradiation of 58±8 s.

After LAVA, we observed no blood leakage in six of eight experiments. The pulse rate was visible distal to the soldering site and a blood flow through the venous end of the flap demonstrated the patency of the vessels for blood. The maximum load and the tensile strength, determined for four of the patent anastomoses, was 1058±265 mN and 138±52 mN/mm^2, respectively (see figure II.11). To test the clinical outcome of a lower irradiance leading to lower temperatures and hence lower tensile strengths, we irradiated one vessel with 1.6 W/cm^2. Here, the required temperature of 80 °C to achieve strong tissue bonding was not reached, leading to a tensile strength of only 23 mN/mm^2. Even in this case the fusion was patent for blood and no leakage occurred, even after touching and slightly pulling the vessel. In two experiments we observed a blood leakage, as the patch was not overlapping due to defective approximation of the vessels and the laser fiber.

II.4 Discussion

The aim of our study was to develop and characterize a patch suitable for LAVA that is easy-to-handle, pliable, biodegradable and that can be adjusted to different shapes and sizes to meet specific surgical needs. The patch should be ready-to-use without further modification in the surgery room. Since it is necessary to ensure a reliable and reproducible anastomosis, a well-defined concentration of the chromophore in the patch is required during the procedure.

Matrix polymers, that have led to promising results for laser tissue soldering, include PCL [15, 20], poly(lactic-co-glycolic acid) (PLGA) [5], and chitosan [6]. We used PCL as a matrix material for laser tissue soldering, since it is biodegradable and biocompatible and approved

by the Food and Drug Administration (FDA) [47]. A further advantage is its low melting point at around 60 °C [48] which, during LAVA, promotes a strong polymer-tissue-interaction by solidifying the polymer at the surface [5]. Additionally, we have chosen PCL over PLGA due to its lower degradation rate leading to a lower inflammatory response [49]. Besides, PCL is an intensively studied polymer with regard to electrospinning. Since PCL is hydrophobic and a linear semi crystalline polymer it is soluble in organic solvents such as chloroform, acetic acid, formic acid and tetrahydrofuran [33, 47]. It is reported that electrospinning of PCL in chloroform as single solvent produces randomly oriented and smooth fibers [33, 42, 50, 51]. By using a binary system with chloroform and a solvent with a high dielectric constant, such as methanol or dimethylformamide, the electrospinnability was enhanced and more uniform fibers with regards to its size distribution were reported [33, 50]. A further reason to use the binary system of chloroform and methanol was the high solubility and the good stability of ICG in methanol compared to aqueous fluids [19].

In this study we present the possibility to fix ICG in various concentrations in polymer fibers by using electrospinning and hence to control the absorption coefficient of the patch. For LAVA we are aiming at a high absorption coefficient [2, 12]. In this study, a 1:10 ratio of ICG:PCL was used as this leads to a higher attenuation coefficient of $1119\pm183\,cm^{-1}$ compared to former approaches with soaked ICG or ICG-loaded nanoshells [15, 45], which was reported to be 96 to $288\,cm^{-1}$ and $145\pm5\,cm^{-1}$, respectively. The high absorption coefficient leads to an energy absorption in the first few micrometers of the patch, which results in a strong accumulation of heat at the interface of the patch and the artery. The strong heat accumulation at the patch-vessel interface together with the water-filled balloon catheter in the lumen result in a steep temperature gradient across the vessel wall. This gradient could be made steeper, when a balloon catheter flushed with a cooling medium, is applied [52]. Due to the temperature gradient a strong tissue bonding is achieved at the patch-tissue interface while keeping the temperature at the Tunica interna low.

Our hypothesis was that embedding ICG into micro-fibers would avoid its flow-off and ensure that peripheral tissue is not stained and hence not heated. The data of the aqueous- and photo-stability experiments show that the amount of absorbing ICG in the patch is reduced by 10 % after immersion in physiological solution after exposure to sunlight. We suggest three factors accounting for the reduction of ICG: (1) the leakage of ICG into the surrounding physiological solution, (2) the photo-degradation of ICG and (3) the instability of ICG in aqueous solution. The leakage of ICG was investigated by measuring the amount of ICG that was released into the extract. A release decreasing with time, as expected, of ICG into physiological solution during the first 8 hours was observed. After this, no further release of ICG was observed. This stagnation could be an evidence for entrapment of the ICG in the PCL fibers, with the initial burst release due to ICG that was not entrapped but loosely attached to the surface of the fibers. A burst release was observed for other molecules entrapped in PCL fibers, such as BSA [53, 54]. The absorbance of the extracts from patches exposed to daylight showed a significantly lower ICG concentration than the samples stored in the dark. This could be due to an effect of photobleaching since ICG is shown to possess poor photo-stability and photo-bleaching in aqueous solution [55]. There was no effect of the exposure to daylight on ICG absorbance measured directly from the subsequently dissolved patches. This could be due to the protection of ICG in PCL-fibers, an effect that was previously observed in silica-polycaprolactone grafted nanocomposites [17]. The degradation of ICG due to storage in aqueous solution was not observed, probably because of the short observation period of 24 hours [41].

Laser tissue soldering is achieved by irreversibly damaging the solder protein and structural proteins of the tissue [2, 7, 56]. Previously, we applied ambiguous end points, such as the change of color, desiccation and the shrinkage of the patch that defined whether the laser irradiation had

to be stopped. The usage of a thermal camera during the soldering process allows to optically observe the temperature and hence to control the applied laser energy. The infrared-camera based approach is easy to apply, however, it has a major drawback: we are mostly interested in the temperature at the vessel-patch-interface, but we are measuring at the outer surface of the solder patch. Additionally, we are just measuring at upper side of the vessel. The lower side might have a different temperature due to the formation of a water droplet. Due to naturally varying parameters, such as the water content of the tissue, tissue type, and tissue thickness, the thermal conduction towards the solder-tissue-interface and the T. interna is affected. Due to the high attenuation coefficient the target temperature of 75 to 85 °C is reached much faster, which reduces the overall irradiation time. Previous studies [12, 15] showed that the soldering time should be maximum 30 s to avoid desiccation and to stay in a clinically acceptable time. Therefore, we decided to keep the duration at the end-point temperature of 75 to 85 °C constant for 30 s. Additional experiments displayed (data not shown), that a longer duration of up to 60 s did not increase the tensile strength. A shorter duration decreased, however, the tensile strength significantly. During tensile strength testing, all anastomoses broke at the patch/tissue-interface, which indicates that the bond is mainly created by adhesive bonding. The histological assessment demonstrated, that the patch is in close contact with the vessel wall over its full lateral length, ensuring a high bonding strength (figure II.10). Thermal damage of the vessel wall was evident, however, the Tunica interna appeared structurally intact. The target temperature of 75–85 °C in *in vitro* soldering was reached after 16±8 s whereas for *in vivo* soldering the target temperature was reached after 28±8 s. This can be explained by the fact that in the clinical setup the humidity of the vessels and the patch was higher due to wound liquid and the wetting of the preparation site to avoid desiccation of the site of incision. This leads to a higher heat diffusion during the *in vivo* situation, and therefore to a stronger thermal damage. The standard deviation of ± 10 °C of the temperature reached during soldering is low compared to previous methods with liquid solder [45]. This low deviation results from the fixation of indocyanine green in the polycaprolactone scaffold and a result of the manual control of the laser power. The reproducibility of the temperature curve was improved by applying an ICG-loaded electrospun patch.

Due to the shrinkage of the patch during soldering, complete wrapping with an overlap has to be ensured during surgery. Therefore, the width of the patch needs to be sufficiently large, but at the same time small enough to avoid a large thermal damage zone. Furthermore, the shrinkage results in formation of a clump, which could be problematic during the healing process. Another challenge might be a tension onto the blood vessels. During our experiments, we did not observe such a tension, but this possible effect should be further investigated.

The time required for the whole surgery, beginning from introducing the balloon catheter until the removal of the balloon catheter lasted 10 min and hence underlines the fast and easy soldering procedure using the patch. The resulting tensile strength of the *in vitro* and *in vivo* experiments was similar, demonstrating the potential of the electrospun patches in a realistic environment. The tensile strength of sutured anastomoses was significantly higher. However, all *in vivo* tests were free of leakage during the observation period, demonstrating that the technique was able to provide water-tight anastomosis. This finding shows that the reported tensile strengths withstand the physiological blood pressure immediately after the anastomosis. The maximum loads at the vessel rupture point were in the same range as our previously reported results [15, 45]. Throughout this thesis, the maximum load was divided by the external diameter of the blood vessel, including the lumen and the vessel wall, and named as "tensile strength". This is certainly not a physically correct measure, but allowed to normalize the impact of the different vessel size of rabbit aorta and pig arteries. Nevertheless, measuring the immediate tensile strength as a quality attribute of LAVA assesses the integrity of the bonding after laser

soldering, and is related to the effect of the laser irradiation, however it provides no information about the patency of the vessels, nor about the immediate tightness. Therefore it is important to assess the leaking point pressure, and the bonding strength after wound healing in a future study.

II.5   Conclusion

In conclusion, we demonstrated the feasibility and applicability of an electrospun ICG-loaded patch for LAVA. Our approach, to embed ICG into fibers and thus to enable quantitative control during the surgery, was confirmed by *in vitro* and *in vivo* experiments. The main advantage of this patch is the entrapment of the chromophore in microfibers and thus the prevention of optical degradation and the staining of peripheral tissue. LAVA by means of the electrospun ICG-loaded patch resulted in an immediate and effective *in vivo* microvascular anastomosis, thus demonstrating the clinical feasibility of this approach and the successful handling of the patch under operative conditions. In terms of outlook, the focus will lay on the application of a layered electrospun patch, where albumin is embedded into polymer fibers. In addition, the mesh could be further loaded with functional molecules and drugs such as anti-inflammatory agents, and antibiotics to promote wound healing, considering their resistance to heat during soldering.

Acknowledgments

Bibliography

[1] Annemarie Schönfeld, Zacharia Mbaidjol Kabra, Kirsten Peters, Mihai A. Constantinescu, and Martin Frenz. Binding of indocyanine green in polycaprolactone fibers using blend electrospinning for laser-assisted vascular anastomosis. *Lasers in Surgery and Medicine*, in prepara:1–28, 2016.

[2] Karen M McNally, Brian S Sorg, Ashley J Welch, Judith M Dawes, and Earl R Owen. Photothermal effects of laser tissue soldering. *Physics in Medicine and Biology*, 44(4):983–1002, apr 1999.

[3] Beat Ott, Mihai A. Constantinescu, Dominique Erni, Andrej Banic, Thomas Schaffner, and Martin Frenz. Intraluminal laser light source and external solder: In vivo evaluation of a new technique for microvascular anastomosis. *Lasers in Surgery and Medicine*, 35(4):312–316, oct 2004.

[4] I.C.D.Y.M. Wolf -de Jonge, J.F. Beek, and R. Balm. 25 Years of Laser Assisted Vascular Anastomosis (LAVA): What Have We Learned? *European Journal of Vascular and Endovascular Surgery*, 27(5):466–476, may 2004.

[5] Dara R. Pabittei, Michal Heger, Sjoerd van Tuijl, Marc Simonet, Wadim de Boon, Allard C. van der Wal, Ron Balm, and Bas A. de Mol. Ex vivo proof-of-concept of end-to-end

scaffold-enhanced laser-assisted vascular anastomosis of porcine arteries. *Journal of Vascular Surgery*, 62(1):200–209, jul 2015.

[6] Giuseppe Esposito, Francesca Rossi, Paolo Matteini, Alba Scerrati, Alfredo Puca, Alessio Albanese, Giacomo Rossi, Fulvio Ratto, Giulio Maira, and Roberto Pini. In vivo laser assisted microvascular repair and end-to-end anastomosis by means of indocyanine green-infused chitosan patches: A pilot study. *Lasers in Surgery and Medicine*, 45(5):318–325, jul 2013.

[7] Lawrence S. Bass and Michael R. Treat. Laser tissue welding: A comprehensive review of current and future. *Lasers in Surgery and Medicine*, 17(4):315–349, 1995.

[8] Franck M P Leclère, Michel Schoofs, Bruno Buys, and Serge Mordon. Outcomes after 1.9 μm diode laser assisted anastomosis in reconstructive microsurgery: Results in 27 Patients. *Plastic and Reconstructive Surgery*, 125(4):1, jan 2010.

[9] De Ti-Sheng Chang. *Principles, techniques, and applications in microsurgery*. World Scientific, 1986.

[10] Mahmut Yasargil. *Microsurgery: Applied to Neurosurgery*. Georg Thieme Verlag, 2006.

[11] W. Z. Yahr, K. J. Strully, and E. S. Hurwiit. Non-occlusive small arterial anastomosis with a neodymium laser. *Surgical forum*, 15:224–6, 1964.

[12] Serge Bogni, Oliver Stumpp, Michael Reinert, and Martin Frenz. Thermal model for optimization of vascular laser tissue soldering. *Journal of Biophotonics*, 3(5-6):284–295, mar 2010.

[13] Ilan Gabay, Irina Barequet, David Varssano, Mordechai Rosner, and Abraham Katzir. Bonding surgical incisions using a temperature-controlled laser system based on a single infrared fiber. *Journal of Biomedical Optics*, 18(11):111416, sep 2013.

[14] Yaron Rabi and Abraham Katzir. Temporal heating profile influence on the immediate bond strength following laser tissue soldering. *Lasers in Surgery and Medicine*, 42(5):425–432, jun 2010.

[15] Daniel S. Schöni, Serge Bogni, Amadé Bregy, Amina Wirth, Andreas Raabe, Istvan Vajtai, Uwe Pieles, Michael Reinert, and Martin Frenz. Nanoshell assisted laser soldering of vascular tissue. *Lasers in Surgery and Medicine*, 43(10):975–983, dec 2011.

[16] Brian S. Sorg and Ashley J. Welch. Laser-tissue soldering with biodegradable polymer films in vitro: Film surface morphology and hydration effects. *Lasers in Surgery and Medicine*, 28(4):297–306, apr 2001.

[17] Andrea Schönbächler, Olfa Glaied, Jörg Huwyler, Martin Frenz, and Uwe Pieles. Indocyanine green loaded biocompatible nanoparticles: Stabilization of indocyanine green (ICG) using biocompatible silica-poly(ϵ-caprolactone) grafted nanocomposites. *Journal of Photochemistry and Photobiology A: Chemistry*, 261:12–19, jun 2013.

[18] Mohammad E Khosroshahi and Mohammad S Nourbakhsh. Enhanced laser tissue soldering using indocyanine green chromophore and gold nanoshells combination. *Journal of Biomedical Optics*, 16(8):088002, 2011.

[19] O. G. Björnsson, R. Murphy, V. S. Chadwick, and S. Björnsson. Physicochemical Studies on Indocyanine Green: Molar Lineic Absorbance, pH Tolerance, Activation Energy and Rate of Decay in Various Solvents. *Clinical Chemistry and Laboratory Medicine*, 21(7):453–458, 1983.

[20] Dara R. Pabittei, Michal Heger, Ron Balm, Han E. H. Meijer, Bas de Mol, and Johan F. Beek. Electrospun Poly(ÉŻ-Caprolactone) Scaffold for Suture-Free Solder-Mediated Laser-Assisted Vessel Repair. *Photomedicine and Laser Surgery*, 29(1):19–25, jan 2011.

[21] Kailash Gupta, Adnan Haider, Yu-ri Choi, and Inn-kyu Kang. Nanofibrous scaffolds in biomedical applications. *Biomaterials Research*, 18(1):5, jan 2014.

[22] Seema Agarwal, Joachim H. Wendorff, and Andreas Greiner. Use of electrospinning technique for biomedical applications. *Polymer*, 49(26):5603–5621, dec 2008.

[23] Gareth R Williams, Nicholas P Chatterton, Tahir Nazir, Deng-Guang Yu, Li-Min Zhu, and Christopher J Branford-White. Electrospun nanofibers in drug delivery: recent developments and perspectives. *Therapeutic Delivery*, 3(4):515–533, apr 2012.

[24] Seeram Ramakrishna, Maedeh Zamani, and Molamma P Prabhakaran. Advances in drug delivery via electrospun and electrosprayed nanomaterials. *International Journal of Nanomedicine*, 8(1):2997, aug 2013.

[25] Young Ju Son, Woo Jin Kim, and Hyuk Sang Yoo. Therapeutic applications of electrospun nanofibers for drug delivery systems. *Archives of Pharmacal Research*, 37(1):69–78, jan 2014.

[26] Travis J. Sill and Horst A. von Recum. Electrospinning: Applications in drug delivery and tissue engineering. *Biomaterials*, 29(13):1989–2006, may 2008.

[27] Nae Gyune Rim, Choongsoo S Shin, and Heungsoo Shin. Current approaches to electrospun nanofibers for tissue engineering. *Biomedical Materials*, 8(1):014102, feb 2013.

[28] J. Lannutti, D. Reneker, T. Ma, D. Tomasko, and D. Farson. Electrospinning for tissue engineering scaffolds. *Materials Science and Engineering: C*, 27(3):504–509, apr 2007.

[29] Ali Tamayol, Mohsen Akbari, Nasim Annabi, Arghya Paul, Ali Khademhosseini, and David Juncker. Fiber-based tissue engineering: Progress, challenges, and opportunities. *Biotechnology Advances*, 31(5):669–687, sep 2013.

[30] Payam Zahedi, Iraj Rezaeian, Seyed-Omid Ranaei-Siadat, Seyed-Hassan Jafari, and Pitt Supaphol. A review on wound dressings with an emphasis on electrospun nanofibrous polymeric bandages. *Polymers for Advanced Technologies*, 21(2):n/a–n/a, 2009.

[31] Pim-on Rujitanaroj, Nuttaporn Pimpha, and Pitt Supaphol. Wound-dressing materials with antibacterial activity from electrospun gelatin fiber mats containing silver nanoparticles. *Polymer*, 49(21):4723–4732, oct 2008.

[32] Martina Abrigo, Sally L. McArthur, and Peter Kingshott. Electrospun Nanofibers as Dressings for Chronic Wound Care: Advances, Challenges, and Future Prospects. *Macromolecular Bioscience*, 14(6):772–792, jun 2014.

[33] C. J. Luo, E. Stride, and M. Edirisinghe. Mapping the Influence of Solubility and Dielectric Constant on Electrospinning Polycaprolactone Solutions. *Macromolecules*, 45(11):4669–4680, jun 2012.

[34] A. Gholipour Kanani and S. Hajir Bahrami. Effect of Changing Solvents on Poly(-Caprolactone) Nanofibrous Webs Morphology. *Journal of Nanomaterials*, 2011:1–10, may 2011.

[35] A. Cipitria, A. Skelton, T. R. Dargaville, P. D. Dalton, and D. W. Hutmacher. Design, fabrication and characterization of PCL electrospun scaffoldsâĂŤa review. *Journal of Materials Chemistry*, 21(26):9419, oct 2011.

[36] Seema Agarwal, Andreas Greiner, and Joachim H. Wendorff. Functional materials by electrospinning of polymers. *Progress in Polymer Science*, 38(6):963–991, jun 2013.

[37] Amir H. Torbati, Ryan T. Mather, Jay E. Reeder, and Patrick T. Mather. Fabrication of a light-emitting shape memory polymeric web containing indocyanine green. *Journal of Biomedical Materials Research Part B: Applied Biomaterials*, 102(6):1236–1243, aug 2014.

[38] Luana Persano, Andrea Camposeo, Cagri Tekmen, and Dario Pisignano. Industrial Upscaling of Electrospinning and Applications of Polymer Nanofibers: A Review. *Macromolecular Materials and Engineering*, 298(5):504–520, may 2013.

[39] Y Li, D; Xia. *Nanofibers - Production, Properties and Functional Applications*. InTech, nov 2011.

[40] Stanislav Petrik and Miroslav Maly. Production Nozzle-Less Electrospinning Nanofiber Technology. *MRS Proceedings*, 1240:1240–WW03–07, jan 2009.

[41] W. Holzer, M. Mauerer, A. Penzkofer, R.-M. Szeimies, C. Abels, M. Landthaler, and W. Bäumler. Photostability and thermal stability of indocyanine green. *Journal of Photochemistry and Photobiology B: Biology*, 47(2-3):155–164, dec 1998.

[42] H. Yoshimoto, Y.M. Shin, H. Terai, and J.P. Vacanti. A biodegradable nanofiber scaffold by electrospinning and its potential for bone tissue engineering. *Biomaterials*, 24(12):2077–2082, may 2003.

[43] Patrick Stähli, Jaro Ricka, Martin Frenz, and Akarcay H. Günhan. Optical extinction measurements on strongly scattering samples by way of imaging. 2017.

[44] RK Schenk, AJ Olah, and W Herrmann. Preparation of calcified tissues for light microscopy. *Methods of Calcified Tissue Preparation*, Amsterdam(Elsevier):1–56, 1984.

[45] Amadé Bregy, Serge Bogni, Vianney J.P. Bernau, Istvan Vajtai, Felix Vollbach, Alke Petri-Fink, Mihai Constantinescu, Heinrich Hofmann, Martin Frenz, and Michael Reinert. Solder doped polycaprolactone scaffold enables reproducible laser tissue soldering. *Lasers in Surgery and Medicine*, 40(10):716–725, dec 2008.

[46] Sharon Thomsen. Pathologic Analysis of Photothermal and Photomechanical Effects of Laser-Tissue Interactions. *Photochemistry and Photobiology*, 53(6):825–835, jun 1991.

[47] Maria Ann Woodruff and Dietmar Werner Hutmacher. The return of a forgotten polymer-Polycaprolactone in the 21st century. *Progress in Polymer Science*, 35(10):1217–1256, oct 2010.

[48] Shoufeng Yang, Kah-Fai Leong, Zhaohui Du, and Chee-Kai Chua. The Design of Scaffolds for Use in Tissue Engineering. Part II. Rapid Prototyping Techniques. *Tissue Engineering*, 8(1):1–11, feb 2002.

[49] Hak-Joon Sung, Carson Meredith, Chad Johnson, and Zorina S Galis. The effect of scaffold degradation rate on three-dimensional cell growth and angiogenesis. *Biomaterials*, 25(26):5735–5742, nov 2004.

[50] Chen Ming Hsu and S. Shivkumar. Nano-sized beads and porous fiber constructs of Poly(ÉŽâĂŃ-caprolactone) produced by electrospinning. *Journal of Materials Science*, 39(9):3003–3013, sep 2004.

[51] Lien Van Der Schueren, Bert De Schoenmaker, Özlem I. Kalaoglu, and Karen De Clerck. An alternative solvent system for the steady state electrospinning of polycaprolactone. *European Polymer Journal*, 47(6):1256–1263, may 2011.

[52] Serge Bogni, Maria Anna Ortner, Istvan Vajtai, Christian Jost, Michael Reinert, Bernard Dallemagne, and Martin Frenz. New laser soldering-based closures: A promising method in natural orifice transluminal endoscopic surgery. *Gastrointestinal Endoscopy*, 76(1):151–158, oct 2012.

[53] Fatemeh Roozbahani, Naznin Sultana, Davood Almasi, and Farnaz Naghizadeh. Effects of Chitosan Concentration on the Protein Release Behaviour of Electrospun Poly(ϵ-caprolactone)/Chitosan Nanofibers. *Journal of Nanomaterials*, 2015:1–11, apr 2015.

[54] Chandra M. Valmikinathan, Steven Defroda, and Xiaojun Yu. Polycaprolactone and Bovine Serum Albumin Based Nanofibers for Controlled Release of Nerve Growth Factor. *Biomacromolecules*, 10(5):1084–1089, may 2009.

[55] Vishal Saxena, Mostafa Sadoqi, and Jun Shao. Degradation kinetics of indocyanine green in aqueous solution. *Journal of Pharmaceutical Sciences*, 92(10):2090–2097, oct 2003.

[56] D P Poppas, S M Schlossberg, I L Richmond, D A Gilbert, and C J Devine. Laser welding in urethral surgery: improved results with a protein solder. *The Journal of urology*, 139(2):415–7, feb 1988.

[57] Michelle K. Leach, Zhang-Qi Feng, Samuel J. Tuck, and Joseph M. Corey. Electrospinning Fundamentals: Optimizing Solution and Apparatus Parameters. *Journal of Visualized Experiments*, 47(47):2494, jan 2011.

[58] Seonok Lee, S Y Christin Chong, Samuel J Tuck, Joseph M Corey, and Jonah R Chan. A rapid and reproducible assay for modeling myelination by oligodendrocytes using engineered nanofibers. *Nature Protocols*, 8(4):771–782, mar 2013.

III. Electrospinning of highly concentrated albumin patches by using auxiliary polymers for laser-assisted vascular anastomosis

Abstract

Background and Objective: Electrospun meshes have been extensively investigated for tissue engineering and drug delivery. The application of this technology is of interest for laser-assisted vascular anastomosis (LAVA) due to the possibility to bind and stabilize macromolecules in fibers.

Materials and Methods: We prepared bovine serum albumin (BSA) blend microfibers from the auxiliary proteins polyethylene oxide (PEO), polycaprolactone (PCL), polyvinyl alcohol (PVA) and gelatin. The thickness and weight of the resulting patches were measured and the morphological characteristics were observed by scanning electron microscopy. The effect of the material composition of the electrospun patches on the bonding strength after LAVA was determined.

Results: The bonding strength of the tissue fusion increased by using higher BSA amounts in the patch. By using PEO, a ratio of 85/15 (w/w) of BSA/PEO was stable during electrospinning, leading to a tensile strength that was similar to patches that were soaked in liquid BSA ($102\pm18\,\mathrm{mN/mm^2}$ and $117\pm30\,\mathrm{mN/mm^2}$, respectively).

Conclusion: This study investigated the maximum amount of BSA possible in electrospun polymer fibers made from PEO, PCL, PVA and gelatin. The process of electrospinning of a BSA/PEO blend was stable for hours, making them a promising material for LAVA.

III.1 Introduction

Laser-assisted vascular anastomosis (LAVA) has potential to enable secure, rapid and easy fusion of blood vessels and might reduce suture and needle trauma, foreign body reactions and bleeding [2–4]. LAVA is based on the inauguration of a thermal effect driven by the absorption of laser light, inducing denaturation and coagulation of proteins. Solder that commonly consists of chromophore indocyanine green (ICG) and protein bovine serum albumin (BSA), is applied onto the soldering site by either dripping [4–6] or by soaking a patch in BSA/ICG solution [7–9]. However, the usage of a liquid solder solution has disadvantages: (1) Dripping of the liquid solution before and during soldering lead to an uncontrollable amount of both, the chromophore and the protein. (2) The difficult localized deposition of the liquid solder and the flow-off of the

---

The content of this chapter was submitted to "Biomedical Materials" in 2016 [1].

solder, results in staining the surrounding tissue and hence heating and thermal damage. (3) Applying solder solution, containing highly concentrated BSA, is a tedious process, due to the stickiness of the solution. (4) The short shelf-life of highly concentrated BSA solution necessitates its fresh preparation prior to surgery to avoid protein degradation and aggregation [10]. A patch, that is soaked in liquid BSA/ICG solution, followed by application to blood vessels, possesses the same disadvantages with regard to liquid highly concentrated BSA solutions, but significantly increases the bonding strength. The increased bonding strength is a result of the larger surface area that is involved in the bonding due to the fusion of the solder patch along the sides of the tissue and not only at the edges of the tissue to be fused, as for liquid solder [7–9]. Our aim is thus to develop and characterize a pliable and tear-proof patch that already encapsulates both ICG and BSA and is ready-to-use without additional modifications in the surgery room.

Electrospinning is a well-studied technique to produce fibers with diameters in the nano- and micrometer range [11]. Electrospun materials can be prepared from a large variety of synthetic or natural polymers, enabling a wide field of applications such as in filtering [12], sensors [13] and textiles [14]. Powerful progress has been achieved in using electrospinning for tissue engineering [15–18], wound dressing [19–21], and the encapsulation of drugs [22–26] and cells [27, 28]. The application of an electrospun scaffold made of ICG-loaded polycaprolactone (PCL) fibers that was soaked in liquid BSA has been shown to improve tissue fusion due to binding of ICG, avoiding its flow-off, and due to easier handling during surgery [29]. To obtain strong tissue fusion during LAVA, the amount of BSA must be high and the BSA layer needs to have direct contact with the underlying tissue ensuring the denaturation and subsequent entanglement of the protein chains [5, 30]. We present a double-layer patch, with the BSA-loaded layer touching the tissue and with the PCL/ICG-absorber layer above. As stated in the literature, the protein BSA does not form fibers during electrospinning, due to its globular structure. To overcome this limitation, blend [31–34], coaxial [35, 36] and emulsion [37–39] electrospinning have been shown to incorporate biomolecules into fibers.

The present study addresses the development of scaffolds with a high BSA-load via blend electrospinning together with an auxiliary polymer. BSA-loaded layers from four different auxiliary polymers and with different weight ratios were prepared and investigated with regard to weight, thickness and fiber morphology. The following biocompatible polymers were tested: polyethylene oxide (PEO), polyvinyl alcohol (PVA), gelatin and PCL. PEO is a biocompatible polymer, water-soluble and known for its good electrospinnability [31, 41, 44]. Protein-loaded PVA nanofibers have been investigated for application in biosensors [33], tissue engineering [47], and protein delivery systems [48, 49]. Gelatin is the irreversibly hydrolized form of collagen, which is a naturally abundant polymer. Gelatin was frequently used in tissue engineering to serve as a matrix material to provide support for cells [50–53], and could therefore be a potential candidate for LAVA. PCL is shown to be suitable as a matrix polymer for the ICG-loaded layer and was therefore investigated as an auxiliary polymer for BSA-electrospinning, see chapter II. The solution and electrospinning parameters were optimized in order to ensure an electrospinning process without dripping of the solution or clogging of the needle tip and to ensure the production of smooth membranes. The applicability of the layered solder patches to LAVA was tested *in vitro* using rabbit aortas by measuring the tensile strength of the anastomoses.

III.2 Materials and Methods

III.2.1 Materials

Polycaprolactone (PCL, M_n = 70000 to 90000), polyethylene oxide (PEO, average M_n =400000), polyvinyl alcohol (PVA, M_n =205000), gelatin (from porcine connective tissue, bloom 175 G),

acetic acid (p.a.), formic acid (p.a.), and lyophilized bovine serum albumin (BSA) were obtained from Sigma Aldrich (Saint Louis, MO). Methanol and chloroform were used in analytical grade from Merck KGaA (Darmstadt, Germany). Indocyanine green (ICG, IR-125) was obtained from Acros Organics (Geel, Belgium). All materials were used as received.

III.2.2 Preparation of patches

Electrospinning of BSA-loaded patches

The electrospinning solutions were prepared by simultaneously adding specific amounts of the polymer and BSA to the solvent mixture, see table III.1. The solutions were stirred overnight at 37 °C. Polymer and BSA concentrations are expressed in % (w/w) relative to the solution.

For electrospinning, the prepared solution was placed in a 5 ml syringe that was connected with Teflon tubings to a truncated needle (21 G, 0.812 mm I.D.). A flow rate of 10–30 µl/min, a collector distance of 10-30 cm and a positive potential of 5–25 kV were employed, depending on the stability of the electrospinning process. The fibers were collected on a rotating aluminum plate to aid even distribution of the deposited fibers. The humidity and the temperature were fixed at 30±5 % RH and 22±1 °C.

Electrospinning of ICG-loaded layer

The preparation of the indocyanine-green loaded layer is described in chapter II. A 9 % (w/w) PCL solution with ICG at a ratio of 1:10 (w/w) ICG:PCL was prepared in chloroform/methanol (75/25 (v/v)). The blend was electrospun for 75 min using a positive potential of 15 kV, 15 cm collector distance and a flow rate of 30 µl/min.

III.2.3 Analysis of the patches

Scanning electron microscopy (SEM)

To examine the fiber morphology, the patches were cut into small pieces, sputter coated with a 10 nm layer of gold and analyzed using scanning electron microscopy. The fiber diameters were analyzed using FIJI (ImageJ 1.51a) [40]. The average fiber diameter and standard deviation were determined by preparing 3 patches and measuring the cross section of 60 fibers per image (n=180).

Weight and thickness

After determining the solution and process parameters that lead to stable electrospinning, the BSA/polymer blend was electrospun directly on a ICG-loaded layer to produce a solder patch. From each blend two solder scaffolds with a diameter of 10 cm were electrospun, from which 5 solder patches were cut and used for the thickness, weight, and tensile strength measurements (n=10). After electrospinning, the solder patches were cut to a width of 10±1 mm and a length of 20±1 mm and weighed. The weight of the ICG-loaded layer was determined to be 9.1±2.3 mg (n=50 ICG-layers) and subtracted from the weight of the layered solder patch. For the determination of the thickness of the layers, a layer was inserted between two microscope slides, followed by measuring the displacement with a height gauge (Trimos V600+, Trimos SA, Renens, Switzerland).

***In vitro* laser-assisted vascular anastomosis**

The applicability of the different solder patches was tested using the LAVA technique shown in figure III.3. Rabbit aortic arteries from a local slaughterhouse were liberated from surrounding fatty tissue, cut transversal and placed onto a water-filled balloon catheter (Armada 35 PTA catheter, Abbott, Illinos). A diffusor laser fiber with a 15 mm active zone (Laser und Medizintechnologie Berlin, Germany) was inserted into the catheter. An 810 nm diode laser (Lina 30d, Intros, Heilbad Heiligenstadt, Germany) was coupled into the laser fiber. The solder patches were wrapped around the blood vessel, with an overlap of 2 mm, and with the BSA-loaded layer in direct contact with the vessel wall. Subsequently, the vessel was irradiated using an average output power of 3 W, in the continuous wave (cw) regime, as opposed to chapter II, where 4 W were used due to more humid vessels and therefore a slower temperature increase. The vessel diameter was measured to be 3.9 ± 0.3 mm (n=30), thus the irradiated surface was 1.8 ± 0.1 cm^2, resulting in an irradiance of 2.2 ± 0.2 W/cm^2. During soldering, the temperature was measured with a thermal camera (A655, FLIR systems, Oregon, USA) and manually controlled by switching the laser on and off. After 75 °C were reached, we irradiated for 30 s at a temperature range between 75 and 85 °C.

Measuring tensile strength

The quality of the fusion was assessed by measuring the tensile strength. A test stand with a fixed force gauge (BFG50, Mecmesin Limited, West Sussex, United Kingdom) was employed to measure the maximum load onto the vessels. The vessels were fixed with two surgical clamps 2 mm from the ends of the patches. The clamps were fixed to a moving table, which was pulled with an electrically driven motor at a constant velocity of 30 mm/min. The maximum load on the probe was recorded and divided by the cross section of the vessel, including the lumen and the vessel wall, giving the tensile strength in mN/mm^2. Similarly, the tensile strength of the electrospun layers before soldering was measured, where the maximum load was divided by the thickness times the width of the layer (n=5 layers).

III.3   Results

III.3.1   Optimization of solution and electrospinning parameters

Table III.1 lists the BSA/polymer ratios and the process parameters used in the further course of this study.

Polyethylene oxide (PEO)

As a starting point, a blend of 7.4 % (w/w) BSA and 1.3 % (w/w) PEO was used as published by Kowalczyk *et al.* [31]. Stable electrospinning of this blend was achieved by applying a gap distance of 15 cm, a feed rate of 15 µl/min and an applied voltage of 15 kV. The solution did neither drip nor clog at the needle tip, and spinning for hours was possible without any adjustment. The appearance of the resulting patch was homogeneous, without any clumping. With the BSA/PEO ratio being 85/15 (w/w), the amount of BSA in the final layer was 10.1 ± 1.6 mg. Experiments involving different BSA amounts, revealed that the tensile strength of the tissue fusion increased with increasing BSA amount. A BSA amount of 10.1 ± 1.6 mg in the patch was the highest obtained during BSA-blend electrospinning. Figure III.1 shows the morphology of the electrospun fibers made from the different polymer/albumin blends. The electrospun nanofibers made from BSA/PEO (85/15 (w/w)) resembled a string of beads. Electrospinning with a lower

Table III.1: Solution and process parameters used for electrospinning of the BSA/polymer blends and the appearance of the process and the patch.

polymer	BSA [% (w/w)]	polymer [% (w/w)]	solvent	voltage [kV]	gap dist [cm]	feed [µl/min]	e-spinnability	appear. patch
PEO	7.4	1.3	water	15	15	15	stable	homogeneous, no flaws
	4.4	4.4	water	15	15	15	stable	homogeneous, no flaws
PVA	7	7	water	20	15	20	rarely dripping	homogeneous, few droplets
Gelatin	10	20	formic acid	15	15	10	stable	homogeneous, no flaws
PCL	6	10	formic/acetic	22	15	15	dripping	homogeneous, no flaws
	20	3.5	acid 70/30 v/v	22	15	15	dripping	homogeneous, few droplets

BSA and higher PEO concentration (4.4 % (w/w)/4.4 % (w/w)) resulted in a solution of higher viscosity and in fibers. However, no effect on LAVA due to the beaded morphology was observed, shown in chapter III.3.3. Scaffolds made from PVA, gelatin and PCL show random fibers with a narrow diameter distribution.

Polyvinyl alcohol (PVA)

By using different BSA/PVA ratios with water as a solvent, BSA/PVA fibers were only obtained at PVA concentrations of 7 % (w/w). At lower concentrations, a consistent jet could not be produced, and the solutions were constantly dripping. Using a blend of 7 % (w/w) BSA and 7 % (w/w) PVA, a homogeneous layer, with a few droplets, was obtained. However, after varying the gap distance, voltage and feed rate, rarely dripping of the solution from the needle tip could not be avoided. By further increasing the BSA ratio, BSA and PVA did not dissolve to a homogeneous blend.

Gelatin

We tested various BSA/gelatin ratios in order to receive a homogeneous layer with a high amount of BSA. BSA/gelatin blends in formic acid produced homogeneous scaffolds at 20 and 10 % (w/w), respectively, and the jet formed during electrospinning was uniform and consistent. Application of higher BSA amounts lead to clogging of the needle tip.

Polycaprolactone (PCL)

For the ICG-loaded layer, PCL was diluted in chloroform/methanol, which lead to stable electrospinning. For blend electrospinning with BSA, another solvent than chloroform was required, as BSA denatured in this solvent. Roozbahani *et al.* [54] demonstrated electrospinning of PCL and BSA in a formic acid and acetic acid solvent system. In our study, a homogeneous layer was achieved by using a blend made of 10 % (w/w) PCL and 6 % (w/w) BSA, with some droplets falling from the needle tip. By decreasing the polymer concentration to 3.5 % (w/w), the BSA concentration could be increased to 20 % (w/w), with the same electrospinning behavior as the blend above.
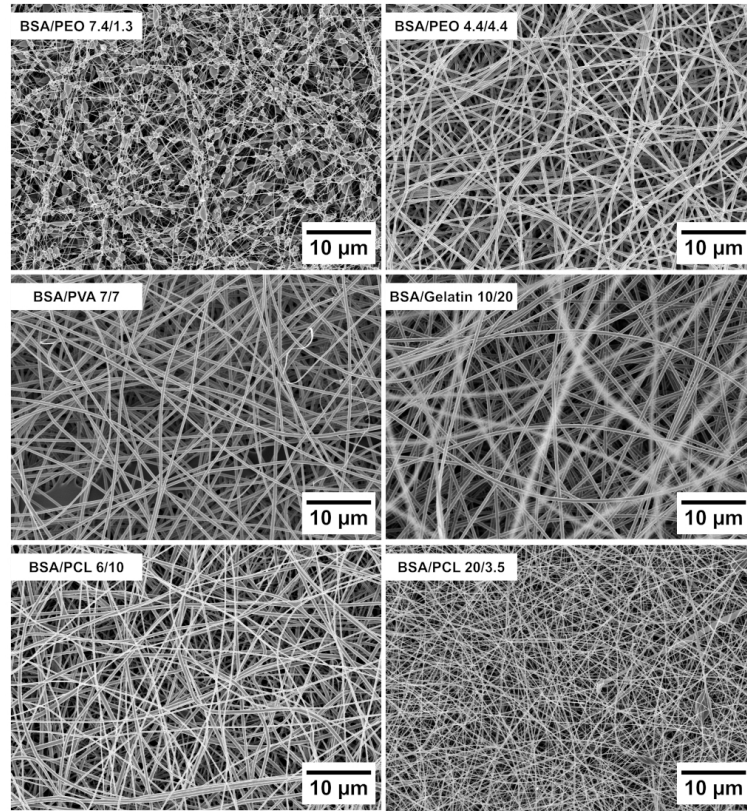
Figure III.1: Fiber morphology of the electrospun polymer and albumin blends. BSA/PEO fibers (7.4/1.3 % (w/w)) display a beads-on-a-string morphology. All other polymer/BSA solutions produced random, straight fibers, with the following fiber diameters: BSA/PEO (4.4/4.4 % (w/w)) 315±62 nm; BSA/PVA (7/7 % (w/w)) 412±75 nm; BSA/gelatin (10/20 % (w/w)) 494±48 nm; BSA/PCL (6/10 % (w/w)) 396±147 nm; BSA/PCL (20/3.5 % (w/w)) 153±63 nm.

III.3.2 Preparation of patches: electrospinning duration, thickness, weight, and tensile strength

Layered BSA- and ICG-loaded patches were prepared by electrospinning a blend of PCL/ICG, followed by a second layer of the blend made from BSA/polymer. To result in a pliable patch with a high amount of protein, we are aiming at a thickness of 200 to 300 µm for the BSA-loaded layer. The required spinning duration, thicknesses and weights of the BSA-layers are shown in table III.2. After electrospinning the BSA/PEO-blend (7.4 % (w/w)/1.3 % (w/w)) for 3 hours, a layer with a thickness of 271±43 µm and a weight of 11.8±1.6 mg was measured. The constant dripping of the blends with PVA and PCL resulted in loss of solution, and therefore a longer electrospinning duration was required, being 5 hours. Still, the weight of the layer was lower compared with the BSA/PEO layer, being in the range of 6.7 to 8.6 mg. The BSA/gelatin blend was electrospun for 5 hours, due to the lower feed rate of 10 µl/min compared to BSA/PEO with 15 µl/min. All layers were flexible and the macroscopic appearance was smooth. The BSA-layers adhered well to the ICG-layer, except for BSA/gelatin, where we could easily pull the BSA-layer off. The removal of the BSA-layer is an unwanted effect, since this complicates the handling of

Table III.2: Properties and results of the BSA-loaded layer of the electrospun patches used for *in vitro* tissue soldering using rabbit aorta. tens=tensile strength

polymer	BSA [% (w/w)]	polymer [% (w/w)]	BSA/polymer [(w/w)]	spinning duration [h]	weight layer [mg]	weight BSA [mg]	thickness layer [μm]	tens layer [mN/mm²]	tens LAVA [mN/mm²]
PEO	7.4	1.3	85/15	3	11.8±1.6	10.1 ±1.6	271±43	97±25	102±18
	7.4	1.3	85/15	1	3.8± 0.8	3.3±0.7	68± 31	113±23	23±11
	4.4	4.4	50/50	3	9.9±3.8	4.9±1.9	119±75	709±122	19±11
PVA	7	7	50/50	5	8.4±1.2	4.2 ± 0.6	180±50	781± 141	21±8
Gelatin	10	20	33/66	5	10.0± 1.0	3.3 ± 0.3	87±23	237±69	18±5
PCL	6	10	37.5/62.5	5	6.7 ± 1.3	2.5 ± 0.2	52± 17	2553±297	10±4
	20	3.5	85/15	5	8.6±2.5	7.3±2.2	37 ± 19	2895±357	13±4

the patch during *in vivo* surgery. The tensile strength of the layers varies significantly with the PCL/BSA layer tearing at $2895\pm357\,\mathrm{mN/mm^2}$ and the BSA/PEO (ratio 85/15 (w/w)) layer at $97\pm25\,\mathrm{mN/mm^2}$. Interestingly, layers from BSA/PEO 50/50 (w/w) were much stronger than the 85/15 (w/w)-layers with $709\pm122\,\mathrm{mN/mm^2}$ which is probably due to its straight fiber morphology instead of beaded fibers that are connected by thin fibers (see figure III.1). The tensile strength of the supporting PCL/ICG layer was $3297\pm414\,\mathrm{mN/mm^2}$, and the tensile strength of the layered patch was specified by this layer and not further affected by the BSA-loaded layer.

III.3.3 Tensile strength after laser-assisted vascular anastomosis

For LAVA, the original polymer concentrations in the solvent are irrelevant; instead we report the weight ratios between BSA and each respective auxiliary polymer in the final layer. Figure III.2 depicts the tensile strengths measured after soldering with the different BSA/polymer patches and soldering with a patch soaked in liquid BSA solution. In LAVAs with BSA-loaded patches made from PVA, PCL, and gelatin low mean tensile strengths, ranging from 10 to $21\,\mathrm{mN/mm^2}$, were measured. LAVAs with the polymer PEO at a ratio of 85/15 (w/w). and a spinning duration of 3 hours, exhibit a significantly higher tensile strength of $102\pm18\,\mathrm{mN/mm^2}$. These values were compared to LAVA with liquid BSA solutions, where we immersed the ICG-loaded layer in BSA dissolved in water at different concentrations. The tensile strengths for the 10, 25 and 40 % (w/w) BSA solutions were 2 ± 2, 60 ± 26 and $103\pm23\,\mathrm{mN/mm^2}$, respectively.

Using PEO as a polymer allowed us to incorporate $10.1\pm1.6\,\mathrm{mg}$ of BSA in the patch after a spinning duration of 3 hours. A lower electrospinning duration of 1 hour reduced the amount of deposited fibers and the weight of the BSA-loaded layer was measured to be $3.8\pm0.8\,\mathrm{mg}$. The BSA amount was therefore calculated to be $3.3\pm0.7\,\mathrm{mg}$. With this patch we obtained a tensile strength after LAVA of $23\pm11\,\mathrm{mN/mm^2}$. A low tensile strength of $19\pm11\,\mathrm{mN/mm^2}$ was obtained when the ratio of BSA/PEO was altered to 50/50 (w/w), where the amount of BSA was $4.9\pm1.9\,\mathrm{mg}$. Soldering with a soaked patch using a 10 % (w/w) BSA solution with an amount of $8.3\pm3.0\,\mathrm{mg}$ BSA, resulted in a lower tensile strength of $2\pm2\,\mathrm{mN/mm^2}$. Patches made from PVA and gelatin, yielded low BSA amounts being 4.2 ± 0.6 and $3.3\pm 0.3\,\mathrm{mg}$, respectively. We
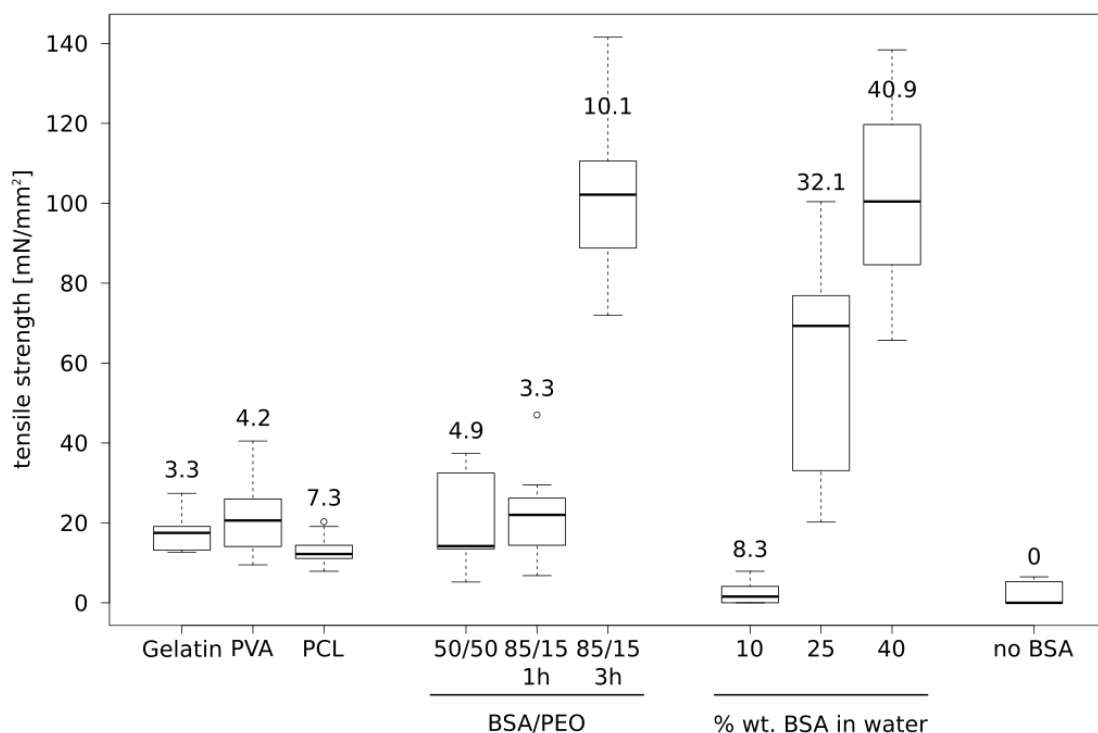
Figure III.2: Tensile strengths received after LAVA for the examined layered patches and ICG-layers soaked in liquid BSA solutions. The native ICG-loaded layer without BSA is depicted as a negative control. The median is represented by the line in the boxes, the fences of the boxes show the lower and upper interquartile range (IQR). The whiskers have the length of 1.5*IQR. The number above the whiskers depicts the mean weight of the BSA amount in the patches in mg.

could not bind higher BSA amounts to PVA or gelatin, since lower concentrations of the polymer did not produce fibers, whereas higher BSA concentrations did not dissolve to a homogeneous solution or led to clogging of the needle tip.

Figure III.3 shows the layered patch made of BSA/PEO before (B) and after LAVA (C). The color of the patch changed from light-green to dark-green and the patch shrank during laser irradiation. The lateral shrinkage was reduced in comparison with the patch soaked in liquid BSA (compare figure II.9, chapter II).

III.3.4 Histological analysis

Applying a blend of BSA/PEO led to a high tensile strength of the anastomosis after LAVA. Histological slides from rabbit aorta after LAVA were prepared using a layered solder patch, composed of a BSA/PEO layer and a PCL/ICG layer, and compared to a PCL/ICG layer soaked in liquid BSA. The micrographs are shown in figure III.4. The preparation of the histologies is described in chapter II. By comparing the native arterial wall and the laser-treated wall, it is evident, that thermal damage occurs using both patch types. Interestingly, the thermal damage is restricted to the area that is covered by the patch, which is probably due to the absence of
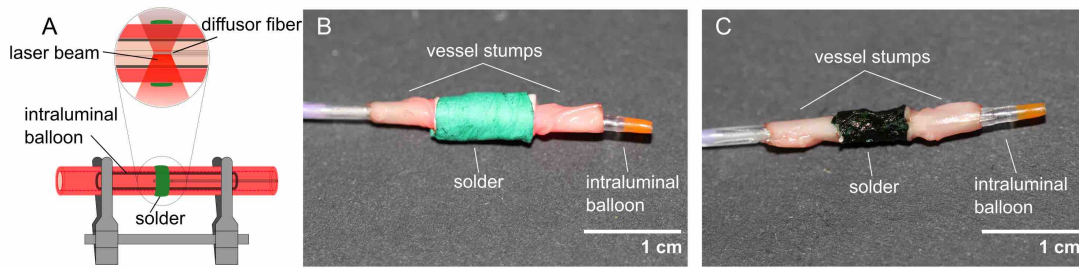
Figure III.3: A: Schematic of the LAVA setup (adapted from Ott *et al.* [4]). B: Experimental setup showing the aligned vessel stumps *in vitro* with the balloon catheter and the patch that was wrapped around the vessel before irradiation. C: LAVA after irradiation. A color change towards dark-green and radial shrinkage was observed.

staining of peripheral tissue. The extent of the thermal damage is similar using both patches, due to same soldering procedure, involving heating at 75 to 85 °C for 30 s. No vacuoles are present in the arterial wall, being one characteristic for overheating. Using the soaked patch, however, more shrinking in lateral direction was observed as by using the layered patch, leading to a thicker patch and therefore a bigger glob. Additionally, the soaked patch is slightly more interfused with small to mid-sized bubbles than the layered patch, that could lead to worse heat conduction due to the insulation by air.

III.4 Discussion

In the first part of this study, the solution and process parameters to achieve stable electrospinning of the BSA/polymer blends were determined. Here "stable" refers to a jet that is uniform, consistent, and not oscillating, the absence of dripping and clogging of the needle tip, and the build-up of a regular, homogeneous scaffold. The electrospinning process is susceptible to many parameters. This includes the constitution of the electrospinning solution regarding the concentration of the polymer and protein, the molecular weight, the viscoelasticity, the dielectric properties, and the surface tension. The electric potential, gap distance between needle and collector, the feed rate and the temperature and humidity are referred to as "process parameters" that influence the outcome of electrospinning [41]. Although some attempts are made to simulate and hence to accelerate the optimization process, it remains a "trial-and-error" procedure [42, 43]. Fiber morphologies, namely straight fibers and beaded fibers, have been correlated with different polymer concentrations and low molecular weights, where no chain entanglements were formed [45, 46]. This was confirmed by our results, were we obtained straight or beaded fibers depending on the concentration and ratio of BSA/PEO.

LAVAs with a higher liquid BSA concentration exhibited a higher tensile strength than those with a lower concentration, which is in agreement with the literature [5, 30]. By involving PCL as an auxiliary polymer, it was possible to bind 7.3 ± 2.2 mg of BSA in the patch. Theoretically this should enable reasonable tensile strengths. However, the tensile strength measured was low, being 13 ± 4 mN/mm^2. This effect can be explained by the entrapment of BSA inside the hydrophilic PCL fibers, which shields BSA from contacting the tissue. For laser-tissue soldering the direct contact of the BSA with the underlying tissue is a prerequisite. Long release durations were reported by Valmikinathan *et al.* [39], who stated the continuous and sustained
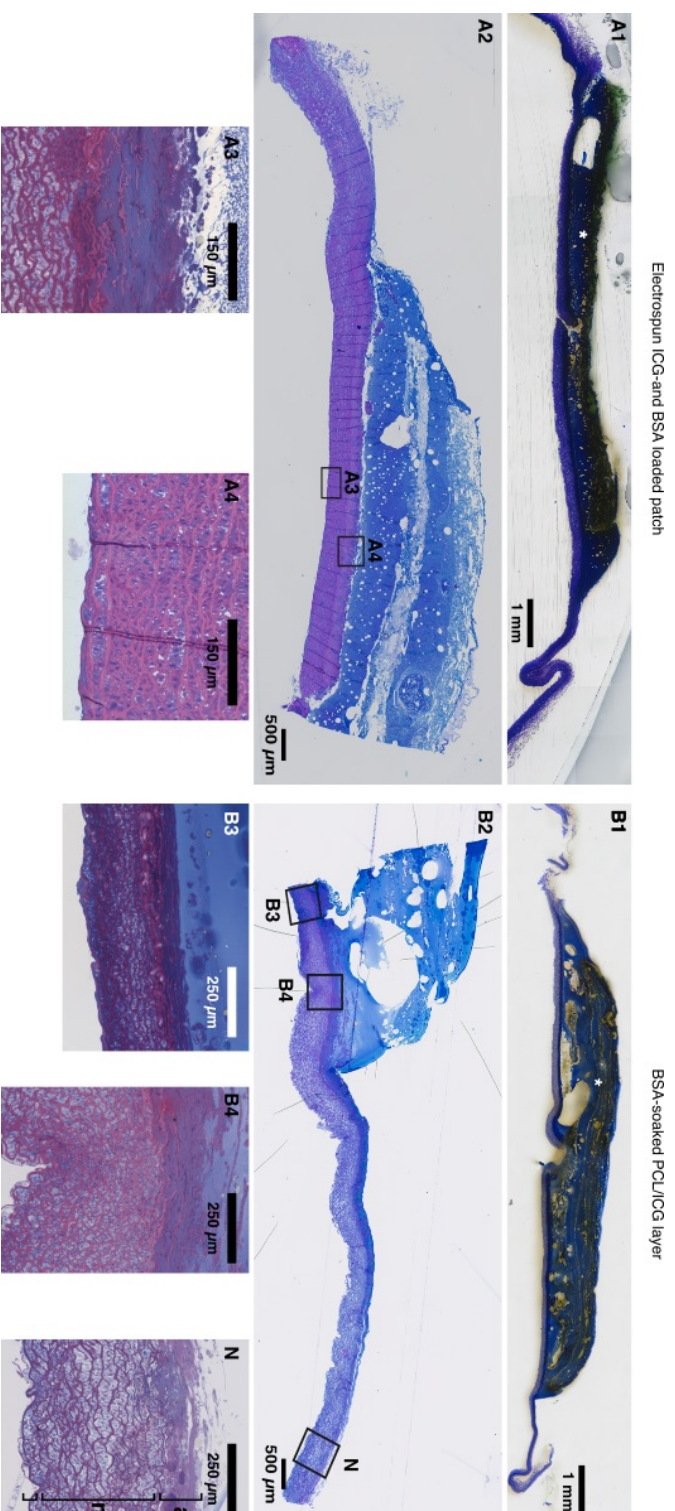
Figure III.4: **Histological Analysis.** Comparison of light micrographs of arterial walls immediately after *in vitro* LAVA using the two-layer electrospun patch and the PCL/ICG layer soaked in liquid BSA. **A1** and **B1:** Longitudinal whole-mount sections show the patch (asterisks) closely adhering to the Tunica adventitia and the position were the anastomosis was performed. **N:** The thermally untreated, native (N) arterial wall with the internal elastic lamina (i), and the Tunica media (m), formed by smooth muscle cells and loosely arranged collagen fibers. The Tunica adventitia (a) blends with the connective tissue that surrounds the artery. After LAVA (**A2** to **A4** and **B2** to **B4**), thermal damage is evident. The Tunica media is densely compressed, while the collagen fibers appear compact and accurately arranged.

release of BSA from PCL/BSA fibers over 28 days. Furthermore, an initial burst of BSA from BSA/PCL/Chitosan fibers followed by a gradual release until 14 days was demonstrated [54]. In contrary, PEO, PVA and gelatin are water-soluble polymers where we observe that the BSA-layer dissolves immediately after wrapping them around the blood vessel, enabling direct contact of BSA with the tissue.

Soldering using the layered patch with BSA/PEO (85/15 (w/w)) showed the same results as soldering with the PCL/ICG layer soaked in liquid 40 % (w/w) BSA, with tensile strengths of 102 ± 18 mN/mm^2 and 103 ± 23 mN/mm^2, respectively. This is remarkable, as the amount of BSA is still four times lower in the BSA/PEO patch. One explanation for this is the easier positioning of the electrospun BSA/PEO patch versus the soaked BSA patch. The electrospun patch dissolves and becomes slightly sticky as soon as it gets in contact with water. Due to the stickiness, the two vessel stumps hold together enabling a better contact with the tissue. The same behavior is observed for BSA-loaded patches made from PVA and gelatin. In contrary, the patch soaked in liquid BSA is sticky from the beginning, and therefore more difficult to handle.

Pre-clinical trials, where we tested the handling of the layered BSA/PEO patch in a realistic setup, demonstrated the advantages of this patch compared to a patch that was soaked in liquid BSA. Due to the dry state of the patch, storage and transport is uncomplicated and does not require continuous cooling. During surgery, the patch can be easily cut to the required size. The patch is pliable, mechanically stable, and can be handled easily. An additional advantage may be the improvement of the chemical stability of BSA by PEO, an effect that is used for drug delivery [55]. The performance of the BSA-loaded patch during surgery, the long-term effects after LAVA and the shelf-life of the patch have to be further tested.

III.5   Conclusion

Electrospinning is a relatively simple technique and enables the entrapment of proteins in polymer fibers. In this study, BSA was successfully encapsulated in microfibers with PEO, PCL, PVA and gelatin using a blending electrospinning technique. By using a BSA/PEO (ratio 85/15 (w/w)) blend, high protein-loading was possible, leading to a tensile strength after LAVA, which is similar to LAVA with application of a patch soaked in liquid albumin solution. Additionally, the BSA/PEO blend was outstanding regarding the stability of the electrospinning process and the patch enabled an easy handling during surgery. In comparison, fibers from PVA, PCL, and gelatin were limited in BSA content, to which a stable electrospinning process is still possible, which in turn leads to a lower bonding strength after LAVA. Our findings support the potential of electrospun scaffolds with protein loading in biomedical applications.

Acknowledgments

Bibliography

[1] Annemarie Schönfeld, Mihai A. Constantinescu, Kirsten Peters, and Martin Frenz. Effects of different auxiliary polymers for electrospinning of albumin on the tensile strength after laser-tissue-soldering. *Biomedical Materials*, submitted:1–12, 2016.

[2] Lawrence S. Bass and Michael R. Treat. Laser tissue welding: A comprehensive review of current and future. *Lasers in Surgery and Medicine*, 17(4):315–349, 1995.

[3] I.C.D.Y.M. Wolf -de Jonge, J.F. Beek, and R. Balm. 25 Years of Laser Assisted Vascular Anastomosis (LAVA): What Have We Learned? *European Journal of Vascular and Endovascular Surgery*, 27(5):466–476, may 2004.

[4] Beat Ott, Mihai A. Constantinescu, Dominique Erni, Andrej Banic, Thomas Schaffner, and Martin Frenz. Intraluminal laser light source and external solder: In vivo evaluation of a new technique for microvascular anastomosis. *Lasers in Surgery and Medicine*, 35(4):312–316, oct 2004.

[5] Karen M McNally, Brian S Sorg, Ashley J Welch, Judith M Dawes, and Earl R Owen. Photothermal effects of laser tissue soldering. *Physics in Medicine and Biology*, 44(4):983–1002, apr 1999.

[6] Brian D. Byrd, Douglas L. Heintzelman, and Karen M. McNally-Heintzelman. Absorption properties of alternative chromophores for use in laser tissue soldering applications. *Biomedical sciences instrumentation*, 39:6–11, 2003.

[7] Giuseppe Esposito, Francesca Rossi, Paolo Matteini, Alba Scerrati, Alfredo Puca, Alessio Albanese, Giacomo Rossi, Fulvio Ratto, Giulio Maira, and Roberto Pini. In vivo laser assisted microvascular repair and end-to-end anastomosis by means of indocyanine green-infused chitosan patches: A pilot study. *Lasers in Surgery and Medicine*, 45(5):318–325, jul 2013.

[8] Daniel S. Schöni, Serge Bogni, Amadé Bregy, Amina Wirth, Andreas Raabe, Istvan Vajtai, Uwe Pieles, Michael Reinert, and Martin Frenz. Nanoshell assisted laser soldering of vascular tissue. *Lasers in Surgery and Medicine*, 43(10):975–983, dec 2011.

[9] Dara R. Pabittei, Michal Heger, Ron Balm, Han E. H. Meijer, Bas de Mol, and Johan F. Beek. Electrospun Poly(ÉŻ-Caprolactone) Scaffold for Suture-Free Solder-Mediated Laser-Assisted Vessel Repair. *Photomedicine and Laser Surgery*, 29(1):19–25, jan 2011.

[10] Wei Wang. Instability, stabilization, and formulation of liquid protein pharmaceuticals. *International Journal of Pharmaceutics*, 185(2):129–188, aug 1999.

[11] Andreas Greiner and Joachim H. Wendorff. Electrospinning: A Fascinating Method for the Preparation of Ultrathin Fibers. *Angewandte Chemie International Edition*, 46(30):5670–5703, jul 2007.

[12] Subramanian Sundarrajan, Kwong Luck Tan, Soon Huat Lim, and Seeram Ramakrishna. Electrospun Nanofibers for Air Filtration Applications. *Procedia Engineering*, 75:159–163, 2014.

[13] Seema Agarwal, Andreas Greiner, and Joachim H. Wendorff. Functional materials by electrospinning of polymers. *Progress in Polymer Science*, 38(6):963–991, jun 2013.

[14] N. M. Bedford and A. J. Steckl. Photocatalytic Self Cleaning Textile Fibers by Coaxial Electrospinning. *ACS Applied Materials & Interfaces*, 2(8):2448–2455, aug 2010.

[15] Quynh P Pham, Upma Sharma, and Antonios G Mikos. Electrospinning of Polymeric Nanofibers for Tissue Engineering Applications: A Review. *Tissue Engineering*, 12(5):1197–1211, may 2006.

[16] Nae Gyune Rim, Choongsoo S Shin, and Heungsoo Shin. Current approaches to electrospun nanofibers for tissue engineering. *Biomedical Materials*, 8(1):014102, feb 2013.

[17] J. Lannutti, D. Reneker, T. Ma, D. Tomasko, and D. Farson. Electrospinning for tissue engineering scaffolds. *Materials Science and Engineering: C*, 27(3):504–509, apr 2007.

[18] Ali Tamayol, Mohsen Akbari, Nasim Annabi, Arghya Paul, Ali Khademhosseini, and David Juncker. Fiber-based tissue engineering: Progress, challenges, and opportunities. *Biotechnology Advances*, 31(5):669–687, sep 2013.

[19] Payam Zahedi, Iraj Rezaeian, Seyed-Omid Ranaei-Siadat, Seyed-Hassan Jafari, and Pitt Supaphol. A review on wound dressings with an emphasis on electrospun nanofibrous polymeric bandages. *Polymers for Advanced Technologies*, 21(2):n/a–n/a, 2009.

[20] Pim-on Rujitanaroj, Nuttaporn Pimpha, and Pitt Supaphol. Wound-dressing materials with antibacterial activity from electrospun gelatin fiber mats containing silver nanoparticles. *Polymer*, 49(21):4723–4732, oct 2008.

[21] Martina Abrigo, Sally L. McArthur, and Peter Kingshott. Electrospun Nanofibers as Dressings for Chronic Wound Care: Advances, Challenges, and Future Prospects. *Macromolecular Bioscience*, 14(6):772–792, jun 2014.

[22] Anne J. Meinel, Oliver Germershaus, Tessa Luhmann, Hans P. Merkle, and Lorenz Meinel. Electrospun matrices for localized drug delivery: Current technologies and selected biomedical applications. *European Journal of Pharmaceutics and Biopharmaceutics*, 81(1):1–13, may 2012.

[23] Gareth R Williams, Nicholas P Chatterton, Tahir Nazir, Deng-Guang Yu, Li-Min Zhu, and Christopher J Branford-White. Electrospun nanofibers in drug delivery: recent developments and perspectives. *Therapeutic Delivery*, 3(4):515–533, apr 2012.

[24] Seeram Ramakrishna, Maedeh Zamani, and Molamma P Prabhakaran. Advances in drug delivery via electrospun and electrosprayed nanomaterials. *International Journal of Nanomedicine*, 8(1):2997, aug 2013.

[25] Young Ju Son, Woo Jin Kim, and Hyuk Sang Yoo. Therapeutic applications of electrospun nanofibers for drug delivery systems. *Archives of Pharmacal Research*, 37(1):69–78, jan 2014.

[26] Travis J. Sill and Horst A. von Recum. Electrospinning: Applications in drug delivery and tissue engineering. *Biomaterials*, 29(13):1989–2006, may 2008.

[27] Suwan N Jayasinghe. Cell electrospinning: a novel tool for functionalising fibres, scaffolds and membranes with living cells and other advanced materials for regenerative biology and medicine. *The Analyst*, 138(8):2215–2223, 2013.

[28] Samantha L. Sampson, Luisa Saraiva, Kenth Gustafsson, Suwan N. Jayasinghe, and Brian D. Robertson. Cell Electrospinning: An In Vitro and In Vivo Study. *Small*, 10(1):78–82, jan 2014.

[29] Annemarie Schönfeld, Zacharia Mbaidjol Kabra, Kirsten Peters, Mihai A. Constantinescu, and Martin Frenz. Binding of indocyanine green in polycaprolactone fibers using blend electrospinning for laser-assisted vascular anastomosis. *Lasers in Surgery and Medicine*, in prepara:1–28, 2016.

[30] Amadé Bregy, Serge Bogni, Vianney J.P. Bernau, Istvan Vajtai, Felix Vollbach, Alke Petri-Fink, Mihai Constantinescu, Heinrich Hofmann, Martin Frenz, and Michael Reinert. Solder doped polycaprolactone scaffold enables reproducible laser tissue soldering. *Lasers in Surgery and Medicine*, 40(10):716–725, dec 2008.

[31] Tomasz Kowalczyk, Aleksandra Nowicka, Danek Elbaum, and Tomasz A. Kowalewski. Electrospinning of Bovine Serum Albumin. Optimization and the Use for Production of Biosensors. *Biomacromolecules*, 9(7):2087–2090, jul 2008.

[32] Rouhollah Mehdinavaz Aghdam, Siamak Najarian, Saeed Shakhesi, Samaneh Khanlari, Keyvan Shaabani, and Shahriar Sharifi. Investigating the effect of PGA on physical and mechanical properties of electrospun PCL/PGA blend nanofibers. *Journal of Applied Polymer Science*, 124(1):123–131, apr 2012.

[33] Christina Tang, A. Evren Ozcam, Brendon Stout, and Saad A. Khan. Effect of pH on Protein Distribution in Electrospun PVA/BSA Composite Nanofibers. *Biomacromolecules*, 13(5):1269–1278, may 2012.

[34] Marina I. Santos, Ronald E. Unger, Rui A. Sousa, Rui L. Reis, and C. James Kirkpatrick. Crosstalk between osteoblasts and endothelial cells co-cultured on a polycaprolactone-starch scaffold and the in vitro development of vascularization. *Biomaterials*, 30(26):4407–4415, sep 2009.

[35] Hong Zhang, ChenGuang Zhao, Yunhui Zhao, Gongwen Tang, and Xiaoyan Yuan. Electrospinning of ultrafine core/shell fibers for biomedical applications. *Science China Chemistry*, 53(6):1246–1254, jun 2010.

[36] Honglin Qu, Suying Wei, and Zhanhu Guo. Coaxial electrospun nanostructures and their applications. *Journal of Materials Chemistry A*, 1(38):11513, 2013.

[37] Xiaoqiang Li, Yan Su, Shuiping Liu, Lianjiang Tan, Xiumei Mo, and Seeram Ramakrishna. Encapsulation of proteins in poly(l-lactide-co-caprolactone) fibers by emulsion electrospinning. *Colloids and Surfaces B: Biointerfaces*, 75(2):418–424, feb 2010.

[38] Ye Yang, Xiaohong Li, Wenguo Cui, Shaobing Zhou, Rui Tan, and Chaoyang Wang. Structural stability and release profiles of proteins from coreâĂŘshell poly (DLâĂŘlactide) ultrafine fibers prepared by emulsion electrospinning. *Journal of Biomedical Materials Research Part A*, 86A(2):374–385, aug 2008.

[39] Chandra M. Valmikinathan, Steven Defroda, and Xiaojun Yu. Polycaprolactone and Bovine Serum Albumin Based Nanofibers for Controlled Release of Nerve Growth Factor. *Biomacromolecules*, 10(5):1084–1089, may 2009.

[40] Johannes Schindelin, Ignacio Arganda-Carreras, Erwin Frise, Verena Kaynig, Mark Longair, Tobias Pietzsch, Stephan Preibisch, Curtis Rueden, Stephan Saalfeld, Benjamin Schmid, Jean-Yves Tinevez, Daniel James White, Volker Hartenstein, Kevin Eliceiri, Pavel Tomancak, and Albert Cardona. Fiji: an open-source platform for biological-image analysis. *Nature Methods*, 9(7):676–682, jun 2012.

[41] Ying Yang, Zhidong Jia, Qiang Li, and Zhicheng Guan. Experimental investigation of the governing parameters in the electrospinning of polyethylene oxide solution. *IEEE Transactions on Dielectrics and Electrical Insulation*, 13(3):580–585, jun 2006.

[42] H. Mohammad Khanlou, B. Chin Ang, S. Talebian, A. Muhammad Afifi, and A. Andriyana. Electrospinning of polymethyl methacrylate nanofibers: optimization of processing parameters using the Taguchi design of experiments. *Textile Research Journal*, 85(4):356–368, mar 2015.

[43] Stuart R. Coles, Daniel K. Jacobs, James O. Meredith, Guy Barker, Andrew J. Clark, Kerry Kirwan, Jon Stanger, and Nick Tucker. A design of experiments (DoE) approach to material properties optimization of electrospun nanofibers. *Journal of Applied Polymer Science*, 117(4):2251–2257, aug 2010.

[44] J Deitzel. Controlled deposition of electrospun poly(ethylene oxide) fibers. *Polymer*, 42(19):8163–8170, sep 2001.

[45] Joachim H. Wendorff, Seema Agarwal, and Andreas. Greiner. *Electrospinning*. Wiley-VCH Verlag GmbH & Co. KGaA, Weinheim, Germany, 1. edition, apr 2012.

[46] Matthew G. McKee, Garth L. Wilkes, Ralph H. Colby, and Timothy E. Long. Correlations of Solution Rheology with Electrospun Fiber Formation of Linear and Branched Polyesters. *Macromolecules*, 37(5):1760–1767, mar 2004.

[47] Y Mohammadi, M Soleimani, M Fallahi-Sichani, a Gazme, V Haddadi-Asl, E Arefian, J Kiani, R Moradi, a Atashi, and N Ahmadbeigi. Nanofibrous poly(epsilon-caprolactone)/poly(vinyl alcohol)/chitosan hybrid scaffolds for bone tissue engineering using mesenchymal stem cells. *The International journal of artificial organs*, 30(3):204–11, mar 2007.

[48] Jun Zeng, Achim Aigner, Frank Czubayko, Thomas Kissel, Joachim H. Wendorff, and Andreas Greiner. Poly(vinyl alcohol) Nanofibers by Electrospinning as a Protein Delivery System and the Retardation of Enzyme Release by Additional Polymer Coatings. *Biomacromolecules*, 6(3):1484–1488, may 2005.

[49] Y. Wang and Y.-L. Hsieh. Immobilization of lipase enzyme in polyvinyl alcohol (PVA) nanofibrous membranes. *Journal of Membrane Science*, 309(1-2):73–81, feb 2008.

[50] Achim Salamon, Sandra van Vlierberghe, Ine van Nieuwenhove, Frank Baudisch, Geert-Jan Graulus, Verena Benecke, Kristin Alberti, Hans-Georg Neumann, Joachim Rychly, José Martins, Peter Dubruel, and Kirsten Peters. Gelatin-Based Hydrogels Promote Chondrogenic Differentiation of Human Adipose Tissue-Derived Mesenchymal Stem Cells In Vitro. *Materials*, 7(2):1342–1359, feb 2014.

[51] Zuwei Ma, Wei He, Thomas Yong, and S Ramakrishna. Grafting of Gelatin on Electrospun Poly(caprolactone) Nanofibers to Improve Endothelial Cell Spreading and Proliferation and to Control Cell Orientation. *Tissue Engineering*, 11(7-8):1149–1158, jul 2005.

[52] Yanzhong Zhang, Hongwei Ouyang, Chwee Teck Lim, Seeram Ramakrishna, and Zheng-Ming Huang. Electrospinning of gelatin fibers and gelatin/PCL composite fibrous scaffolds. *Journal of Biomedical Materials Research*, 72B(1):156–165, jan 2005.

[53] Wei Fu, Zhenling Liu, Bei Feng, Renjie Hu, Xiaomin He, Hao Wang, Meng Yin, Huimin Huang, Haibo Zhang, and Wei Wang. Electrospun gelatin/PCL and collagen/PLCL scaffolds for vascular tissue engineering. *International Journal of Nanomedicine*, 9(1):2335, may 2014.

[54] Fatemeh Roozbahani, Naznin Sultana, Davood Almasi, and Farnaz Naghizadeh. Effects of Chitosan Concentration on the Protein Release Behaviour of Electrospun Poly(ϵ-caprolactone)/Chitosan Nanofibers. *Journal of Nanomaterials*, 2015:1–11, apr 2015.

[55] S. Dhawan, K Dhawan, M Varma, and V R Sinha. Applications of Poly (ethylene oxide) in drug delivery systems. *Pharmaceutical Technology*, 29(9):82–96, 2005.

IV. *In vivo* laser-assisted vascular anastomosis using an electrospun layered solder patch: A pilot study

Abstract

Background and Objective: In this study we investigated the feasibility and efficacy of the layered electrospun patch to laser-assisted vascular anastomosis *in vivo* using pigs.

Materials and Methods: A blend of polycaprolactone and indocyanine green was electrospun, followed by electrospinning of albumin and polyethylene oxide to produce a pliable patch. The left rectus abdominis muscle was dissected and the artery of this flap was prepared for microsurgical anastomosis with the right cranial epigastric artery. The solder patch was wrapped around the blood vessel stumps; an intraluminal balloon catheter enabled an easy alignment and held the setup in place. The soldering energy was delivered via a diffusor fiber from the vessel lumen using a diode laser at 810 nm. After surgery, the pigs were observed for one week, followed by euthanasia and assessment of the viability of the flap.

Results: 4 pigs were treated. All anastomoses were patent after the surgery, no bleeding was observed. The animals behaved normal throughout the observation period, there were no complications. After the observation period of 6 to 8 days, however, the flap was devitalized and swollen, there was no perfusion of the flap for all animals. After opening, the site of the anastomosis was stuck to hard tissue and the vessel stumps looked grayish. In 3 of 4 experiments, the distal vessel end slipped easily out of the patch, and the stumps were occluded.

Conclusion: This study shows that the strength of the anastomosis was withstanding the blood flow and the blood pressure as no rupture or leakage was found. The handling of the layered patch was easy and straight forward. However, the flaps did not survive during the observation period, the vessels were not patent but occluded, showing denaturation in the Tunica media of the vascular wall. The thermal denaturation of the vascular wall has therefore to be limited by future optimized thermal modulation during the soldering procedure. Additionally, the cytotoxicology of the patches should be investigated.

IV.1 Motivation

Chapter III describes the development of a layered electrospun patch for LAVA. The aim of this pre-clinical study is to evaluate the handling of the newly developed patch during surgery, the patency of the anastomosis and the short-term success-rate of the new technique.

Previous *in vivo* studies in our group [1] investigated the applicability of a new solder carrier material [2], by performing LAVA on the saphenous artery. They described the superior handling properties of a 200 µm thin solder material possessing a good flexibility and pliability. It was

suggested, that the total irradiation time should be standardized and the thermal damage has to be investigated in order to improve the reproducibility of LAVA.

In this report, LAVA was performed using a flap model in pigs [Leckenby et al., manuscript in preparation]. This model was chosen because it enabled a direct evaluation of the vitality of the flap during the follow-up period. Furthermore, it allowed to observe the patency of the LAVA for blood immediately after surgery, as the flap should turn pink after the removal of the vessel clamps. Importantly, the position of the flap was easy to reach and unproblematic during recovery. For LAVA, no stay sutures were used, and an intraluminal setup was applied [3]. The follow-up time was 6 to 8 days for each of the 4 animals.

IV.2   Materials and Methods

IV.2.1   Materials

Polycaprolactone (PCL, average $M_n = 80000$), bovine serum albumin (BSA, lyophilized), and polyethylene oxide (PEO, average $M_n = 400000$)) were obtained from Sigma Aldrich (Saint Louis, MO). Methanol and chloroform were used in analytical grade from Merck KGaA (Darmstadt, Germany). Indocyanine green (ICG, IR-125) was obtained from Acros Organics (Geel, Belgium). All materials were used as received.

IV.2.2   Solder patches

For this *in vivo* study we used electrospun layered protein- and chromophore loaded patches. A ICG:PCL solution with a ratio of 1:10 was electrospun for 75 min. A 8.7 % (w/w) BSA/PEO (85/15 (w/w)) solution was directly spun onto the PCL/ICG layer for 180 min. The patch was cut into pieces of 10x20 mm and stored in the dark at room temperature, and used for *in vivo* experiments within one week.

For scanning electron microscopy (SEM), both layers were separately sputter coated with a 10 nm layer of gold and analyzed with the SEM (Zeiss, DSM982) (see chapter II and III). The micrographs are shown in figure IV.1. The total thickness of the patches was $550\pm 43\,\mu m$ (n=10 patches), with the PCL/ICG-layer being $279\pm62\mu m$ and the BSA/PEO-layer being $271\pm43\mu m$. The weight of the patch was $18.1\pm3.3\,mg$ (n=70 patches), the PCL/ICG layer weight $9.2\pm2.4\,mg$ and the BSA/PEO-layer $8.9\pm3.3\,mg$. The amount of BSA in the patch was thus calculated to be $7.5\pm2.8\,mg$.
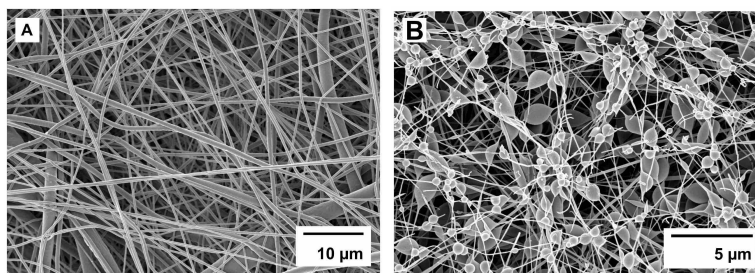

Figure IV.1: Scanning electron micrographs of electrospun fibers. Left: ICG-doped PCL fibers. Right: The albumin-doped PEO layer is directly electrospun onto the PCL/ICG layer.

IV.2.3 Surgical Protocol

This subsection was adapted from an original surgical protocol by Zacharia Mbaïdjol Kabra.

All animal experimentation were performed with the approval of the Animal Care Committee of the Canton of Bern, Switzerland BE137/14 and in accordance with the guidelines for the care and use of experimental animals of the *National Institutes of Health*. Four white female adult pigs with a weight of approximately 40 kg each were used for this study. They were transported 4 days prior to surgery from the breeder to the Animal hospital in Bern were they underwent a physical examination by the veterinary from the Experimental Research Unit (ESI, Insel Hospital, Bern). They were housed in a controlled environment, fed a standard diet until 12 hours prior to surgery and given an unrestricted access to water. All surgical procedures were performed under general anesthesia.

The animals were sedated intramuscularly with 20 mg/kg ketamine (Vetoquiol AG, Ittigen, Switzerland) and 2 mg/kg xylazine (Vetoquiol AG, Ittigen, Switzerland), followed by tracheal intubation 10 min later and intravenous administration of 0.5 mg/kg midazolam (University Hospital Bern, Switzerland) and 0.05 mg/kg atropine (University Hospital Bern, Switzerland). The animals were closely monitored during the operation and general anesthesia was maintained with halothane and 79 % nitrous oxide in oxygen. Ventilation was maintained with oxygen/air 1:3 and isoflurane (University Hospital Bern, Switzerland) 1–1.5 % vol. The intubated pigs were placed in a supine position and prepped and draped in a sterile manner. The same team of surgeons performed all the operations in a standardized way.

A left para-median incision was made extending from the junction of the costal margin and xiphoid process, down to approximately 5 cm inferior to the umbilicus with a 5x10 cm skin island. The external and internal oblique muscles were divided and the anterior rectus sheath was exposed. The sheath was opened to expose the rectus abdominis muscle. The cranial epigastric vessels emerged from the notch between the costal margin and xiphoid process and is accompanied by two veins. The arteries were ligated using medium Ligaclips (Ethicon US. LLC, Ohio, US). The muscle was then dissected in a proximal to distal fashion, ligating the medial and lateral rows of perforators given off at each of the multiple tendinous intersections. The distal rectus abdominis sheath was also opened on the distal part of the flap exposing the distal extremity of the flap's pedicle. The two veins were isolated and left intact while the artery was sectioned. The musculocutaneous flap, including the external and internal oblique muscles, were finally elevated off the rectus sheath. Arterial flow measurements were recorded at 7 cm from the xiphoid notch on the left and 7 cm from the distal left end (perivascular flow module, TS420, Transonic Systems Inc., Ithaca NY).

A second incision on the contra-lateral side was made extending inferiorly from the right xiphoid notch for 10 cm to expose the right cranial epigastric vessels. The vessels were then laid in a way that the distal end was level with the proximal extremity of the flap and were ligated using Ligaclips. A subcutaneous tunnel was then created inferior to the xiphoid process and the right cranial epigastric artery was passed to the left side. The left cranial epigastric artery was prepared for microsurgical anastomosis to the right cranial epigastric artery. The anastomosis was performed using intraluminal LAVA [3].

IV.2.4 Laser-assisted vascular anastomosis

A balloon catheter (Fox Plus, PTA Catheter, max dia = 3 mm, AP12003, Abbott, ALVE Ltd Beringen, Switzerland) was introduced in the distal end of the cranial epigastric artery and was retrogradely advanced through the whole flap, while flushing with saline water. The tip of the catheter was positioned in the proximal part of the right cranial epigastric artery. The right and left stumps were then carefully adjusted over the balloon catheter and held in place with

ST microsurgical clamps (Synovis, Birmingham, AL, USA). The diffusor laser fiber (400 µm core diameter, Laser und Medizintechnologie, Berlin, Germany) was introduced into the working channel of the balloon catheter advanced to the repair site. The solder patch with a size of 10x20 mm was wrapped around the vessel, sticking by itself, with an overlap of approximately 2 mm. The perfect alignment of the fiber is mandatory to melt the patch homogeneously over its whole length. The solder was then irradiated with the laser operating at an average output power of 3 W (continuous wave). The temperature was recorded on the surface of the patches and controlled during the laser irradiation with a thermal camera (A655, FLIR Systems, Inc., Wilsonville, Oregon). Therefore, a 6 mm^2 rectangle was positioned over the anastomosis, in which the temperature was averaged in real-time. After reaching an average surface temperature of 75 °C we continued irradiating the vessel for 30 s. To avoid that the temperature exceeded 85 °C during the soldering process, the irradiation was controlled by manually switching the laser on and off. The irradiation duration and the temperature were standardized, being 30 s at 75 to 85 °C. The total irradiation duration was in a narrow range between 50 and 58 s, ensuring that all vessels were equally treated. This technique enabled an equal endpoint for all anastomoses, and was independent from the surgeon. After soldering, the laser fiber and the balloon catheter were removed and the distal cranial epigastric artery clipped (figure IV.2). 5,000 U Heparin were given just prior to the removal of vessel clamps. Patency of the anastomosis and viability of the flap were assessed and arterial flow was again recorded 25 mm proximal and distal to the anastomosis. Laser Doppler images were obtained prior to the removal of the clamps and directly after. Finally, the wound was closed by stitching of 3 layers and Opsite spray (Smith and Nephew GmbH, Hamburg, Germany) was applied on the skin. After complete recovery from sedation, the pigs were discharged to the veterinary hospital for surveillance.
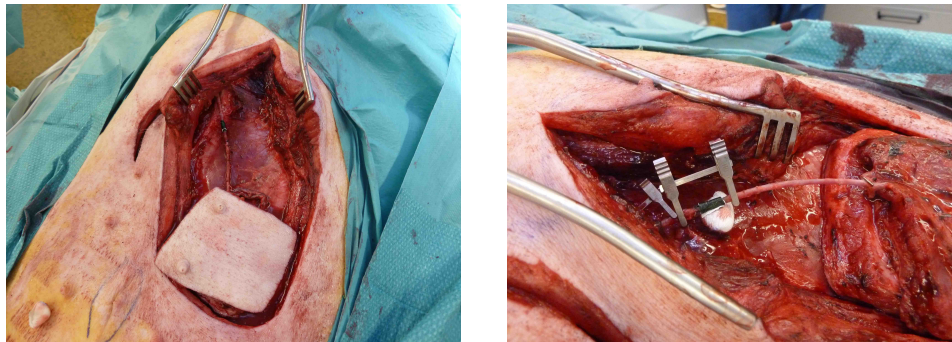
Figure IV.2: Anastomosis after LAVA. Left side: Overview. The rectus abdominis muscle was exposed, with the two veins distal to the muscle still attached. LAVA of the right and left cranial epigastric artery was performed. Right side: Zoomed picture with the green solder patch.

IV.2.5   Euthanasia and follow-up

6 to 8 days later, the pigs were re-operated. First, Laser Doppler images (EasyLDI, Aïmago, SA, Lausanne, Switzerland) were taken. Thereafter, access to the anastomosis was gained by opening the flap through the previous stitches. The viability of the flap was assessed and the vessel was harvested for histology and stored in 4 % formaldehyde solution (G256, Dr. Grogg Chemie AG, Stettlen, Switzerland). The pigs were euthanized by intravenous perfusion of 40 mmol potassium chloride (University Hospital Bern, Switzerland) given during deep anesthesia. The 1-week time-point for the follow-up was chosen because initial wound healing should be finished by then.

IV.2.6 Temperature curve

After surgery, the temperature data were analyzed and processed using Matlab (version R2012b, MathWorks, Inc., Natick, Massachusetts, US). The average temperature of a $6\,mm^2$ surface was calculated for each camera frame and plotted versus the irradiation time. The surface was determined by a 2 times $3\,mm$ rectangle centered over the hottest spot of the solder surface.

IV.2.7 Histological assessment

After fixation and storage in formaldehyde, the specimens were embedded in epon resins, sectioned, and stained with toluidine-blue and basic fuchsin. The detailed procedure is described in chapter II.

IV.3 Results

The patch was flexible and pliable and could easily be applied to blood vessels, which can reduce the operation time. If kept dry, the patch was not sticky and could be easily manipulated with forceps. As soon as the albumin layer got in contact with liquids, it became slightly sticky. This effect helped to align the patch and the vessels stumps and hold them together. Additionally, the patch could be easily cut and adapted to different vessel sizes during surgery. The patch can be sterilized by using methods such as ethylene oxide or UV radiation [6]. The handling of the solder patch was improved, as compared to liquid solder [3] or a patch soaked in liquid BSA [4, 5].

Immediately after LAVA the arteries of all experiments were intact, tight, and patent for blood. The flaps appeared pink, demonstrating blood perfusion. Flow measurements revealed a flow through the anastomosis and the 2 veins (see figure IV.1). Laser Doppler images showed the perfusion of the flaps (figure IV.3A). The whole operation, starting with the first incision and ending with the closure of the wound, took $3\,h\,15\,min$ to $4\,h\,10\,min$. Laser tissue soldering, starting and ending with the insertion/removal of the balloon catheter, lasted 12 to $20\,min$. The surgeons were satisfied with the presented LAVA technique, the handling of the patch, and awaited a positive outcome of the surgery.
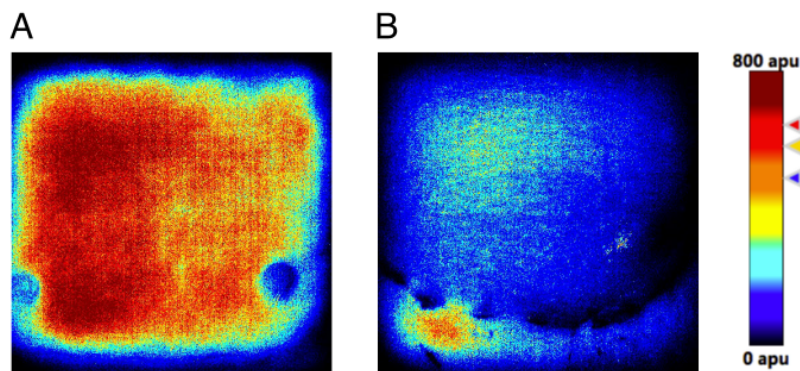

Figure IV.3: Doppler Images. **A:** Immediately after LAVA. **B:** During follow-up after 1 week.

Table IV.1: Flow measurements before and directly after LAVA. Before LAVA, the flow was recorded at the right cranial epigastric artery (proximal) and the left cranial epigastric artery (distal). Measurements at the left cranial epigastric artery were performed without clipping the left epigastric artery distal to the flap, except for pig 1, where we thus measured a reduced flow. Additionally, the flow of the left cranial epigastric artery distal to the flap was determined. After LAVA, we measured the cranial epigastric artery distal and proximal to the anastomosis, and the two veins distal to the flap. For pig 1 only one vein was measured, due to a mistake.

		proximal to anastomosis [ml/min]	distal to anastomosis [ml/min]	distal to flap [ml/min]	veins, distal to flap [ml/min]
pig 1	before LAVA	17.1	5.6 (artery clipped)	n.a.	-
	after LAVA	4.7	3.7	-	2.7
pig 2	before LAVA	10.9	19.7	13.8	-
	after LAVA	3.4	3.5	-	(1) 1.3 and (2) 0.5
pig 3	before LAVA	8.8	13.0	3.5	-
	after LAVA	2.9	2.9	-	(1) 0.8 and (2) 0.4
pig 4	before LAVA	11.2	21.3	3.6	-
	after LAVA	7.8	7.9	-	(1) 3.9 and (2) 0.1

All four pigs survived the procedure and the observation period. During the first days, the pigs behaved normal and there were no complications. After 4 to 6 days, the flap started to appear violet. After 6 to 8 days the animals were euthanized, as intended. The flaps looked macroscopically devitalized, swollen and violet (figure IV.6). The patches were stuck to hard tissue and the position of the anastomosis was difficult to find. No vessel rupture has been observed, but the distal vessel stumps slipped easily out of the patch sleeve for 3 out of 4 cases. All vessels were thrombotic and the flap was not perfused with blood.

The temperature curve during soldering is shown in figure IV.4. The temperature increased fast, the target temperature of 75 °C for all pigs was reached after approx. 5 s. During *in vitro* experiments the increase was slower, see chapter VI, figure VI.1. Furthermore, the irradiation duration at the target temperature was longer than expected, ranging from 35 to 43 s.

Figure IV.5 shows a scheme of the soldering setup with the vessel wall and the layered patch. Histological assessment after follow-up (see figure IV.7) revealed well-maintained structures of the Tunica adventitia, media and interna across the anastomotic site. The T. interna with its endothelium seemed to be intact and the patch adhered closely to the T. adventitia. The T. media, however, was compressed and shrunk. The blood vessels were occluded and an amalgam-like structure, including cells, was visible. These histologies were compared to an acute experiment, where the artery was dissected directly after LAVA (see figure IV.8). Again, the patch adhered closely to the T. adventitia. Alterations of the arterial wall are clearly visible when comparing them to native arteries. As can be seen in figures IV.7 and IV.8, the part of the arterial wall that was covered with the patch was compressed and appears very dense over its full cross section. On the contrary, loosely arranged collagen fibers were visible in the uncovered tissue. The endothelium appeared structurally intact by the treatment.
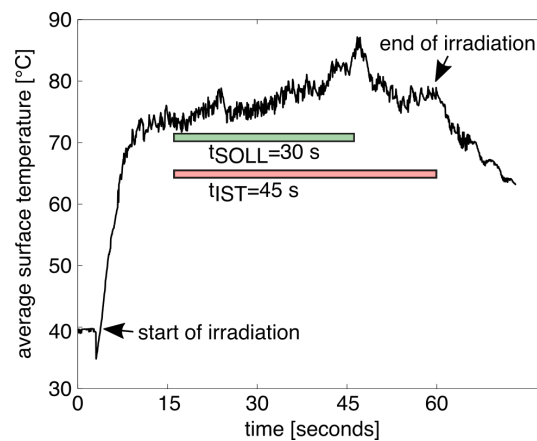
Figure IV.4: Typical average surface temperature of the patch surface during soldering.
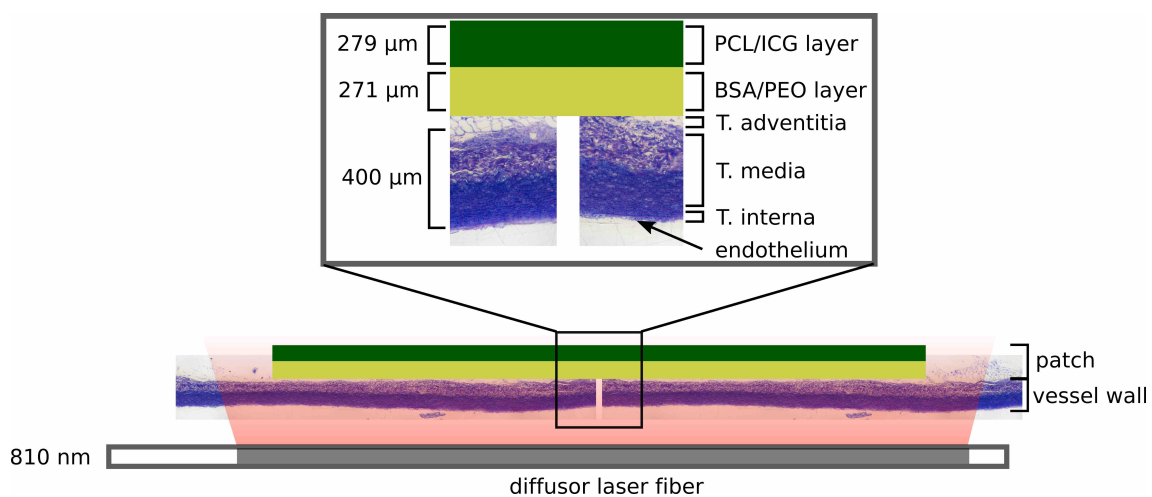
Figure IV.5: Scheme of soldering setup with the blood vessel wall, the layered patch, and the laser diffusor fiber. The thicknesses are illustrated to scale. The length of the patch is 10 mm and the length of the diffusor fiber is 15 mm.

IV.4   Discussion

Chapter II and III demonstrated the potential of electrospun patches for LAVA in *in vitro* experiments using rabbit aortas. In this *in vivo* study, involving pigs, we have shown that soldered blood vessels withstand the blood pressure immediately after laser anastomosis. Furthermore, we observed that after a few days the thermally damaged vessels occluded in the area of thermal exposure and that the flap was not perfused with blood. The future development of the LAVA technique will thus have to focus on an optimized thermal modulation during the soldering procedure to limit vascular wall denaturation and subsequent clotting. Alternative measures would include higher oral or intravenous anticoagulation dosages in the protocol. A sutured

Figure IV.6: Follow up after 1 week. Left side: The flap appeared devitalized, swollen and violet. Right side: The site of anastomosis and the patch were surrounded by necrotic tissue.

control group was not yet included in this study according to the animal approval to reduce the number of sacrificed animals and due to a large number of reports in the literature d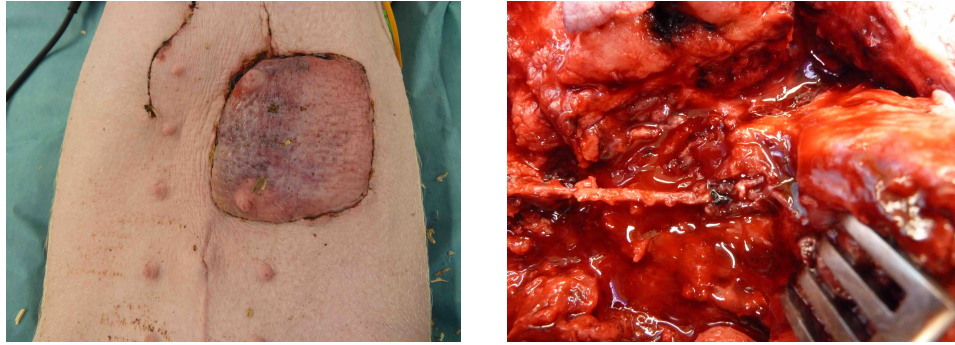escribing patency rates of over 90 %. However, a control group is vital to investigate and understand the causes for vessel occlusion.

No leakage of the chromophore during soldering was observed, demonstrating the great advantage of ICG-loaded fibers. This ensures that peripheral tissue was not stained and remained unheated, as histologies have demonstrated.

Currently an infrared camera on a tripod was used to observe the surface temperature of the patch during soldering. This method was not very efficient due to the limited space near the operating table. While setting up the thermal camera, a rectangle of $6\,mm^2$ is positioned at the place the anastomosis. According to this area, the average temperature during soldering is monitored in real-time to assess the target temperature and the temperature range of 75 to 85 °C and thus to start the timer and to manually control the laser. This setup is simple and straightforward during *in vitro* testing, however, *in vivo* this process is problematic. One reason is the smaller field of view due to the farther positioning of the thermal camera. Another difficulty is the continuous respiratory movement of the pig, that displaces the $6\,mm^2$ rectangle. Therefore, the temperature of the patch surface during soldering was underestimated and the soldering duration was too long. Another serious drawback of the temperature evaluation was that we were mainly interested in the temperature at the T. interna, but measuring at the surface of the patch. Thermocouples that are placed within the tissue could be helpful, however, the steel needle probe might lead to photon absorption. Hence, the patch-surface-temperature would lower than the actual measurement result. Moreover, the contact with the steel needle probe might conduct the heat during soldering, leading to unwanted cooling. A potential alternative are infrared fibers to monitor the temperature in real-time [7–9].

Although the surgery itself apparantly went very well, the patch was surrounded be necrotic, hard tissue for all 4 experiments after one week of recovery time. This could be due to the compression and alteration of the collagen wall, as histologies showed. Sharon Thomsen *et al.* demonstrated that laser-induced effects lead to different tissue damages, including non-lethal and lethal cellular damage. The repair and healing processes are not specific to laser irradiation and depend on the extent of damage and the sort of damage, i.e. photothermal, photochemical, or photomechanical. Typical healing processes are DNA and protein synthesis, resolution of tissue edema, thrombosis, hemorrhage and wound healing with scar tissue formation [10]. A reduction of the temperature during soldering might be required and is investigated in chapter V.

The importance of an intact endothelium to prevent pathological vascular changes has been
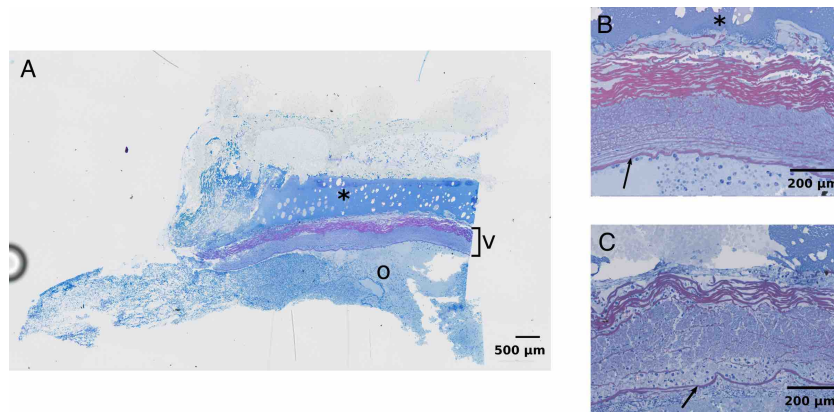
Figure IV.7: Histological assessment during the follow up at 1 week, using epon embedding. **A:** Longitudinal whole-mount sections show the patch (asterisks) closely adhering to the vessel wall (marked with v). The lumen of the vessel was occluded, and cells were visible in the amalgam-like structure (marked with o). **B:** Detailed view of the arterial wall after thermal treatment. Structural alterations were observed, after comparing to untreated arterial wall (**C**). The collagen fibers of the thermally treated vessel appear dense and well sorted, whereas the collagen fibers of untreated vessel wall are loosely arranged. The T. interna with its endothelium (arrow) was intact after LAVA.

stated elsewhere [11–13]. Shaw *et al.* suggested, that damages of the endothelial cell layer leads to the activation of platelets and fibrin and erythrocyte activation that produce an organized, occlusive thrombus [14]. However, in all histologies, the T. interna with its endothelium was clearly visible and seemed to be structurally unaffected by the heat treatment. Another study reports damage of endothelial layer solely by inflation with a balloon catheter [15]. Hence, a control, that is not soldered, but treated with the balloon catheter, should be included in upcoming *in vivo* studies.

Another major reason for the formation of scar tissue could be responses to foreign material or to non-sterility of the patch. Thus, the patch should be sterilized before surgery. The cytotoxicity of the patch is investigated and discussed in the following chapter.

IV.5   Conclusion

This study serves as a pre-clinical step towards the application of LAVA and shows the potential of the layered electrospun patch. All vessels were patent directly after LAVA, demonstrating an adequate bonding strength. After a few days, however, all vessels were occluded and the flaps were not perfused with blood. Possible reasons for this are thermal damage and toxicity of the patch. These two problems will be addressed in the following chapters.
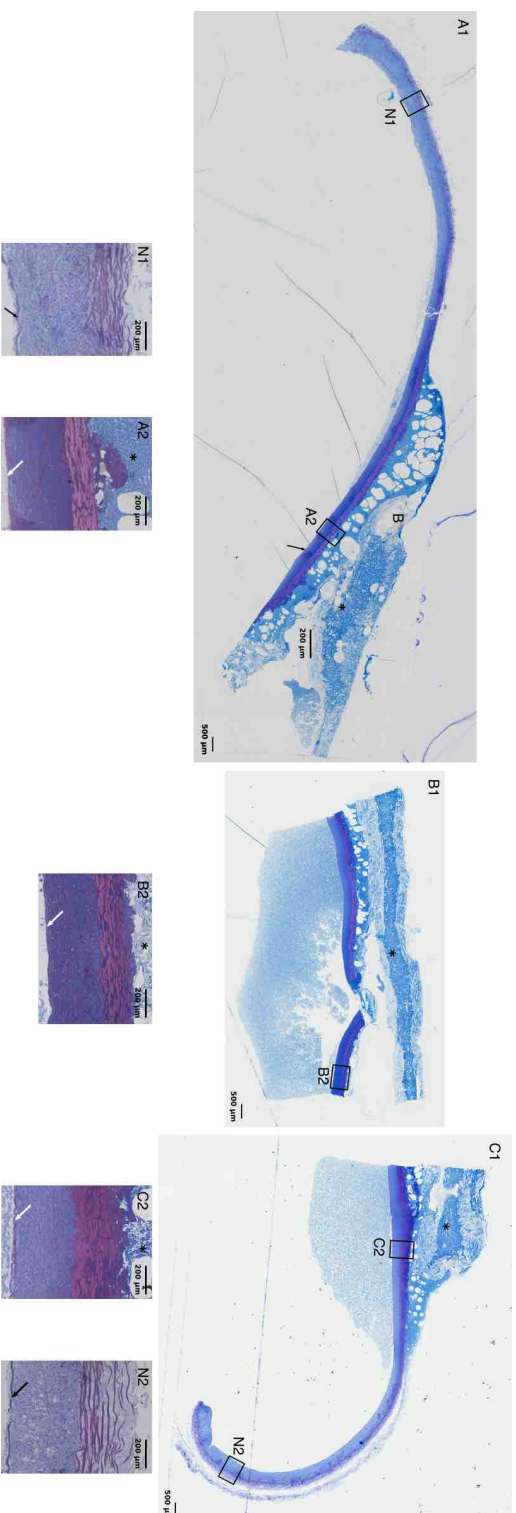
Figure IV.8: Histological assessment directly after LAVA, using epon embedding. **A1, B1, C1:** Longitudinal whole-mount sections showing the patch (asterisks) closely adhering to the T. adventitia. **A2, B2, C2:** Detailed view of the arterial wall after thermal treatment. Structural alterations were observed, the T. media was compressed and was shrinking. Fewer cell cores (blue) were visible as compared to native vessels, and the collagen fibers appeared well-structured. **N1, N2:** Detailed view of native (N) arterial wall, were the collagen fibers of the T. media seem loosely arranged. The internal elastic lamina (arrow) appeared not affected after LAVA, and the effect of the thermal treatment was restricted to the part of the arterial wall that was covered with the patch.

Bibliography

[1] Serge Bogni. *Improvement of the physical parameters for vascular and gastric laser soldering.* PhD thesis, University of Bern, 2011.

[2] Amadé Bregy, Serge Bogni, Vianney J.P. Bernau, Istvan Vajtai, Felix Vollbach, Alke Petri-Fink, Mihai Constantinescu, Heinrich Hofmann, Martin Frenz, and Michael Reinert. Solder doped polycaprolactone scaffold enables reproducible laser tissue soldering. *Lasers in Surgery and Medicine*, 40(10):716–725, dec 2008.

[3] Beat Ott, Mihai A. Constantinescu, Dominique Erni, Andrej Banic, Thomas Schaffner, and Martin Frenz. Intraluminal laser light source and external solder: In vivo evaluation of a new technique for microvascular anastomosis. *Lasers in Surgery and Medicine*, 35(4):312–316, oct 2004.

[4] Daniel S. Schöni, Serge Bogni, Amadé Bregy, Amina Wirth, Andreas Raabe, Istvan Vajtai, Uwe Pieles, Michael Reinert, and Martin Frenz. Nanoshell assisted laser soldering of vascular tissue. *Lasers in Surgery and Medicine*, 43(10):975–983, dec 2011.

[5] Annemarie Schönfeld, Zacharia Mbaidjol Kabra, Kirsten Peters, Mihai A. Constantinescu, and Martin Frenz. Binding of indocyanine green in polycaprolactone fibers using blend electrospinning for laser-assisted vascular anastomosis. *Lasers in Surgery and Medicine*, in prepara:1–28, 2016.

[6] A. Cipitria, A. Skelton, T. R. Dargaville, P. D. Dalton, and D. W. Hutmacher. Design, fabrication and characterization of PCL electrospun scaffoldsâĂŤa review. *Journal of Materials Chemistry*, 21(26):9419, oct 2011.

[7] Yaron Rabi and Abraham Katzir. Temporal heating profile influence on the immediate bond strength following laser tissue soldering. *Lasers in Surgery and Medicine*, 42(5):425–432, jun 2010.

[8] A. Abergel, I. Gabay, D. M. Fliss, A. Katzir, and Z. Gil. A Multi-wavelength Fiber-Optic Temperature-Controlled Laser Soldering System for Upper Aerodigestive Tract Reconstruction: An Animal Model. *Otolaryngology - Head and Neck Surgery*, 144(6):872–876, jun 2011.

[9] Ilan Gabay, Irina Barequet, David Varssano, Mordechai Rosner, and Abraham Katzir. Bonding surgical incisions using a temperature-controlled laser system based on a single infrared fiber. *Journal of Biomedical Optics*, 18(11):111416, sep 2013.

[10] Sharon Thomsen. Pathologic Analysis of Photothermal and Photomechanical Effects of Laser-Tissue Interactions. *Photochemistry and Photobiology*, 53(6):825–835, jun 1991.

[11] Peramaiyan Rajendran, Thamaraiselvan Rengarajan, Jayakumar Thangavel, Yutaka Nishigaki, Dhanapal Sakthisekaran, Gautam Sethi, and Ikuo Nishigaki. The Vascular Endothelium and Human Diseases. *International Journal of Biological Sciences*, 9(10):1057–1069, 2013.

[12] David Abraham and Oliver Distler. How does endothelial cell injury start? The role of endothelin in systemic sclerosis. *Arthritis Research & Therapy*, 9(Suppl 2):S2, 2007.

[13] Bruce Alberts, Alexander Johnson, Julian Lewis, Martin Raff, Keith Roberts, and Peter Walter. Blood Vessels and Endothelial Cells. In *Molecular Biology of the Cell*. Garland Science, New York, 4th edition, 2002.

[14] C J Shaw, G R ter Haar, I H Rivens, D A Giussani, and C C Lees. Pathophysiological mechanisms of high-intensity focused ultrasound-mediated vascular occlusion and relevance to non-invasive fetal surgery. *Journal of The Royal Society Interface*, 11(95):20140029–20140029, mar 2014.

[15] Theodore H Spaet, Michael B Stemerman, Frank J Veith, and I. Lejnieks. Intimal injury and regrowth in the rabbit aorta; medial smooth muscle cells as a source of neointima. *Circulation Research*, 36(1):58–70, jan 1975.

V. Adhesion and toxicity assay: Reactions of human primary cells on the electrospun, laser-soldered patch

Abstract

Background and Objectives: Chromophore- and protein-loaded electrospun patches may have potential application for laser-assisted vascular anastomosis. Here, I addressed the adhesion of cells at the patch and the cytotoxicity of the patch.

Materials and Methods: A solder patch, with a layer of polycaprolactone and indocyanine green and a second layer of polyethylene oxide and bovine serum albumin, was produced by electrospinning. The patches were irradiated with a diode laser, followed by ethylene-oxide sterilization. Human dermal microvascular endothelial cells and mesenchymal cells from liposuction tissue were seeded onto the patches to investigate the adhesion of cells. Additionally, these cells were incubated with extracts from patches for toxicology studies.

Results: The MTS assay and the vitality stain showed that no cells adhered to the patches. The cells exposed to the patch extracts showed severe changes in their morphology, indicating cytotoxicity.

Conclusion: A procedure for the measure of cell adhesion and cytotoxicity for the electrospun, laser soldered patch was developed. All materials of the patch, as well as potential ethylene oxide residues, should be tested towards cytotoxicity. A reduction of the indocyanine green amount might be required.

V.1 Motivation

We developed an electrospun patch that is composed of two layers. The first layer is made of a blend of the polymer polycaprolactone (PCL) together with the chromophore indocyanine green (ICG), see chapter II and the second layer is electrospun on top, consisting of bovine serum albumin (BSA) and the polymer polyethylene oxide (PEO), see chapter III. All materials are bio-compatible and FDA-approved. This pliable patch resulted in high and reproducible bonding strengths during *in vitro* experiments and ensured a constant concentration of the chromophore during soldering.

Little is known about the adhesion of cells at the surface of the laser-treated patch. The goal was thus to test the adhesion and proliferation of human primary cells on the laser-treated patch. Blood vessels consist of three layers which are built up by the following main cell types: The Tunica interna with endothelial cells, the T. media made of smooth muscle cells and the T. adventitia consisting of connective tissue with fibroblasts [1]. Preliminary tests were made with human dermal microvascular endothelial cells (HDMEC) and human mesenchymal stem or stromal cells from processed lipoaspirat (adipose tissue derived mesenchymal stromal cells/adMSC).

V.2 Materials and Methods

V.2.1 Preparation and laser-irradiation of the layered patch

Materials

Polycaprolactone (PCL, average M_n = 80000), polyethylene oxide (PEO, average M_n =400000), and bovine serum albumin (BSA, lyophilized) were obtained from Sigma Aldrich (Saint Louis, MO). Methanol and chloroform were used in analytical grade from Merck KGaA (Darmstadt, Germany). Indocyanine green (ICG, IR-125) was obtained from Acros Organics (Geel, Belgium). All materials were used as received.

Electrospinning

A blend 9 % (w/w) PCL and ICG at a ratio of 1:10 based on PCL in chloroform/methanol (75/25 (v/v)) was used to produce the first layer of the patch by electrospinning. Subsequently, a second layer of fibers was added made from 8.7 % (w/w) PEO and BSA (85/15 (w/w)) in water. More details about the preparation can be found in chapters II and III.

Laser treatment

The patches were fixed with pins on a Teflon plate. 3 ml of sterile PBS solution (Dulbecco's phosphate-buffered saline (DPBS), Gibco, Thermo Fisher Scientific, Waltham, MA, US) was added onto the patches to mimic the humid environment during *in vivo* soldering. Subsequently, the patches were irradiated using a diode laser at 810 nm with an irradiance of 2.5 W/cm^2. The temperature was observed with a thermal camera and controlled to be in the range of 75 to 85 °C with a manual switch. The irradiation was stopped after 45 s and the patches were allowed to dry overnight in the dark. The next day they were punched to a diameter of 14 mm. For sterilization the patches were treated with ethylene oxide (Institute for virology and immunology, Mittelhäusern, Switzerland), followed by keeping them in the dark for minimum 3 weeks, in order to aerate the patches and to get rid of ethylene oxide residues.

V.2.2 Cell culture

Culturing of cells

HDMEC and PLA cells were isolated by the team of the stem cell biology group and stored at passage 2 (P2) in liquid nitrogen. The cells were cultured in 75 cm^2 flasks (Greiner Bio-One GmbH, Frickenhausen, Germany) in cell culture medium at 37 °C in a humidified atmosphere with 5 % CO$_2$. Cell culture medium for HDMEC cells was endothelial cell medium MV2 (Promocell, Heidelberg, Germany), containing 5 % fetal calf serum, supplements and 1 % penicillin, streptomycin (Gibco, Thermo Fisher Scientific, Waltham, MA, US). For PLA cells we used Dulbecco's modified Eagle medium (DMEM, Invitrogen, Carlsbad, US) with 10 % fetal calf serum (PAN-Biotech, Aidenbach, Germany), and 1 % penicillin, streptomycin (Gibco). Generally, cells were plated at passage 4 (P4), HDMEC cells with a density of 32000 cells per cm^2 and PLA cells were seeded using 20000 cells per cm^2.
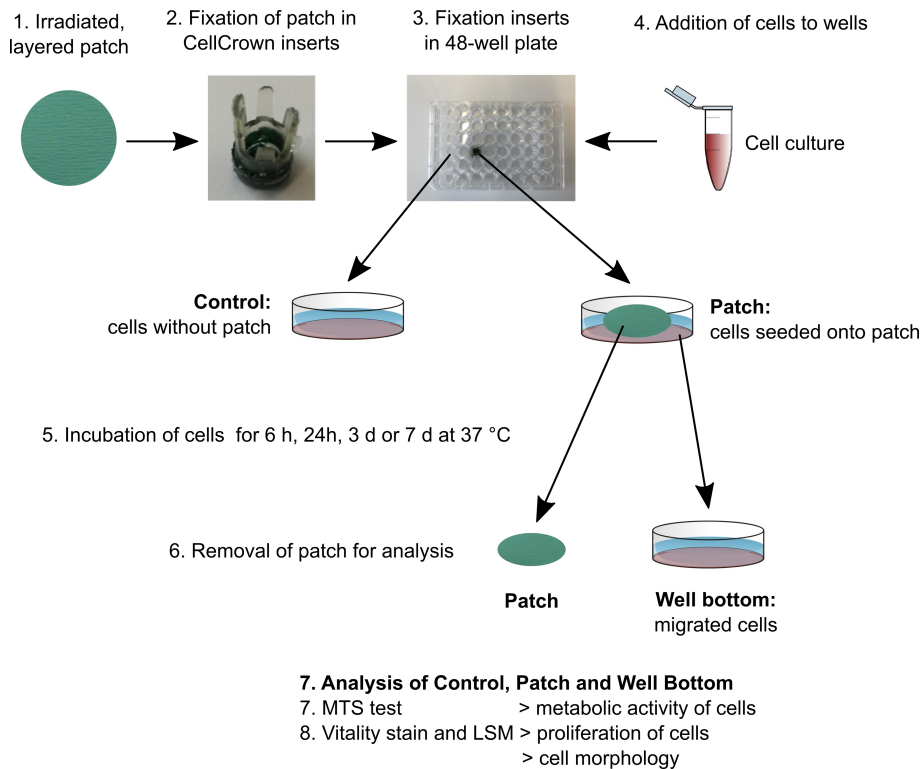
Figure V.1: Scheme of the adhesion assay. The irradiated patch was fixed into a 48-well plate using CellCrown inserts. Previously cultivated cells were added onto the patches and as a control directly onto wells. Cells were then incubated, followed by the transfer of the patches to fresh wells. The control, the patch, and the well bottom were analyzed using MTS assay and vitality stain.

Adhesion assay

Figure V.1 schematically shows the experiments performed to investigate the adhesion of cells onto the patch. The laser-treated patches were fixed in 48-well culture plates (Greiner) with CellCrown inserts (Scaffdex Oy, Tampere, Finland). The beforehand cultivated cells were washed twice with DPBS (PAN-Biotech GmbH, Aidenbach, Germany) and trypsinated at 37 °C for 4 to 5 min. Trypsination was stopped by adding cell culture media, followed by the centrifugation of the cells. Cells were re-suspended in 1 ml media and counted by using the Cellometer (Nexcelom Bioscience LLC, Lawrence, MA, USA). Cells were then seeded onto the patches and onto the 48-well plate directly as control with a seeding volume of 500 µl, using the cell density as written above. The cells were cultured for a period ranging from 6 hours to 7 days. The cell culture medium was exchanged with fresh medium after 24 hours, and then every other day. After cultivation, the patch with the insert was removed from the well and transferred into a fresh well, followed by addition of fresh media. Subsequently, the control, the patch and the well bottom were analyzed using MTS assay and vitality stain. The MTS and staining solution were added directly onto the patch, therefore enabling to observe the metabolic activity and the morphology of cells adhering to the patch.
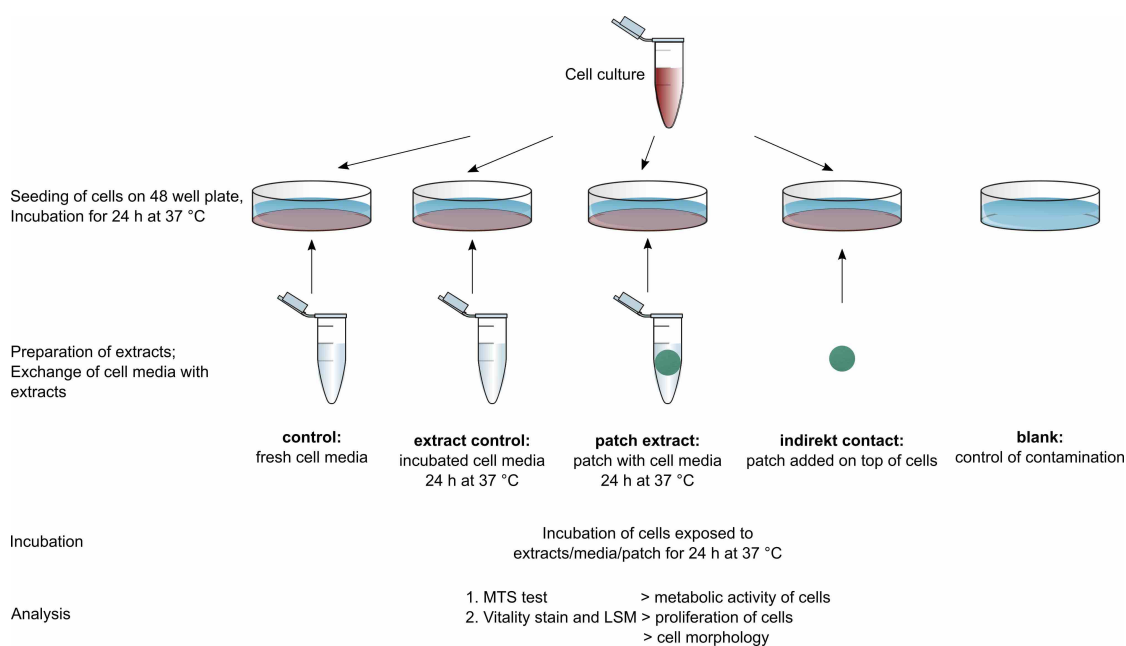
Figure V.2: Scheme of the toxicity assay. Previously cultivated cells were seeded onto a 48-well plate and incubated. Meanwhile, extracts of the patch were prepared by incubating patches in cell culture medium. As a control, cell culture medium without patches was incubated as well. Then, both extracts were added onto the seeded cells. An additional control was added, being fresh cell culture media. Furthermore, patches were added onto seeded cells, named as indirect contact test. A blank, being fresh media only, was included to explore potential contaminants. The cells with the extracts/media/patches were incubated for further 24 hours, followed by analysis using MTS assay and vitality stain.

Toxicity assay

A scheme of the toxicity assay can be seen in figure V.2. Cells were seeded into 48-well plates (Greiner) with a seeding volume of $500\,\mu l$ and cultured for 24 hours to receive approx. $80\,\%$ confluence. In parallel, extracts of the patch in cell culture media were prepared by adding 1 patch to $500\,\mu l$ medium and incubation at $37\,°C$ without agitation for 24 hours. Cell culture medium without patches was used as a control and incubated as well. In addition, patches were fixed into CellCrown inserts and carefully added onto the seeded cells for indirect contact tests, followed by addition of fresh cell culture medium. After cultivation of cells and preparation of all extracts, the cell medium was exchanged with the extracts. Cells were incubated with extracts and patches for further 24 hours and then analyzed.

V.2.3 Analysis

MTS assay for cell metabolic activity

The MTS assay with 3-(4,5-dimethylthiazol-2-yl)-5-(3-carboxymethoxyphenyl)-2-(4-sulfophenyl)-2H-tetrazolium, inner salt (MTS) was used to determine the metabolic activity of the cells, which could be related to the number of viable cells. MTS is converted into soluble formazan with dehydrogenase enzymes and is directly proportional to the number of cells, if the metabolic activity

of the cells remains unchanged.

For this assay, the depleted cell culture medium was removed and fresh medium was added. 20 µl per 100 µl medium MTS solution (CellTiter 96 Aqueous non-radioactive cell proliferation assay, Promocell, Heidelberg, Germany) was added and incubated with the cells for 1 or 2 hours at 37 °C. 100 µl of this solution were added to 96-well-plates (Greiner) and absorption was measured at 400 nm with background reduction at 620 nm using a microplate reader (Anthos 2010, Anthos Mikrosysteme GmbH, Krefeld, Germany).

Vitality stain and morphology

A staining solution was prepared as follows: Hoechst 33342 (1:2000, PanReac AppliChem GmbH, Darmstadt, Germany), Calcein AM (1:3000, AAT Bioquest, Inc., Sunnyvale, CA, US) and Propidiumiodid (PI, 1:50, Invitrogen, Carlsbad, US) were added to fresh media. The media of the cells was exchanged with the staining solution and incubated for 7 min (HDMEC) or 15 min (PLA). Then, the staining solution was removed from the wells and fresh media was added. The cells were observed with a laser scanning microscope (LSM780, Zeiss, Jena, Germany). A 20x objective with a numerical aperture of 0.5 and a working distance of 2.0 mm without immersion was used (EC Plan-Neofluar, Zeiss, Jena, Germany). Image size was usually 512 x 512 pixels, and 2 times averaging was used. Excitation wavelengths were 405 nm (diode laser, Hoechst 33342), 488 nm (argon laser, Calcein AM), and 514 nm (argon laser, PI).

V.3 Results

V.3.1 Adhesion assay

In general, no bacterial contamination of the wells was observed and the control cells grew without complications or abnormalities. The viability of the HDMEC after 6 and 24 hours and 3 and 7 days and adMSCs after 24 hours of seeding on the soldered patches is shown in table V.1. The viability was compared to cells cultured on the same well plate, which is made of tissue culture polystyrene (TCPS). For both cells types, no or a very low MTS conversion was found on the incubated patches. Reduced MTS conversion was measured at the bottoms of the wells where the patches were previously positioned. Due to the brittleness of the patches after laser irradiation, cracks in the patches could not be avoided when placing the patches into the cell culture inserts. The cells could therefore migrate through the patches and grow on the well bottom. In consequence of the usage of CellCrown inserts, a migration of cells around the patch can be excluded.

Microscopic analysis by LSM revealed a few, strongly vacuolized cells on the patches, see figure V.4 and V.3. On the well bottoms, where the patch was previously positioned, some cells could be detected, ranging from vacuolic cells (see figure V.4) to long and stretched cells (figure V.3). Thus, the phenotype of both cell types differed strongly from the TCPS controls. The intensity of the cell cores and the cytoplasm varies with the cell types, due to slight concentration changes of the staining solution. Additionally, the duration from the removal of the staining solution until taking the micrograph varies, which could be a reason for different intensities.

Additionally, I tested the behavior of the adMSC and HDMEC on the layered, non-irradiated patch and the non-irradiated PCL/ICG-layer (data not shown, no ethylene-oxide sterilization). Again, we found no cells on the surface of the patch. As for the irradiated patches, some intact cells on the well bottoms were detected.

Table V.1: Adhesion assay after incubation with MTS: Absorbance after incubation of HDMEC 01/16 and adMSC with MTS for 1 hour, and HDMEC 07/15 for 2 hours. Blank measurements being fresh media with MTS were subtracted and data represent 3 measurements each. AdMSC were measured in passage P3 and P4, both from the same donor.

cell type/donor	time point	control	well bottom	patch
HDMEC 07/15	6 h	0.236±0.013	0.121±0.023	0.018±0.009
	24 h	0.320±0.008	0.004±0.003	-0.019±0.023
	3 d	0.299±0.007	0.014±0.003	-0.003±0.007
	7 d	0.491±0.031	0.052±0.117	-0.013±0.008
HDMEC 01/16	24 h	0.153±0.004	0.030±0.016	0.004±0.008
adMSC 14/16 P3	24 h	0.240±0.005	0.126±0.025	0.030±0.021
adMSC 14/16 P4	24 h	0.106±0.003	0.081±0.034	0.011±0.007

Figure V.3: Typical confocal microscope images of the adhesion tests for HDMEC 01/16. Cell nuclei were stained blue, cytoplasm were stained green, dead cells appear red. Intact cells found in the well bottom of the soldered patch showed long and stretched cytoplasm. Scale bar is 50 µm.
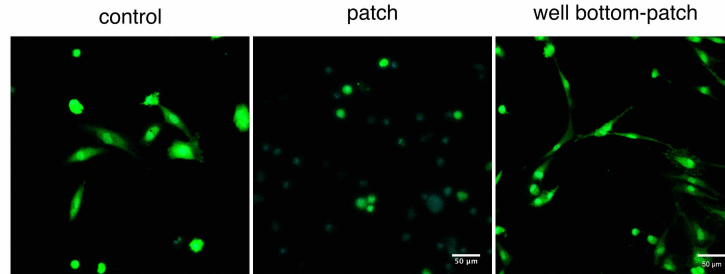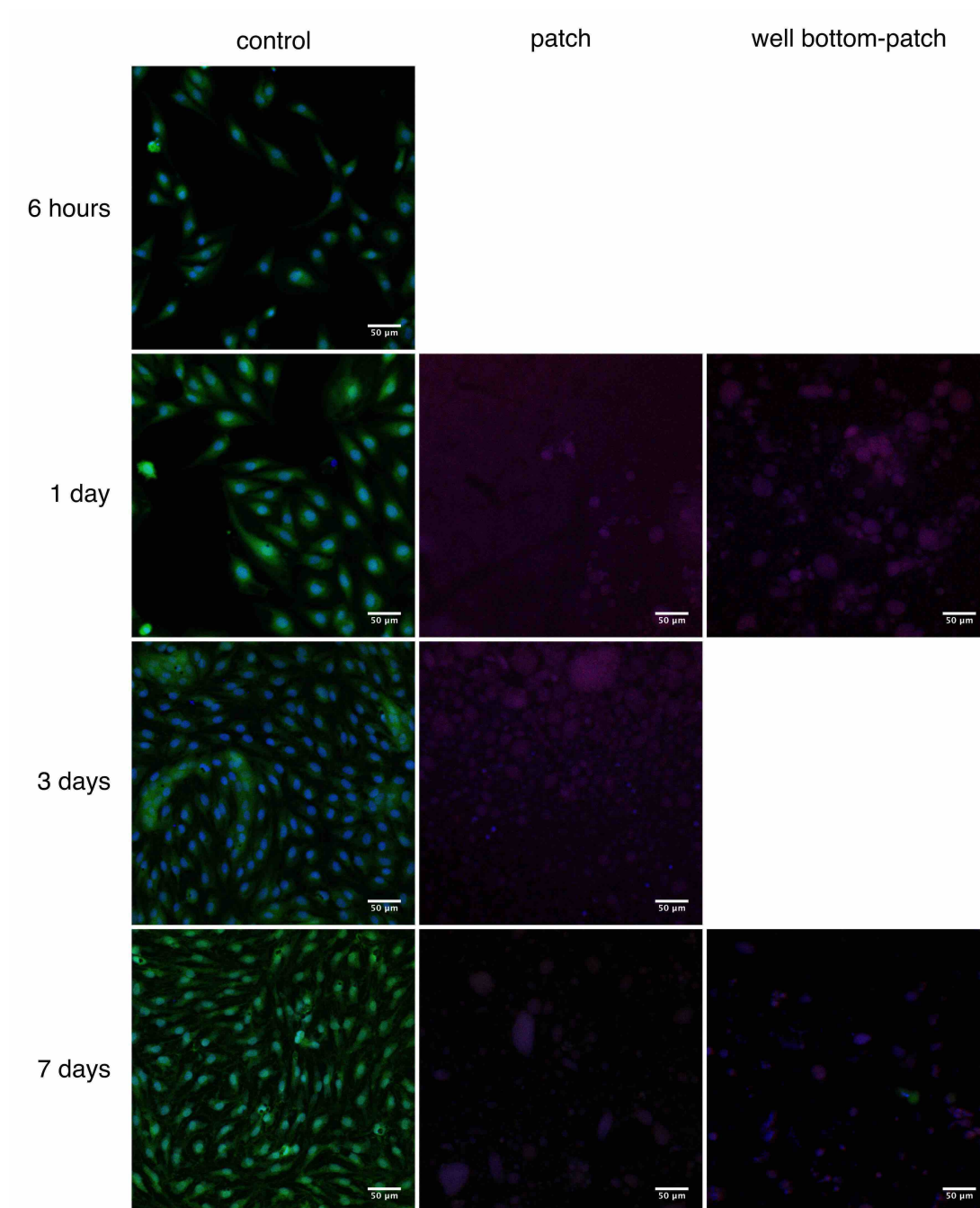
Figure V.4: Typical confocal microscope images of the adhesion tests for HDMEC 07/15. Cell nuclei were stained blue, cytoplasm was stained green, dead cells appear red. Some micrographs were not recorded due to time constraints. After 3 days of incubation the control cells were 100 % confluent and showed the typical microvascular endothelial morphology. Scale bar is 50 μm.

V.3.2 Toxicity assay

Due to the results of cell adhesion tests, toxicity tests were performed to evaluate whether the patch is cytotoxic. The control and the extract control showed the same absorbance amongst each cell type (table V.2). The metabolic activity after exposure to the patch extracts was decreased to approximately 60 % for HDMEC, for the adMSC it had no influence. After exposure with the patches (indirect contact test), the metabolic activity was decreased to approx. 75 % for both HDMEC and adMSC. After observation of these cells with the phase contrast microscope (no images taken) and the LSM (figure V.5), the differences between the controls and the extracts/indirect tests are more obvious. Fewer cells were observed for the HDMEC. However, the cytoskeleton was affected. The cells appeared vacuolic, and the cell membranes were less pronounced. Additionally, the cells were much smaller and the shape of the cells became spherical. After exposure to patch extract, the amount of cells was unchanged for the adMSC in comparison with the control. Although from the same donor, the adMSC P3 were intact after exposure to the patch extract, whereas the adMSC P4 were smaller and spherical. This effect cannot yet be explained, yet longer incubation with the extracts could lead to more significant results.

Table V.2: Toxicity assay after incubation with MTS: Absorbance after incubation of HDMEC and adMSC with MTS for 1 hour. AdMSC P3 and P4 were from the same donor. Blank measurements with fresh media and MTS with and without patch were subtracted and data represent 3 measurements each. In one case a methodical problem evolved. Therefore the result might be of limited value.

cell type/donor	time point	control	extract control	extract patch	indirect contact
HDMEC 01/16	24 h	0.267±0.005	0.280±0.028	0.165±0.032	0.221±0.062
adMSC 14/16 P3	24 h	0.204±0.013	0.191±0.009	0.226±0.021	(0.085±0.034)
adMSC 14/16 P4	24 h	0.124±0.009	0.108±0.008	0.102±0.002	0.087±0.009

V.4 Discussion

In this study, preliminary *in vitro* tests were performed to evaluate the adhesion and growth of cells on the soldered patch.

It was difficult to handle the soldered patches during cell culture. The patch bent in the cell culture medium and floated up to the surface. Special care had to be taken during the media changes, where the patch was attracted by the pipette tips. A solution to these problems was the usage of cell culture inserts [2], which immobilized the patch between two rings and enabled easy media exchange.

A further challenge was the sterilization of the electrospun patches. Common sterilization methods used are ethylene oxide, UV radiation, and soaking in ethanol [3]. Soaking in ethanol was not suitable, as the BSA/PEO layer dissolved in ethanol. We avoided the use of UV radiation, as it could potentially lead to the degradation of PCL [4]. Therefore, we chose to sterilize the patches using ethylene oxide. Due to the aeration of more than 3 weeks, we assumed that no ethylene oxide contaminants were left in the patches. However, the complete removal of ethylene oxide has to be thoroughly tested [5]. Furthermore, potential influence on the chemical or mechanical properties of ethylene oxide on the patch should be investigated.

Electrospun fibers elicited interest in tissue engineering, because the fiber structure can resemble the structure of the extracellular matrix and provides a 3-D framework for the attachment
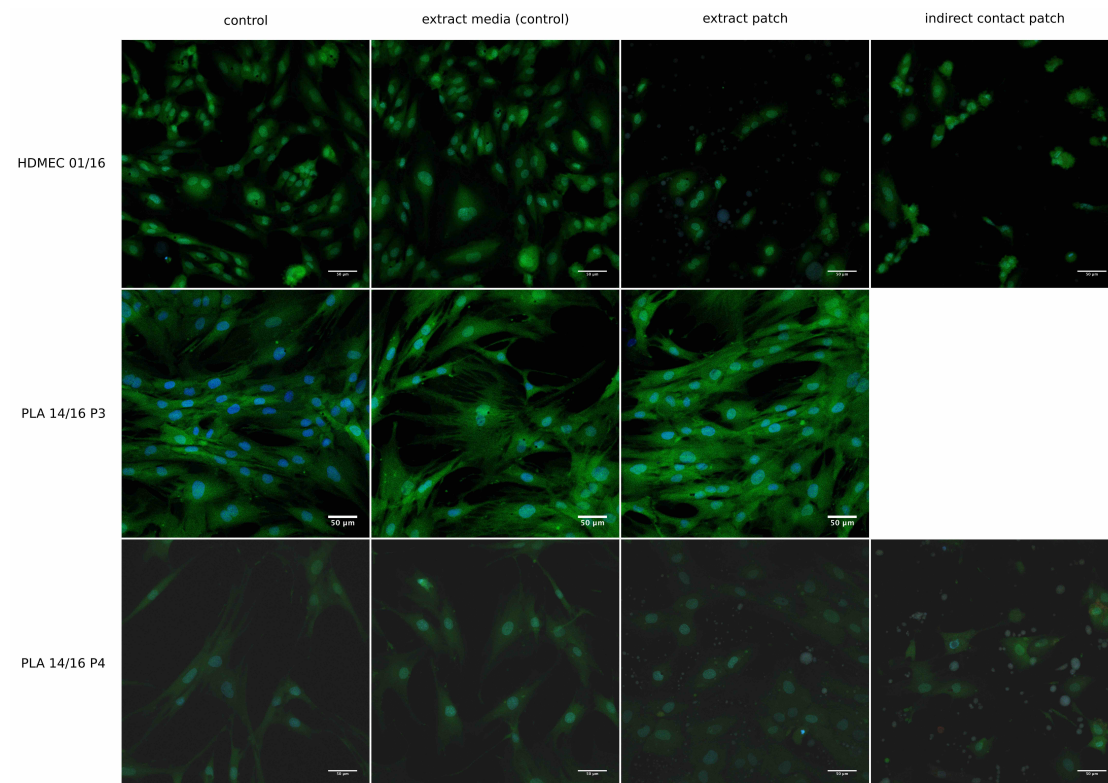
Figure V.5: Typical confocal microscope images of the toxicity tests. Cell nuclei were stained blue, cytoplasm was stained green, dead cells appear red. HDMEC and adMSC images were obtained with the same parameters, however the adMSC P4 images had to be contrast-enhanced. Due to a methodical problem with adMSC P3 with the indirect contact test no image was taken. Scale bar is 50 µm.

of cells [6, 7]. Additionally, the thickness of the fibers, the surface structure, and the porosity of the fibers are tunable, which are desirable features for tissue engineering [8]. However, the two polymers PCL and PEO, used for the solder patch, have melting points at 60 and 65 °C, respectively [9]. Due to melting, the soldered patches in this study are not composed of fibers, but possess a smooth surface (chapter II). The adhesion of cells on surfaces underlies a complex regulation and depends on many factors [10]. Furthermore, the success of biomaterials after implantation depends on many complex processes, such as repair processes, neo-vascularization, and inflammation [11].

Based on the results, no cells could adhere to the soldered patches and the patch is potentially cytotoxic. Interestingly, the MTS assay alone did not indicate a toxic reaction in the toxicity assay, which could be due to the short incubation period of 24 hours. Even though all used materials are biocompatible, more experiments have to be performed to systematically test the single electrospun materials for cell toxicity, before further experiments about cell adhesion should be conducted. Concerning ICG, a dose-depended ICG-related toxicity after staining the retina was reported [12–14]. Additionally, toxicity of ICG was observed in mitochondria of rat liver [15]. In our study, the cells were exposed to an ICG concentration of 1.3 ± 0.2 mg/ml. An effect on the toxicity after reduction of the ICG concentration in the patches should be investigated.

The BSA/PEO layer dissolves after in contact with liquids, it is therefore assumed that this layer has only minor impact on cell attachment. On the contrary, PCL is hydrophobic and a slowly degrading polymer [16]. PCL fibers have been extensively studied for applications as biomaterials and for tissue engineering. However, due to its hydrophobic properties, it lacks cell attachment and requires modification [3]. One possibility is its usage in blended fibers [8, 17, 18], another possibility is surface modification [19–21].

Numerous challenges have been investigated for reconstructive arterial surgery, among these are inflammatory processes that lead to thrombus formation, poor patency rates, tissue ingrowth, the polymer degradation, and the elasticity of the grafts [22, 23]. As a consequence, additional cell-based tests and *in vivo* experiments are required in order to optimize the properties of the patch used for LAVA.

V.5 Conclusion

In this study I tested the behavior of two human primary cell types on the laser-soldered patch. MTS assays were performed to measure the metabolic activity and the morphology of the cells was observed with fluorescence microscopy. No intact cells adhered on the surface of the patch. A toxicity assay with patch extracts and an indirect contact test was performed to evaluate the toxicity of the patch. It could be demonstrated, that the patch leads to smaller, vacuolic and round-shaped cells, indicating toxic effects. Based on these preliminary results, residues after ethylene oxide sterilization should be investigated first. Next, all materials have to be tested towards cytotoxicity and a reduction of the ICG-content might be required.

Bibliography

[1] Bruce Alberts, Alexander Johnson, Julian Lewis, Martin Raff, Keith Roberts, and Peter Walter. Blood Vessels and Endothelial Cells. In *Molecular Biology of the Cell*. Garland Science, New York, 4th edition, 2002.

[2] Lucie Bacakova, Parizek, Douglas, Kromka, Brady, Renzing, Voss, Jarosova, Palatinus, Lisa, Warnke, Lucie Bacakova, Bozena Novotna, Tesarek, Ryparova, and dos Santos. Nanofibrous

poly(lactide-co-glycolide) membranes loaded with diamond nanoparticles as promising substrates for bone tissue engineering. *International Journal of Nanomedicine*, 7:1931, apr 2012.

[3] A. Cipitria, A. Skelton, T. R. Dargaville, P. D. Dalton, and D. W. Hutmacher. Design, fabrication and characterization of PCL electrospun scaffoldsâĂŤa review. *Journal of Materials Chemistry*, 21(26):9419, oct 2011.

[4] Dong Yixiang, Thomas Yong, Susan Liao, Casey K. Chan, and S. Ramakrishna. Degradation of Electrospun Nanofiber Scaffold by Short Wave Length Ultraviolet Radiation Treatment and Its Potential Applications in Tissue Engineering. *Tissue Engineering Part A*, 14(8):1321–1329, aug 2008.

[5] P Vink and K Pleijsier. Aeration of ethylene oxide-sterilized polymers. *Biomaterials*, 7(3):225–230, may 1986.

[6] Quynh P Pham, Upma Sharma, and Antonios G Mikos. Electrospinning of Polymeric Nanofibers for Tissue Engineering Applications: A Review. *Tissue Engineering*, 12(5):1197–1211, may 2006.

[7] Seema Agarwal, Joachim H. Wendorff, and Andreas Greiner. Use of electrospinning technique for biomedical applications. *Polymer*, 49(26):5603–5621, dec 2008.

[8] Marina I. Santos, Kadriye Tuzlakoglu, Sabine Fuchs, Manuela E. Gomes, Kirsten Peters, Ronald E. Unger, Erhan Piskin, Rui L. Reis, and C. James Kirkpatrick. Endothelial cell colonization and angiogenic potential of combined nano- and micro-fibrous scaffolds for bone tissue engineering. *Biomaterials*, 29(32):4306–4313, nov 2008.

[9] Maria Ann Woodruff and Dietmar Werner Hutmacher. The return of a forgotten polymer-Polycaprolactone in the 21st century. *Progress in Polymer Science*, 35(10):1217–1256, oct 2010.

[10] M Lotfi, M Nejib, and M Naceur. Cell Adhesion to Biomaterials: Concept of Biocompatibility. In Rosario Pignatello, editor, *Advances in Biomaterials Science and Biomedical Applications*, chapter 8, pages 207–240. InTech, mar 2013.

[11] Ronald E. Unger, Anne Sartoris, Kirsten Peters, Antonella Motta, Claudio Migliaresi, Martin Kunkel, Ulrike Bulnheim, Joachim Rychly, and C. James Kirkpatrick. Tissue-like self-assembly in cocultures of endothelial cells and osteoblasts and the formation of microcapillary-like structures on three-dimensional porous biomaterials. *Biomaterials*, 28(27):3965–3976, sep 2007.

[12] Peter Stalmans, Elisabeth H. Van Aken, Marc Veckeneer, Eric J. Feron, and Ingeborg Stalmans. Toxic effect of indocyanine green on retinal pigment epithelium related to osmotic effects of the solvent. *American Journal of Ophthalmology*, 134(2):282–285, aug 2002.

[13] A Gandorfer, C Haritoglou, and A Kampik. Toxicity of indocyanine green in vitreoretinal surgery. *Dev Ophthalmol. Basel, Karger*, 42:69–81, 2008.

[14] Eduardo B. Rodrigues, Carsten H. Meyer, Stefan Mennel, and Michel E. Farah. Mechanisms of Intravitreal Toxicity of Indocyanine Green Dye. *Retina*, 27(7):958–970, sep 2007.

[15] Y Laperche. Toxic effects of indocyanine green on rat liver mitochondria. *Toxicology and Applied Pharmacology*, 41(2):377–387, aug 1977.

[16] Hak-Joon Sung, Carson Meredith, Chad Johnson, and Zorina S Galis. The effect of scaffold degradation rate on three-dimensional cell growth and angiogenesis. *Biomaterials*, 25(26):5735–5742, nov 2004.

[17] Wei He, Thomas Yong, Wee Eong Teo, Zuwei Ma, and Seeram Ramakrishna. Fabrication and Endothelialization of Collagen-Blended Biodegradable Polymer Nanofibers: Potential Vascular Graft for Blood Vessel Tissue Engineering. *Tissue Engineering*, 11(9-10):1574–1588, sep 2005.

[18] Y Mohammadi, M Soleimani, M Fallahi-Sichani, a Gazme, V Haddadi-Asl, E Arefian, J Kiani, R Moradi, a Atashi, and N Ahmadbeigi. Nanofibrous poly(epsilon-caprolactone)/poly(vinyl alcohol)/chitosan hybrid scaffolds for bone tissue engineering using mesenchymal stem cells. *The International journal of artificial organs*, 30(3):204–11, mar 2007.

[19] Nikola Kasálková, Petr Slepička, ZdeÅĹka Kolská, Petra Hodačová, Štěpánka Kučková, and Václav Švorčík. Grafting of bovine serum albumin proteins on plasma-modified polymers for potential application in tissue engineering. *Nanoscale Research Letters*, 9(1):161, oct 2014.

[20] Yuanyuan Duan, Zhongyi Wang, Wei Yan, Shaohai Wang, Shaofeng Zhang, and Jun Jia. Preparation of collagen-coated electrospun nanofibers by remote plasma treatment and their biological properties. *Journal of Biomaterials Science, Polymer Edition*, 18(9):1153–1164, jan 2007.

[21] Jeong Soo Park, Jung-Man Kim, Sung Jun Lee, Se Geun Lee, Young-Keun Jeong, Sung Eun Kim, and Sang Cheon Lee. Surface hydrolysis of fibrous poly(ϵ-caprolactone) scaffolds for enhanced osteoblast adhesion and proliferation. *Macromolecular Research*, 15(5):424–429, aug 2007.

[22] Swathi Ravi and Elliot L Chaikof. Biomaterials for vascular tissue engineering. *Regenerative Medicine*, 5(1):107–120, jan 2010.

[23] Toshiharu Shinoka, Dominique Shum-Tim, Peter X. Ma, Ronn E. Tanel, Noritaka Isogai, Robert Langer, Joseph P. Vacanti, and John E. Mayer. Creation Of Viable Pulmonary Artery Autografts Through Tissue Engineering. *The Journal of Thoracic and Cardiovascular Surgery*, 115(3):536–546, mar 1998.

VI. Influence of continuous versus pulsed temperature profiles on laser-assisted vascular anastomosis with an electrospun chromophore- and protein-loaded patch

Abstract

Background and Objectives: Laser-assisted vascular anastomosis using the chromophore indocyanine green (ICG) and the protein albumin (BSA) is an effective technique for the bonding of tissues. The objective of this study was to investigate the influence of different temperature profiles on the immediate bonding strength and to examine the thermal damage.

Materials and Methods: Rabbit aortas were subjected to *in vitro* LAVA, using an electrospun ICG-and BSA-loaded patch. The solder surface temperature was observed with an infrared camera, serving as a feedback to manually control the laser irradiation. Continuous temperature profiles with surface endpoint temperatures at 60, 70, 80, and 90 °C were explored, followed by tensile strength measurement. Arteries were embedded in MMA and epon and cut perpendicular to study thermal damage. Additionally, the influence of pulsed laser irradiation on the temperature profile and the tensile strength was explored.

Results: The endpoint temperatures, ranging from 60 to 90 °C using the continuous temperature profile led to tensile strengths from 69 ± 32 to $153\pm23\,\mathrm{mN/mm^2}$. The analysis of the histologies demonstrated similar thermal damage across these temperature ranges. Using pulsed laser irradiation, tensile strengths ranging from 47 ± 9 to $79\pm32\,\mathrm{mN/mm^2}$ were obtained.

Conclusions: The endpoint temperature during LAVA has a significant influence on the tensile strength and the thermal damage. Effective and reproducible LAVA might be achieved at endpoint temperatures from 60 to 70 °C. Pulsed energy deposition has potential to reduce thermal damage while achieving good tissue bonding, but requires a feed-back system to ensure reproducible results during surgery.

VI.1 Introduction

Tissue bonding of incisions is an important step in most surgical procedures. Conventional methods, namely sutures and staples, possess serious drawbacks, such as additional tissue injury, foreign body reactions, and difficult and tedious execution. Laser-tissue-soldering (LTS) can be faster, easier to apply, and less traumatic [1–3]. In LTS, laser energy is used to heat a solder that is applied to the approximated tissue edges. The tissue is subsequently heated by heat diffusion, leading to the alteration of the molecular structure. The tissue molecules can form bonds leading to tissue fusion.

The application of a solder consisting of the chromophore indocyanine green (ICG) and the protein albumin (BSA, from bovine serum) has been shown to be an effective tissue sealant [4, 5]. ICG selectively absorbs the laser wavelength, with a maximum of absorption at 800 nm, and converts the laser energy to heat, while BSA enhances the tissue fusion. A previous study (see chapter IV), involving laser-assisted vascular anastomosis (LAVA) of pig arteries, has shown, that the immediate bonding strength of this technique was withstanding the blood pressure. However, histological assessment revealed, that the tissue was thermally damaged, leading to the necrosis of the vessels and finally the occlusion of the arteries.

The endpoint of laser irradiation during LAVA is still ambiguous. Solder color change [6, 7] is one determinant for stopping laser irradiation, however by using this technique, the temperature profile is unknown, leading to thermal damage or low bonding strengths. This results in a low reproducibility of the tissue bonding and requires an experienced surgeon. Another common attempt is the application of a specific laser power and irradiation duration [8, 9]. This technique, though, ignores different tissue structures and thicknesses and different hydration states of the tissue. Another possibility is the usage of thermocameras, thermocouplers or infrared fibers to control the temperature by controlling the laser irradiance [10–12]. This approach is promising, but it requires prior knowledge about temperature curves that lead to a high bonding strength but at the same time minimally damaging the tissue. Bregy *et al.* demonstrated that there is only a narrow temperature range were LTS is effective. Low temperature lead to a weak bonding strength, whereas high temperatures lead to thermal damage [13].

During *in vivo* experiments we used an infrared camera to control the temperature during LAVA. The temperature at the solder surface was observed with the infrared camera, and hence the laser irradiation was manually controlled to keep the temperature between 75 and 85 °C for 30 s. Bogni *et al.* has introduced a thermal model to optimize the laser parameters and to understand the temperature distribution inside tissue during LAVA. Their simulations suggest the application of a pulsed irradiation with a high laser power, short pulses, and a highly absorbing solder, allowing repetitively heating the solder/vessel interface while remaining a physiological temperature at the endothelium [14].

The objective of this study is to investigate the influence of different end-point temperatures on the bonding strength and to assess thermal damage by using histology. Additionally, the feasibility of a pulsed energy deposition is investigated and the resulting temperature profiles are shown.

VI.2 Materials and Methods

VI.2.1 Materials

Polycaprolactone (PCL, average $M_n = 80000$), bovine serum albumin (BSA, lyophilized), and polyethylene oxide (PEO, average $M_n = 400000$)) were obtained from Sigma Aldrich (Saint Louis, MO). Methanol and chloroform were used in analytical grade from Merck KGaA (Darmstadt, Germany). Indocyanine green (ICG, IR-125) was obtained from Acros Organics (Geel, Belgium). All materials were used as received.

VI.2.2 Electrospinning of the layered patches

A 9 % (w/w) PCL solution in chloroform/methanol (75/25 (v/v)) with ICG at a ratio of 1:10 (w/w) ICG:PCL and a 8.7 % (w/w) BSA/PEO (85/15 (w/w)) solution in water was prepared.

Both solutions were stored in the dark, the PCL/ICG solution was kept at room temperature and the BSA/PEO solution was stored in the fridge at 4 °C.

For electrospinning, both blends were loaded into 5 ml syringes with a truncated needle (0.812 mm I.D.) that was connected with electrodes to a power supply. For the PCL/ICG blend a flow rate of 30 µL/min, a gap distance of 15 cm between the needle tip and the grounded collector plate, and an applied positive potential of 15 kV were employed and electrospun for 75 min. The BSA/PEO blend was electrospun subsequently and directly onto the PCL/ICG layer, by applying the following settings: flow rate of 30 µL/min, a gap distance of 15 cm, and a positive potential of 15 kV, with a duration of 180 min. The fibers were collected on a rotating aluminum plate at 1 rpm with a diameter of 10 cm to ensure a homogeneous distribution of the fibers. The whole setup was placed in a chamber, where the temperature and the humidity were well controlled to be 22 ± 1 °C and 30 ± 5 % RH. The resulting patches were stored in the dark at room temperature, and used for *in vitro* experiments within one month.

VI.2.3 *Ex vivo* laser soldering technique

The setup for LAVA, including treatment of the rabbit aortas, is described in detail in chapter II.

The patch was cut in pieces of 2x1 cm and topically applied over the position where the anastomosis has to be performed, with the PEO/BSA layer in direct contact with the artery. For the experiments with a continuous temperature profile, the laser was operated with an output power of 3 W in the continuous wave regime. Soldering was observed by involving an infrared camera (A655, FLIR Systems, Inc., Wilsonville, Oregon) and according to the surface temperature the laser was switched on and off manually to stabilize the desired temperature. End-point temperatures were 60, 70, 80 and 90 °C, and the irradiation was stopped after 45 s. For each trial ten measurements were made. The arteries used in this study had a diameter of 4.0 ± 0.2 mm (n=70 vessels), thus the irradiated surface was equal to 1.9 ± 0.1 cm^2 resulting in an irradiance of 1.6 ± 0.1 W/cm^2.

Different pulse lengths from 5 to 125 ms and frequency rates ranging from 0.25 to 10 Hz were applied for pulsed laser irradiation, while the output peak power was kept at 30 W, the highest power possible using the laser system Lina-30D (Intros Lasertechnologie GmbH, Heilbad Heiligenstadt, Germany).

VI.2.4 Evaluation of the temperature profile

During LAVA, the temperature on the surface of the patch was recorded. The camera was calibrated for a temperature range from -40 to 150 °C allowing an accuracy of $\pm$ 2 °C. The temperature was recorded with a frequency of 25 Hz. After soldering, the temperature data were analyzed and processed using Matlab (version R2014a, MathWorks, Inc., Natick, Massachusetts, USA). The average temperature of a 6 mm^2 surface was calculated for each camera frame and plotted versus the irradiation time. The surface was determined by a 2 times 3 mm rectangle centered over the hottest spot of the solder surface.

VI.2.5 Measurement of the tensile strength

The tensile strength of the soldered vessels was evaluated using a test stand with a fixed force gauge (BFG50, Mecmesin Limited, West Sussex, United Kingdom). The measurement was done 1 min after soldering, to avoid any desiccation of the sample. The vessel was fixed 2 mm from the

end of the patch with two surgical clamps that were attached to a moving table. The table was pulled with an electrically driven motor at a constant velocity of 30 mm/min. The maximum load on the specimen was recorded. The tensile strength was calculated by dividing the maximum load at the rupture time point by the cross-sectional area of the blood vessel, including the lumen and the vessel wall. Therefore, the external diameter of the vessel was measured with a caliper before LAVA.

VI.2.6 Histological assessment

The laser-induced thermal damage was assessed using histology with light microscopy. For histological assessment, rabbit aortas were obtained from the slaughterhouse, transported on ice, and processed within 4 hours. Immediately after soldering, the tissue samples were fixed in 4 % formaldehyde (G256, Dr. Grogg Chemie AG, Stettlen, Switzerland) and routinely processed in methylmethacrylate (MMA). Therefore, the samples were rinsed in water, dehydrated in ascending ethanol fractions, infiltrated and embedded in MMA. The embedded blocks were serially cut into 500 µm thick sections using a diamond saw. Subsequently, the specimens were mounted onto acrylic glass slides, and the sections were ground to a final thickness of 80 µm and stained superficially with toluidine blue combined with basic fuchsin.

For epon embedding, the specimen were subdivided into smaller samples and embedded in epon resin (Fluka, Buchs, Switzerland). Sections were cut and stained with toluidine blue and basic fuchsin, and studied using a Zeiss Axioplan microscope (Carl Zeiss GmbH, Jena, Germany). To assess the extent of thermal damage, rabbit aortas that were subjected to LAVA were fixed in formalin, followed by embedding in methyl methacrylate (MMA) or Epon. The evaluation of the embedding technique was not trivial. Paraffin embedding of tissues is a standard technique, however, paraffin could not infiltrate the electrospun patch and the aorta. Sectioning of paraffin embedded samples was therefore impossible, as the patch was very brittle and teared off the tissue. Additionally, it required washes with xylene, being a solvent for PCL. On the other hand, MMA is very hard and used for embedding of undecalcified bone [15]. Using MMA, the whole rabbit aorta could be sectioned, giving a overview about the tissue-patch interface. Additionally, embedding in epon was performed, which allowed thinner sectioning than was possible with MMA, and therefore enabled detailed evaluation of the structural characteristics of the arterial wall.

VI.3 Results

For both, the continuous and the pulsed temperature profile, the irradiation time was identical, being 45 s, to keep the duration in a clinically acceptable time and to avoid desiccation, while ensuring a good bonding strength. Temperatures above 100 °C were avoided, to circumvent too strong thermal damage, as well as the melting of the laser fiber and the balloon catheter.

VI.3.1 Continuous temperature profile: tensile strength and thermal damage

The results show that the temperature profile is an important parameter during LAVA. The continuous temperature profiles with endpoint temperatures ranging from 60 to 90 °C are shown in figure VI.1. The standard deviation for endpoint temperatures of 60 to 80 °C were in the range of ± 5 °C, whereas the standard deviation at 90 °C was higher with ± 10 °C. While lower endpoint temperatures from 60 to 80 were easy to control, the 90 samples were harder to control.
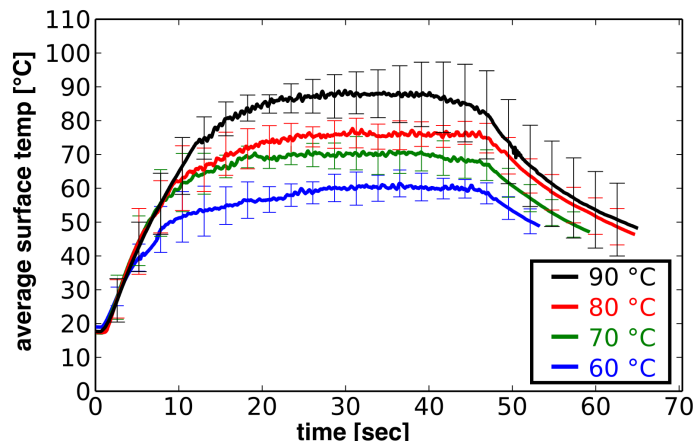
Figure VI.1: Solder-surface temperature of *in vitro* experiments. The graph shows the average temperature of a $6\,\mathrm{mm}^2$ surface of the patch during laser irradiation for endpoint temperatures between 60 and $90\,^{\circ}\mathrm{C}$ (n=10 experiments per end-point temperature). The error bars show the standard deviation.

This was because the temperature increase and decrease was steeper and thus more difficult to adjust. The immediate tensile strengths were 69±32, 99±29, 128±30, and $153{\pm}23\,\mathrm{mN/mm}^2$ at an endpoint temperature of 60, 70, 80, and $90\,^{\circ}\mathrm{C}$, respectively. For all endpoint temperatures, the color of the patch changed from light-green to dark-green, and was shrinking radially. The lateral shrinkage was negligible. No bubbles were visible during the irradiation.
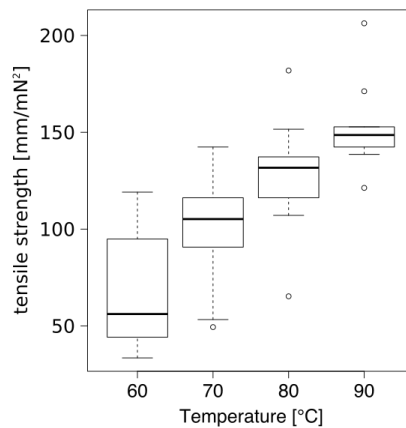
Figure VI.2: Tensile strength after laser soldering with continuous temperature curve at different end-point temperatures.

By comparing the native arterial wall of rabbit aorta and the laser-treated wall (see figure VI.3), it was evident, that thermal damage occurred across all temperature ranges. No vacuoles were present in the arterial wall that would indicate overheating. The T. interna with its endothelium appeared structurally intact in all samples. Especially for the samples treated with an

Figure VI.3: Histological analysis of the arterial wall after *in vitro* LAVA using rabbit aorta. **A**: Longitudinal whole-mount sections after MMA embedding show the patch (asterisks) closely adhering to the T. adventitia and the position were the anastomosis was performed. The end-point temperatures using continuous laser soldering were 60, 80 and 90 °C (**1A, 2A, 3A**, respective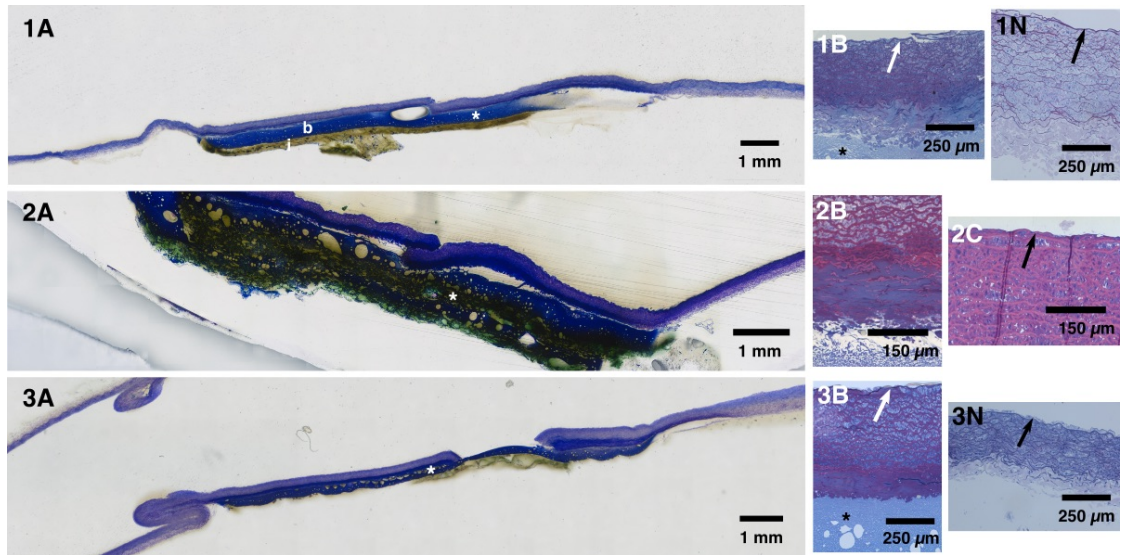ly). After irradiation at 80 and 90 °C the patch was completely molten, while the two-layer structure of the patch was clearly visible in the 60 °C-sample (**1A**, with **b** being the BSA layer and **i** being the ICG layer). The patch shown in 2A was significantly thicker. A reason might be, that the specimen was cut in a way where the overlap was present. All other micrographs show embedding in epon resin demonstrating the alterations of the arterial wall after LAVA. The native arterial wall (**1N, 3N**) consists of the T. interna with its endothelium (arrow), the T. media, and the T. adventitia that blends with the connective tissue that surrounds the artery. After LAVA (**1B, 2B, 2C and 3B**) thermal damage was evident. The T. media was compressed, while the collagen fibers appeared compact and accurately arranged. For samples treated with 60 and 90 °C, a gradient of thermal damage was observable, showing compressed tissue close to the T. adventitia, and lower compression at the site of the vessel lumen.

end-point temperature of 60 °C, a gradient of the thermal damage was visible. The T. adventitia and the underlying layers of the T. media appeared compressed, while the deeper layers of the T. media were loosely connected by collagen fibers. This effect is not observed at an end-point temperature of 80 °C. On the contrary, applying a continuous end-point temperature of 90 °C, the layers of the T. media that are close to the vessel lumen appear intact.

It seems that the patch was not homogeneously molten after irradiation to 60 °C, as the two-layer-structure is still visible. We did not observe this effect at temperatures above 70 °C. For all samples, the patch adhered well to the vessel over its whole length, however, some interspace was visible.

VI.3.2   Pulsed laser soldering: temperature curves and tensile strengths

Preliminary experiments have shown, that the average laser power for pulsed irradiation should be in the range of 0.7 to 1.5 W to ensure a temperature at the solder surface between 50 and 100 °C. Two parameters were varied: the average power and the pulse length. Therefore, the frequency rate of the pulses had to be adjusted, as the output peak power was kept constant at 30 W for all experiments. An overview of the parameters and the resulting tensile strength is given in table VI.1. For all experiments, the color of the patch changed from light to dark green and the patch was shrinking in lateral direction and therefore melting around the blood vessel, as for continuous laser soldering. The color change was faster with increasing average laser power. Figure VI.4 shows the development of the surface temperature during pulsed laser irradiation over time. By using a pulse length of 5 ms, the temperature increase was slow, after approximately 30 s, 50 °C were reached. Due to the low pulse energy of 0.15 J the temperature increase after each pulse was flat. The frequency rate was relatively high, resulting in a short time without irradiation were the tissue was allowed to cool. Hence, no temperature decrease after the pulses was observed and the temperature curve looks similar to the curve with a continuous laser irradiation, see figure VI.1. With a ten-fold increase of the pulse length to 50 ms, the laser pulses were visible in the temperature curves. A pulse energy of 1.5 J, results in a steep temperature increase. Furthermore, a frequency rate of 0.5 to 1 Hz, allows a temperature relaxation. Still, these frequencies allow only a low temperature relaxation, resulting in a temperature difference between the peak and the baseline of 10 to 20 °C. By using a pulse length of 100 ms and a frequency rate of 0.25 to 0.5 Hz, the peaks were more distinct and the height of the peaks was approximately 30 °C.

The tensile strengths reached after pulsed laser soldering is in the range of 47 to 79 mN/mm^2. A high average laser power, and therefore a higher temperature course, resulted in a higher tensile strength. The effect of the pulse length on the tensile strength is minor. Compared to continuous soldering, the tensile strengths were lower, however, soldering by using an pulse length of 100 ms and a frequency of 0.5 Hz, results in a similar tensile strength as continuous soldering with an end-point temperature of 60 °C, and could potentially reduce thermal damage.

Table VI.1: Overview of the parameters and the resulting tensile strength for pulsed laser soldering. The tensile strength displays the mean and the standard deviation of three samples.

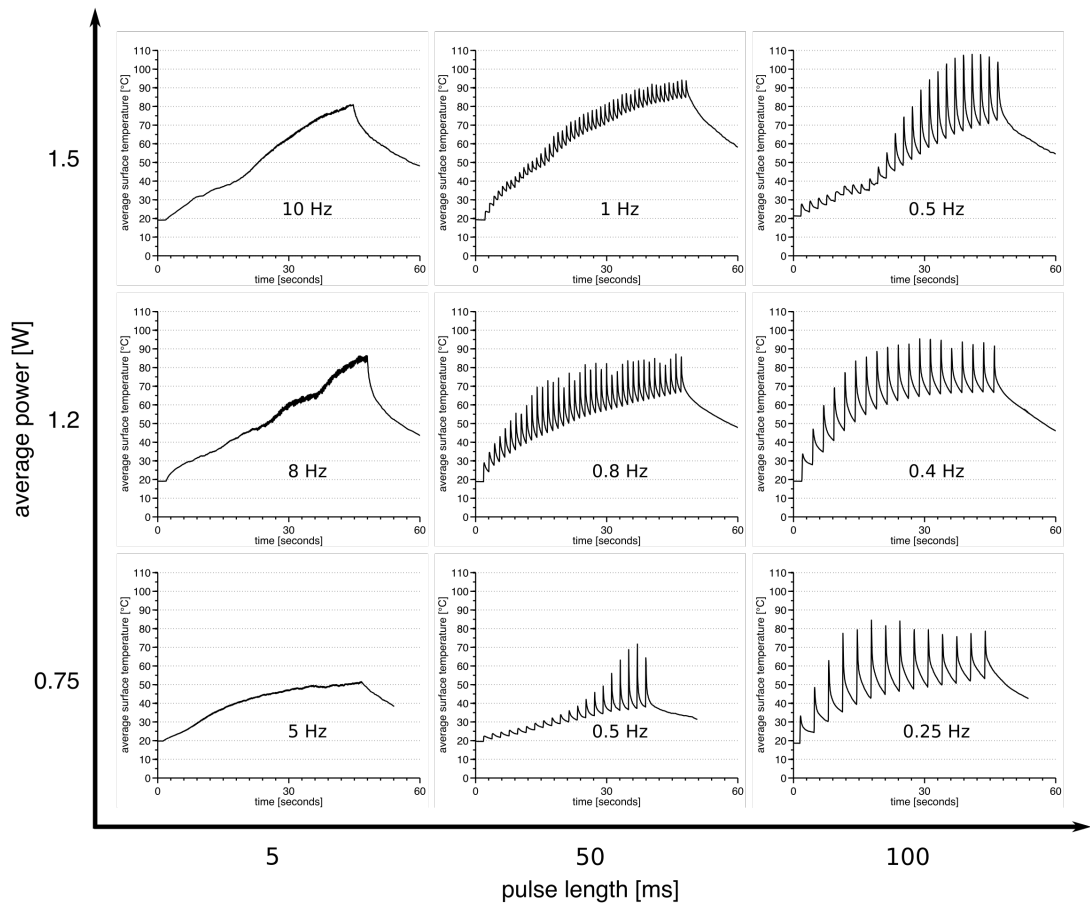| Average power [W]	Pulse length [ms]	Frequency [Hz]	Duty cycle [%]	tensile strength [mN/mm^2]
0.75	5	5		47±9
0.75	50	0.5	2.5	57±15
0.75	100	0.25		76±7
1.2	5	8		64±4
1.2	50	0.8	4	52±26
1.2	100	0.4		52±11
1.5	5	10		79±32
1.5	50	1	5	76±31
1.5	100	0.5		75±23

Figure VI.4: Typical solder-surface temperature of *in vitro* experiments with pulsed laser irradiation. The pulse length was varied between 5 and 100 ms, and the average power was kept constant between 0.75 and 1.5 W, therefore adjusting the frequency of the laser pulses. The graphs demonstrate the average temperature of a 6 mm^2 surface of the patch during laser irradiation.

VI.4 Discussion

In this study, the influence of different heating profiles during LAVA on the tensile strength was investigated. The tensile strength after continuous irradiation with an end-point temperature of 90 °C was twice as high than after irradiation to a temperature of 60 °C, which is in agreement with literature [10]. Histological assessment has shown, that the internal elastic lamina is structurally intact across all temperature ranges. The integrity of the endothelial cell layer is indispensable, as it facilitates the blood flow, keeps the tone of the blood vessels, and hinders the aggregation of platelets, therefore avoiding the occurrence of thrombosis [16]. Notwithstanding, cell-vitality should be investigated using fresh aorta directly after harvesting from the animals. During LAVA, the temperature at the T. interna should stay as low as possible, to avoid thermal damage of the vascular endothelial cell layer. Still, high enough temperatures are required to ensure the denaturation of BSA and the proteins of the blood vessel in order to achieve good bonding strength. A solution to this contradiction is a temperature gradient across the vessel wall, ensuring a high temperature at the T. adventitia and a low temperature at the T. interna. This gradient is visible in the histologies, applying 60 and 90 °C, however, we could not observe it using an end-point temperature of 80 °C. A study that involves a higher number of experiments is therefore required to ensure the reproducibility of the experiments.

A scheme of the soldering setup and the temperature distribution is shown in figure VI.5. Since the attenuation coefficient of the ICG-layer is $1119\pm183\,cm^{-1}$, 99 % of the laser energy is absorbed within a layer of approx. 15 µm [4]. The heating of the BSA-layer and the underlying tissue of the blood vessel is thus the result of heat diffusion.
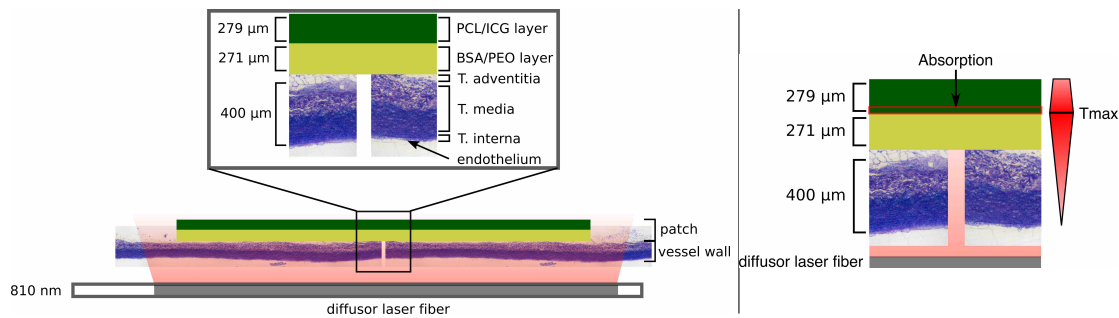

Figure VI.5: **Left:** Scheme of soldering setup with the blood vessel wall, the layered patch, and the laser diffusor fiber. The thicknesses are illustrated to scale. The length of the patch is 10 mm and the length of the diffusor fiber is 15 mm. **Right:** Most of the laser energy is absorbed in the first µm's of the PCL/ICG layer, thus the temperature is assumed to be maximal at this position. After heat deposition, the heat diffuses towards the surface of the patch, as well as towards the BSA-layer and the vessel wall. The temperature durring soldering is, however, observed at the surface of the patch.

In this experimental study, the application of pulsed laser irradiation with a peak energy larger than 1.5 J leads to a fast temperature increase. The heat is then diffusing into the surrounding tissue, followed by the next laser pulse. It is important that the pulse energy, and thus the pulse length, is sufficiently high, as otherwise the temperature increase is very small, and the temperature profile is similar to a continuous temperature profile (compare figure VI.1 and VI.4 (5 ms)). Due to the low thermal relaxation time of tissue [17], long pulse intervals are required, to allow a complete dissipation of the heat. However, our diode laser is limited to a frequency of minimum 0.3 Hz, leading to a built-up of the heat (see temperature curves, figure

VI.4). Furthermore, a low frequency requires too long total irradiation to reach reasonable tensile strengths, and might therefore not be applicable for surgeries.

For LAVA, we are mainly interested in the temperature at the patch-tissue-interface and the T. interna of the blood vessel. However, as we chose a non-contact measurement involving an infrared camera, the temperature at the surface of the patches is measured. Since the ICG-layer and the BSA-layer are similarly humid, I assume that the heat conductivity and heat capacity are in the same order of magnitude. As the thickness of both layers is similar, the heat conducted to the air-ICG-layer interface and the tissue-BSA-layer interface should be roughly equal. The temperature measured at the tissue-BSA-layer interface will however be lower than the temperature at the air-ICG-layer interface due to a higher thermal conductivity of tissue than air. Thus, the tissue-BSA-layer interface will be cooled more efficiently. The histologies (figure VI.3) confirm that most of the thermal damage occurs at the interface of the BSA-layer and the vessel while the deeper layers of the vessel undergoes reduced thermal damage.

By using a pulse length of 100 ms and an average power of 1.2 to 1.5 W/cm^2 a similar baseline of the temperature curve is observed as for continuous soldering at 60 °C, but with additional peaks that could lead to a better bonding strength. Thus, I assume, that thermal damage in both cases is in the same range, but with an improved tensile strength. The tensile strength using pulsed soldering is slightly higher in this case, being 75 ± 23 and 69 ± 32 mN/mm^2, respectively. More experiments have to be performed to investigate a statistical significance. Due to time constraints, a histological assessment of the thermal damage after pulsed laser irradiation was not yet feasible.

A drawback of pulsed soldering with high pulse energies might be the introduction of bubbles in the solder patch and the tissue due to an explosive temperature rise. Rabi et al. [10] suggests a gradual heating procedure that in a first step solidifies the albumin solder and afterwards heats the solder to higher temperatures in a second step. This procedure would avoid the deformation of the tissue or the swelling of the tissue. Such a procedure would nevertheless elongate the irradiation duration, possibly leading to desiccation of the tissue.

The intraluminal soldering setup used in this study ensures an easy positioning of the vessel stumps and the inflation of the blood vessel ends. By applying the balloon catheter, the vessel lumen is filled with water, which supports the cooling of the T. interna. However, the balloon used is only partially filled with water, as air bubbles in the balloon are hardly to avoid due to thin tubings. Moreover, during the positioning of the balloon, the fiber, the blood vessels and the solder patch, the water will heat up to body temperature. A continuous flow of cold water would be beneficial, but is hard to achieve [14].

A previous *in vivo* study has shown, that an anastomosis with a tensile strength of 23 mN/mm^2 was withstanding the blood pressure immediately after surgery (chapter II). Therefore, I assume that the bonding strength reached after continuous irradiation to 60°C as well as after pulsed laser irradiation is stable enough for LAVA. The measurement of the leaking point pressure or pulsatile bursting pressure, as described in [2] and [18], is required to investigate the water-tightness of the anastomosis.

The electrospun layered patch can easily be wrapped around the blood vessels. Due to the humidity of the vessel, the patch becomes slightly sticky after contact with the blood vessel and therefore holds the vessel stumps together. Furthermore, the patch can be applied to the vessels without the appearance of interstices, and no bubbles were observed during soldering for all temperature curves. Using a patch soaked in liquid BSA [4], small interstices were recorded after applying the patch. Interstices and bubbles however, are filled with gas, which has a low thermal conductivity and can therefore lead to an insulating layer between the patch and the vessel [19]. We therefore assume that the heat conduction is improved by using the electrospun layered patch.

By applying the intraluminal LAVA-setup [3], I chose a model that is mimicking *in vivo* surgery, in order to realistically investigate the influence and feasibility of the temperature curve. Although great care was taken to ensure good reproducibility of the experiments, the standard deviation of the tensile strength is high. This is probably due to the following reasons: the rabbit aortas are differing in circumference, wall thickness, humidity and tissue composition. Thus, different temperature curves will be observed for the same laser irradiation. Pulsed irradiation without a direct temperature feedback will therefore always lead to different temperatures, to different protein denaturation and therefore to more or less thermal damage and to varying tensile strengths. A direct feedback that controls the laser irradiation is inevitable for reproducible LAVA [10, 12, 20]. Another cause for the high standard deviation is the tensile strength measurement itself. Main uncertainties are the measurement of the cross section of the vessels, the alignment of the vessel stumps and the shape and the location of the rupture. In the pulsed irradiation group only three experiments were performed for each combination of parameters. More experiments should be conducted in order to improve the significance of the resulting tensile strength.

VI.5 Conclusion

The objective of LAVA is to create a rapid and immediate leakage-free bonding with little thermal damage. It was demonstrated in this work that the bonding strength increases with higher end-point temperatures, but at the same time the thermal damage increases. The tensile strength after soldering with an end-point temperature of $60\,^\circ$C could be sufficiently high and has to be tested *in vivo*. LTS using pulsed irradiation is feasible and achieves reasonable tensile strengths. A probable reduction of thermal damage of the tissue has to be investigated. However, a feedback control of the temperature and the laser irradiation will be indispensable for reproducible results. These findings support the further development of LAVA with a solder patch.

Bibliography

[1] Lawrence S. Bass and Michael R. Treat. Laser tissue welding: A comprehensive review of current and future. *Lasers in Surgery and Medicine*, 17(4):315–349, 1995.

[2] I.C.D.Y.M. Wolf -de Jonge, J.F. Beek, and R. Balm. 25 Years of Laser Assisted Vascular Anastomosis (LAVA): What Have We Learned? *European Journal of Vascular and Endovascular Surgery*, 27(5):466–476, may 2004.

[3] Beat Ott, Mihai A. Constantinescu, Dominique Erni, Andrej Banic, Thomas Schaffner, and Martin Frenz. Intraluminal laser light source and external solder: In vivo evaluation of a new technique for microvascular anastomosis. *Lasers in Surgery and Medicine*, 35(4):312–316, oct 2004.

[4] Annemarie Schönfeld, Zacharia Mbaidjol Kabra, Kirsten Peters, Mihai A. Constantinescu, and Martin Frenz. Binding of indocyanine green in polycaprolactone fibers using blend electrospinning for laser-assisted vascular anastomosis. *Lasers in Surgery and Medicine*, in prepara:1–28, 2016.

[5] Annemarie Schönfeld, Mihai A. Constantinescu, Kirsten Peters, and Martin Frenz. Effects of different auxiliary polymers for electrospinning of albumin on the tensile strength after laser-tissue-soldering. *Biomedical Materials*, submitted:1–12, 2016.

[6] Dara R. Pabittei, Michal Heger, Johan F. Beek, Sjoerd Van Tuijl, Marc Simonet, Allard C. Van Der Wal, Bas A. De Mol, and Ron Balm. Optimization of suture-free laser-assisted vessel repair by solder-doped electrospun poly(ϵ-caprolactone) scaffold. *Annals of Biomedical Engineering*, 39(1):223–234, may 2011.

[7] Serge Bogni, Maria Anna Ortner, Istvan Vajtai, Christian Jost, Michael Reinert, Bernard Dallemagne, and Martin Frenz. New laser soldering-based closures: A promising method in natural orifice transluminal endoscopic surgery. *Gastrointestinal Endoscopy*, 76(1):151–158, oct 2012.

[8] Giuseppe Esposito, Francesca Rossi, Paolo Matteini, Alba Scerrati, Alfredo Puca, Alessio Albanese, Giacomo Rossi, Fulvio Ratto, Giulio Maira, and Roberto Pini. In vivo laser assisted microvascular repair and end-to-end anastomosis by means of indocyanine green-infused chitosan patches: A pilot study. *Lasers in Surgery and Medicine*, 45(5):318–325, jul 2013.

[9] Mohammad E Khosroshahi and Mohammad S Nourbakhsh. Enhanced laser tissue soldering using indocyanine green chromophore and gold nanoshells combination. *Journal of Biomedical Optics*, 16(8):088002, 2011.

[10] Yaron Rabi and Abraham Katzir. Temporal heating profile influence on the immediate bond strength following laser tissue soldering. *Lasers in Surgery and Medicine*, 42(5):425–432, jun 2010.

[11] A. Abergel, I. Gabay, D. M. Fliss, A. Katzir, and Z. Gil. A Multi-wavelength Fiber-Optic Temperature-Controlled Laser Soldering System for Upper Aerodigestive Tract Reconstruction: An Animal Model. *Otolaryngology - Head and Neck Surgery*, 144(6):872–876, jun 2011.

[12] Ilan Gabay, Irina Barequet, David Varssano, Mordechai Rosner, and Abraham Katzir. Bonding surgical incisions using a temperature-controlled laser system based on a single infrared fiber. *Journal of Biomedical Optics*, 18(11):111416, sep 2013.

[13] Amadé Bregy, Serge Bogni, Vianney J.P. Bernau, Istvan Vajtai, Felix Vollbach, Alke Petri-Fink, Mihai Constantinescu, Heinrich Hofmann, Martin Frenz, and Michael Reinert. Solder doped polycaprolactone scaffold enables reproducible laser tissue soldering. *Lasers in Surgery and Medicine*, 40(10):716–725, dec 2008.

[14] Serge Bogni, Oliver Stumpp, Michael Reinert, and Martin Frenz. Thermal model for optimization of vascular laser tissue soldering. *Journal of Biophotonics*, 3(5-6):284–295, mar 2010.

[15] Vivianne Chappuis, Yeliz Cavusoglu, Reinhard Gruber, Ulrike Kuchler, Daniel Buser, and Dieter D Bosshardt. Osseointegration of Zirconia in the Presence of Multinucleated Giant Cells. *Clinical Implant Dentistry and Related Research*, 18(4):686–698, aug 2016.

[16] David Abraham and Oliver Distler. How does endothelial cell injury start? The role of endothelin in systemic sclerosis. *Arthritis Research & Therapy*, 9(Suppl 2):S2, 2007.

[17] Joseph T. Walsh., Thomas J Flotte, R Rox Anderson, and Thomas F Deutsch. Pulsed CO2 laser tissue ablation: Effect of tissue type and pulse duration on thermal damage. *Lasers in Surgery and Medicine*, 8(2):108–118, 1988.

[18] Dara R. Pabittei, Michal Heger, Sjoerd van Tuijl, Marc Simonet, Wadim de Boon, Allard C. van der Wal, Ron Balm, and Bas A. de Mol. Ex vivo proof-of-concept of end-to-end scaffold-enhanced laser-assisted vascular anastomosis of porcine arteries. *Journal of Vascular Surgery*, 62(1):200–209, jul 2015.

[19] Karen M McNally, Brian S Sorg, Ashley J Welch, Judith M Dawes, and Earl R Owen. Photothermal effects of laser tissue soldering. *Physics in Medicine and Biology*, 44(4):983–1002, apr 1999.

[20] Meir Cohen, Avi Ravid, Vered Scharf, Daniel Hauben, and Abraham Katzir. Temperature controlled burn generation system based on a CO2 laser and a silver halide fiber optic radiometer. *Lasers in Surgery and Medicine*, 32(5):413–416, jun 2003.

VII.   Summary

Summary and Discussion

The focus of this thesis was the development of an electrospun solder patch and the exploration of the applicability of the patch for LAVA using medium-sized arteries. Generally, an ideal vascular anastomosis is one that reproduces the continuity of the vessel, causing the least disruption of blood and one that retains the endothelial lining of the vessel without inducing a foreign body or immune reaction. This thesis aimed at achieving an ideal anastomosis by introducing a new solder material.

In **chapter II**, an ICG-loaded electrospun patch was developed. Due to binding the chromophore ICG in PCL fibers, leakage of ICG was prevented, and the concentration of ICG during soldering was stabilized ensuring a reproducible temperature course. Preliminary *in vivo* experiments demonstrated successful handling of the patch under operative conditions and resulted in an effective microvascular anastomosis. However, soaking the ICG-loaded patch in liquid BSA before soldering was tedious and not very practical.

Chapter III showed the development of a second electrospun layer, where the protein BSA was embedded into microfibers using polymers PEO, PCL, PVA, and gelatin. By using a BSA/PEO blend, electrospinning was stable and a high protein-load was achieved. The solder patch was now made of two electrospun layers - an absorbing layer made of PCL and ICG, and a protein layer made of BSA and PEO. The production of this patch was easy, quick, reproducible, and cheap, and more importantly, could be scaled up for industrial processing. *In vitro* LAVA using the layered patch lead to efficient bonding, and the tensile strength reached was in the same range as for patches soaked in liquid BSA, being $102\pm18\,\mathrm{mN/mm^2}$ and $117\pm30\,\mathrm{mN/mm^2}$, respectively.

In **chapter IV**, we investigated the feasibility of the newly developed layered electrospun patch for *in vivo* LAVA. Using the patch during surgery was comfortable, thanks to its pliability and tear-resistance. The patch became slightly sticky after contact with liquids, which helps for coaptation of the vessel ends. A perfect alignment of the vessel ends it still indispensable, to ensure strong bonding and to retain a smooth endothelial lining. During laser irradiation, the patch does neither drip, and therefore not stain peripheral tissue, nor shrink in lateral direction. Due to the relatively low melting points of PCL and PEO at $60\,^{\circ}\mathrm{C}$, the polymers melt during soldering and adapt to the vessel walls, without interstices or bubbles. The surgery itself was successful, the immediate bonding strength was strong enough to withstand the blood pressure and all pigs survived. However, the vessels occluded after a few days, which was not acceptable.

The occlusion of the arteries can have many reasons. One could be the damage of the arteries during surgery due to desiccation or damage with the balloon catheter. A second reason might be insufficient alignment of the vessel walls, leading to turbulence of the blood stream. The histological examinations demonstrated, that a perfect alignment was not achieved, although great care was taken. A third possibility is the toxicology of the patches, that was investigated in **chapter V**. Cell culture experiments showed a cytotoxicity of the layered patch, which is most

probably because of a high ICG concentration. Thus, a reduction of the ICG amount might be required, which would, after all, change the absorption coefficient and thus the heating behavior. Additionally, all materials and possible residues from sterilization should be investigated.

In **chapter VI** I tried to reduce the most relevant reason for the vessel occlusion: Thermal damage. Histologies revealed a shrinkage and morphological alteration of the blood vessel wall at end-point temperatures at the patch-surface higher than 70 °C. A reduction of the temperature to 60 °C significantly reduced the tensile strength of the bonding. However, it might withstand physiological blood pressure. Furthermore, pulsed laser irradiation has potential to minimize thermal damage at the inner vessel wall, while ensuring strong tissue bonding. In both cases an automated feed-back control of the temperature profile and the laser irradiation during LAVA is required. Additionally, active cooling of the lumen of the vessel might be indispensable. The measurement of the leakage point pressure instead of tensile strength will be a more realistic measure to assess the quality of the tissue bonding.

Outlook

Tissue repair is an important step in most surgical procedures. The application of the layered electrospun patch for laser tissue soldering has enormous potential in medical fields, such as wound closure, pyeloplasty, natural orifice transluminal endoscopic surgery, vasovasostomy, fallopian tubes reconstruction, and nerve reconnection.

The electrospun chromophore-and protein-loaded patch improved LAVA and might be a valuable material for other biomedical fields. An alternative application of electrospun PCL/ICG scaffolds are biosensors, due to changing physiochemical characteristics of ICG at different pH values or after binding to proteins and lipoproteins [1, 2]. Another application might be a PCL/ICG-coating of medical devices, such as stents, gastric tubes and implants, followed by real-time fluorescence imaging, to allow tracking and correct placement. Electrospun BSA/PEO layers can be used in numerous applications, including dressings for wound healing, substrates for tissue engineering, and biosensors. A BSA-coating of medical implants could improve their biocompatibility. These coatings could be further functionalized with bioactive molecules, such as growth factors, antifungals, and vasodilators.

Conclusion

This thesis demonstrates the whole development process of a soldering material for LAVA— starting with the idea of a two-layer electrospun patch all the way to pre-clinical experiments. This patch includes all required substances for LAVA and results in an immediate and effective tissue bonding. Still, there is a long way to go for LAVA to become clinically applied, and this thesis presents a stepstone on that path.

Bibliography

[1] R C Benson and H a Kues. Fluorescence properties of indocyanine green as related to angiography. *Physics in Medicine and Biology*, 23(1):017, jan 1978.

[2] O. G. Björnsson, R. Murphy, V. S. Chadwick, and S. Björnsson. Physicochemical Studies on Indocyanine Green: Molar Lineic Absorbance, pH Tolerance, Activation Energy and Rate of Decay in Various Solvents. *Clinical Chemistry and Laboratory Medicine*, 21(7):453–458, 1983.

Acknowledgements

During the past years I met a number of people who helped me in accomplishing this PhD thesis. Especially, I would like to thank the following people:

Prof. Dr. Martin Frenz for giving me the opportunity to work in the exciting field of Biomedical Photonics, for his supervision and valuable and critical inputs.

PD Dr. Kirsten Peters for supervising this thesis and for giving me the opportunity to work in a cell biology lab.

I want to thank René Nyffenegger for his uncountable help regarding technical and chemical questions of the IAP, as well as the mechanics and electronic workshop for building the weirdest things.

The collaborators of the Insel hospital, Prof. Dr. Mihai Constantinescu, Dr. Zacharia Mbaïdjol Kabra and Dr. Jonathan Leckenby, are acknowledged for helping in medical questions, for the interesting discussions and for supporting the clinical experiments.

The *in vivo* experiments would not have been possible without the help of the ESI team. I want to thank Dr. Daniel Mettler and Olgica Beslać for introducing me into surgery.

The team of the Veterinary Anatomy of the Vetsuisse Faculty in Bern is acknowledged for advice regarding histologies and the anatomy of blood vessels and for letting me use the SEM. Prof. Dr. Michael Stoffel thank you for the fruitful discussions we had, for proof-reading this thesis, and for your encouraging comments.

The histologies were made in the Robert K. Schenk Laboratory of Oral Histology, thank you Prof. Dr. Dieter Bosshardt and Silvia Owusu for your support.

The Cell Biology Group in Rostock is acknowledged for introducing me to Cell Biology.

Serge Bogni thank you so much for reviewing and revising the *in vivo*- and temperature-chapter.

I had a great time in the Biomedical Photonics Group. Thank you all for the various inputs, for the lunch breaks and the amazing time we spend together. I want to thank especially the Bachelor student Pascal Moll for performing experiments regarding electrospinning of BSA.

Dominik, thank you for all the interesting scientific discussions we had during the last years, for proof-reading this thesis, and for your relentless support.

Eidesstattliche Versicherung

Ich versichere eidesstattlich durch eigenhändige Unterschrift, dass ich die Arbeit selbstständig und ohne Benutzung anderer als der angegebenen Hilfsmittel angefertigt habe. Alle Stellen, die wörtlich oder sinngemäß aus Veröffentlichungen entnommen sind, habe ich als solche kenntlich gemacht. Die Arbeit ist noch nicht veröffentlicht und ist in gleicher oder ähnlicher Weise noch nicht als Studienleistung zur Anerkennung oder Bewertung vorgelegt worden. Ich weiß, dass bei Abgabe einer falschen Versicherung die Prüfung als nicht bestanden zu gelten hat.

Kopenhagen,

_____   _____

        Abgabedatum   Vollständige Unterschrift

Annemarie Schönfeld

ADDRESS:	Borgergade 26, 4.5
	1300 København K
	Denmark
PHONE:	+45 40 29 18 86
EMAIL:	annemarie@schoenfeld.li
DATE OF BIRTH:	27 March 1986	Zwickau, Germany

Education

JAN 2013 – TODAY	**PhD in Medical Sciences** (Dr. rer. hum.) *Department of Cell Biology, University Medicine Rostock, Germany*
FEB 2011 – NOV 2012	**Master of Science in Life Sciences** (MSc (FHNW)) *University of Applied Sciences Northwestern Switzerland, Muttenz*
SEPT 2004 – JAN 2009	**Engineer in Pharmaceutical Biotechnology** (Dipl.-Ing. (FH)) *University of Applied Sciences Jena, Germany*
SEPT 1996 – JULY 2004	**Abitur** *Gymnasium Wilkau-Hasslau, Germany*

Work Experience

JUNE 2017 – TODAY	**Research Scientist** *Protein Characterisation and Stability, Novozymes A/S, Bagsværd, Denmark*
JAN 2013 – DEC 2016	**PhD Candidate at Biomedical Photonics Group** *Institute of Applied Physics, University of Bern, Switzerland* Thesis: "An electrospun protein- and chromophore-loaded patch: Application to laser-assisted vascular anastomosis"
MAR 2012 – NOV 2012	**Master thesis at Biomedical Photonics Group** *Institute of Applied Physics, University of Bern, Switzerland* Thesis: "Electrospinning of a nanoparticle-doped patch improves laser-tissue-soldering"
DEC 2008 – FEB 2011	**Scientist for High-Throughput Lab Automation** *Biologics, Novartis Pharma AG, Basel, Switzerland*
APR 2008 – OCT 2008	**Diploma thesis Pharmaceutical and Analytical Development** *Novartis Pharma AG, Basel, Switzerland* Thesis: "Development of concentrated liquid antibody formulations applying DoE with focus on pH, ionic strength and stabiliser concentration"
SEPT 2007 – JAN 2008	**Internship at Bacterial Infection and Immunity Group** *Institute of Food Research, Norwich, United Kingdom* Report: "The development of recombinant *Lactococcus lactis* expressing chemokines that target cells *in vivo*"